BIOPRINTING OF CHONDROCYTE-LADEN HYDROGEL CONSTRUCTS AND THEIR *IN-VITRO* CHARACTERIZATION FOR CARTILAGE TISSUE ENGINEERING

A Thesis Submitted to the College of

Graduate and Postdoctoral Studies

In Partial Fulfillment of the Requirements

For the Degree of Doctor of Philosophy

In the Division of Biomedical Engineering

University of Saskatchewan

Saskatoon

By

FU YOU

Permission to Use

In presenting this thesis in partial fulfillment of the requirements for a Postgraduate degree from the University of Saskatchewan, I agree that the Libraries of this University may make it freely available for inspection. I further agree that permission for copying of this thesis in any manner, in whole or in part, for scholarly purposes may be granted by the professor or professors who supervised my thesis work or, in their absence, by the Head of the Department or the Dean of the College in which my thesis work was done. It is understood that any copying or publication or use of this thesis or parts thereof for financial gain shall not be allowed without my written permission. It is also understood that due recognition shall be given to me and to the University of Saskatchewan in any scholarly use which may be made of any material in my thesis.

Requests for permission to copy or to make other uses of materials in this thesis/dissertation in whole or part should be addressed to:

Head of the Division of Biomedical Engineering
57 Campus Drive, University of Saskatchewan
Saskatoon, Saskatchewan S7N 5A9
Canada

OR

Dean
College of Graduate and Postdoctoral Studies
University of Saskatchewan
116 Thorvaldson Building, 110 Science Place
Saskatoon, Saskatchewan S7N 5C9
Canada

Abstract

Articular cartilage lines the ends of bones, provides low friction and load bearing, and allows for efficient joint movement. Once damaged, articular cartilage has difficulty of repairing itself due to lack of blood and nerve supply. Cartilage tissue engineering (CTE) aims to provide solutions to cartilage defects and involves the use of cells, scaffolds, and stimulating factors, alone or in combination. Hydrogel, a crosslinked polymeric network containing large amounts of water, is regarded as the ideal scaffolding material for CTE due to its structural similarity to native cartilage. Encapsulating chondrocytes in hydrogels is a promising approach to provide high cell seeding density, uniform cell distribution and a suitable microenvironment for encapsulated chondrocytes. However, fabrication of hydrogel scaffolds with desired microstructure/internal structure and living cells is the key issue, which limits hydrogel's applications in cartilage tissue engineering. To address these issues, this thesis aimed to bioprint cartilage constructs that incorporate living cells and characterize them *in vitro* for CTE. This aim was achieved via pursuing the following three specific objectives.

The first objective was to fabricate CTE scaffolds based on the bioprinting technique and to study the influence of scaffold design on the mechanical performance. Gelatin and alginate mixtures were synthesized and printed into porous hydrogel scaffolds with the help of thermal/submerged ionic crosslinking process. The scaffold geometries, including stand orientation and the spacing between them, were adjusted for bioprinting and their influence on the scaffold mechanical properties were investigated. Results showed that there was a significant influence of internal design on the mechanical performance of printed hydrogel scaffolds and porosity, contact area between strands and spacing variation were three key factors that influence the mechanical performance of scaffolds.

The second objective was to develop a 3D Bioplotting technique or process supplemented with the submerged cross-linking mechanism to fabricate alginate hydrogel constructs with living cells. *In vitro* biological performance of the printed alginate constructs was evaluated in terms of cell viability, proliferation and secretion of sulfated glycosaminoglycan (GAG) and Collagen type II. Chondrocytes were homogeneously distributed in the bioprinted hydrogels and cell viabilities were around 80%. Cartilage extracellular matrix (ECM) including glycosaminoglycan (GAG) and Collagen type II were synthesized by embedded chondrocytes, demonstrating the promising biocompatibility of this bioprinting technique.

The third objective was to test the hypothesis that homogeneously dispersed hydroxyapatite in alginate hydrogel promotes the formation of calcified cartilage matrix. Cell growth, extracellular matrix (ECM) production, and mineralization potential were evaluated in the presence or absence of hydroxyapatite particles for comparison. The hydroxyapatite (HAP) phase was evenly dispersed into alginate hydrogel with the addition of a surfactant-sodium citrate (SC). Chondrocytes embedded in this composite hydrogel demonstrated expression of alkaline phosphatase (ALP) after 14 days of culture. Characteristic ECM in calcified cartilage such as minerals and Collagen type X showed a significantly higher synthesis in composite hydrogels with pre-incorporated HAP than that of alginate hydrogels. These results provided researchers with a facile technique to bioprint porous chondrocyte-laden hydrogel constructs for application in CTE and demonstrated a technique of inducing chondrocytes to synthesize calcified cartilage matrix by simply mixing HAP into hydrogel.

Taken all together, this thesis presented the techniques/methods developed to bioprint cartilage constructs with living cells and would bring forward the fabrication of constructs for the repair of cartilage defects.

Acknowledgments

I would like to express my gratitude to my supervisors, Dr. Daniel Chen and Dr. Brian Eames, for their inspiring research advices and strong supports during my Ph.D. studies. I would also like to thank the Advisory Committee members, Dr. Assem Hedayat, Dr. Bill Kulyk, and Dr. Ning Zhu, for their valuable comments and suggestions from proposal defense, annual meeting, comprehensive exam all the way to my thesis defense. I appreciate the technical help from Dr. Tuanjie Chang, Dr. Zohreh Izadifar, Dr. Ajay Rajaram and Dr. David Cooper regarding scaffold fabrication techniques, biological experiments, CT image acquisition and analysis. Selfless help from friends and lab mates in the Tissue Engineering Research Group (TERG) and Eames Lab are highly appreciated.

The financial support from the China Scholarship council, Saskatchewan Health Research Foundation (SHRF) and the University of Saskatchewan is greatly acknowledged.

Last, my deepest gratitude goes to my family for my parents Zemin You and Shuxian Xing' unconditional love, my wife Xia Wu's heartwarming supports, and for the joy brought by my son Eddie. I also would to extend my thanks to the rest of my family, my grandfather Huaili Xing, grandmother Xiaohuan Zhang, my ant Shujing Xing, my uncle Zhongyuan Xing.

Table of Contents

List of Tables

List of Figures

Table of Abbreviation

Abbreviation	Explanation
AC	Articular cartilage
OA	Osteoarthritis
ACI	Autologous chondrocyte implantation
OAT	Osteochondral autologous transplantation
TE	Tissue engineering
CTE	Cartilage tissue engineering
GAG	Glycosaminoglycan
ECM	Extracellular matrix
3D	Three dimensional
BMP	Bone morphogenetic protein
IGF	Insulin-like growth factor
TGF-β	Transforming growth factor beta
FGF	Fibroblast growth factors
EBB	Extrusion-based bioprinting
HA	Hyaluronic acid
PEG	Polyethylene glycol
PVA	Poly (vinyl alcohol)
UV	Ultraviolet
RP	Rapid prototyping
CAD	Computer aided design
MSC	Mesenchymal stem cell
BMSC	Bone marrow stem cells
ASC	Adipose stem cells
PCL	Polycaprolactone
PMHMGCL/PCL	Methacrylated poly(hydroxymethylglycolide-co-e-caprolactone)/ polycaprolactone
GelMA	Gelatin methacrylamide
PEGDMA	poly (ethylene glycol) dimethacrylate
dECM	Decellularized extracellular matrix
PEI	Polyethylenimine
SA	Sodium alginate
PBS	Phosphate buffered saline
DDW	Double distilled water
BMIT	BioMedical Imaging & Therapy facility
CLS	Canadian Light Source
BSA	Bovine serum albumin
DMEM	Dulbecco's modified Eagle's medium
FBS	Fetal bovine serum
HBSS	Hank's balanced salt solution
TBS	Tris-buffered saline
GF	Growth factors
HAP	Hydroxyapatite

ALG	Alginate
SC	Sodium citrate
Pi	Inorganic phosphate
ALP	Alkaline phosphatase
pNP	p-nitro-phenol
pNP-PO_4	p-nitrophenyl phosphate
TEM	Transmission electron microscopy
SEM	Scanning electron microscopy
EDS	Energy dispersive spectroscopy

Chapter 1: Introduction

1.1 Articular Cartilage Defects and Osteoarthritis

There are three major types of cartilage existing in human body, hyaline cartilage (found in the elbows, hips, knees, sternum and rib cage), fibrocartilage (found in intervertebral discs) and elastic cartilage (found in the external ear, epiglottis). This thesis will focus on the regeneration of articular cartilage, a type of hyaline cartilage. Articular cartilage (AC) is a thin layer of highly hydrated and specialized tissue that lines the ends of diarthrodial joints and functions to provide a low-friction, wear-resistant, and load-bearing surface for efficient joint movement (1, 2). Besides water (70-80% by total weight), the solid fraction of mature articular cartilage is made up of collagens (50-75%), proteoglycans (15-30%) with the remaining composition including chondrocytes and other minor protein molecules. Collagen type II is the major collagen type in articular cartilage, comprising more than half the dry weight of the tissue. Articular cartilage also has globular and fibrillar collagen types, like Collagen types V, VI, IX, and XI (3). Although the roles of these collagen types are yet fully understood, they are believed to play a key role in modulating the structure of collagen type II and intermolecular interactions (4). For instance, Collagen type IV is mainly found in the pericellular matrix and probably contribute to regulate interactions between the chondrocyte and extracellular matrix (ECM) (5, 6). Collagen type X, mainly found in the calcified cartilage, seems to play a role in building an interface between cartilage and the subchondral bone (7). The primary proteoglycan in articular cartilage is aggrecan, consisting of a protein core and sulfated GAG side chains. Other types of proteoglycans in articular cartilage include biglycan, lubricin, fibromodulin, which are also comprised of core proteins with various glycosaminoglycan species attached as side chains (8). Many proteoglycans grouping into large macromolecular complexes is critical for the functionality of cartilage tissue. An integrated network is formed by collagens and proteoglycans that lay the foundation for the distinct mechanical performance of articular cartilage (9).

Although the thickness of articular cartilage is no more than several millimeters (10), it is divided into four zones, i.e., superficial zone, middle zone, deep zone, and calcified zone, based on the morphology and composition of its components. In superficial zone, densely packed collagen fibers are oriented parallel to the cartilage surface and proteoglycan content is relatively low. Chondrocytes exhibit discoidal, flattened shapes (11). In middle zone, collagen fibers are

randomly oriented and proteoglycan content reaches its maximum. Chondrocytes show spherical shape with a much lower density than superficial zone (11). In deep zone, collagen fibers are oriented perpendicular to the articular surface and proteoglycan content is much lower than middle zone. Chondrocytes are grouped in a columnar organization with the lowest density compared with any other of zone in articular cartilage (11). Below these zones is the calcified cartilage. In calcified cartilage, hypertrophic chondrocytes are embedded in a mineralized matrix. It not only facilitates cartilage-to-bone integration but also serves as a physical barrier that enables pressurization of articular cartilage. This barrier is important for maintaining the integrity of repaired cartilage and thus, successful regeneration of the calcified cartilage layer essential for functional cartilage repair. Underlying calcified zone is the subchondral bone (12-14).

Articular cartilage injury is common and its pathogenesis is multifactorial (15). It can be caused by sports, trauma, obesity, and lack of movement (16). Once damaged, articular cartilage has difficulty repairing itself due to its avascular and aneural nature (16). Depending on the depth, cartilage defects can be categorized into two types: chondral defects and osteochondral defects (17). Chondral defects do not extend to the subchondral bone and patients will not feel any pain due to its aneural nature (18). Meanwhile, tissue self-repair is insufficient because of lack of vascular network. This may lead to the eventual development of osteochondral lesions, which will penetrate into subchondral bone (19). In this case, progenitor cells from bone marrow are recruited to fill and regenerate the defects with impaired functionality (20). The regenerated tissue is mainly fibrocartilage, which results in an inferior quality of repair tissue (21, 22). Previous studies have demonstrated that this repair tissue is structurally and biomechanically inferior to the articular cartilage and may not be suitable for a long-term load-bearing function (23, 24).

Due to the limited ability of articular cartilage for self-repair, and the biomechanically weak repair tissue, cartilage defects may gradually expand to cover most area of the articular surface under long-term compressive loading, leading to osteoarthritis (OA). OA is the most common type of arthritis and affects more than 10% of Canadians aged 15 or older and nearly 27 million Americans (25). Moreover, ageing and extended life expectancy would make OA the fourth leading cause of disability by 2020 (26). OA is also associated with extremely high economic burden, involving the expense of treatment, disability rehabilitation, and early retirement (27).

Treatments for articular cartilage defects include microfracture, autologous chondrocyte implantation (ACI) and osteochondral autologous transplantation (OAT). In microfracture procedure, impaired cartilage is removed and the subchondral bone is penetrated to expose bone marrow. The bone mesenchymal stem cells in bone marrow will access and fill the cartilage defects. Nevertheless, as mentioned before, the newly formed tissue is fibrocartilage which mainly consists of Collagen type I, while the major type collagen in articular is Collagen type II. Fibrocartilage shows much lower biomechanical properties to articular cartilage and may lead to further degeneration under long-term load (28). In ACI procedure, patient's chondrocytes are isolated from a healthy region and expanded in tissue culture laboratory. Cells are re-implanted into the damaged area once enough cells have been obtained. Articular cartilage or fibrocartilage are newly formed by ACI technique. Disadvantages of ACI include donor site morbidity, scarce cell sources, and second invasive surgeries (one surgery to collect chondrocytes, one surgery to put chondrocytes back to defect area) (29). During OAT surgery, healthy cartilage along with part of its underlying bone is transferred to fill the damaged cartilage area. This surgery will come with donor site morbidity, which are not desirable for patients (30).

Surgeries including osteotomy (31) and arthroplasty (32) are usually needed once small focal defects develop into OA. Osteotomy relieves pressures of the defect area by reshaping bone to change its alignment towards the healthy area and thus relieving pain in early-stage OA. However, due to the serious nature of the procedure and in long-term run, it could result in joint deterioration, it is being replaced by arthroplasty especially for seniors. Arthroplasty, or joint replacement, is used to treat serious OA and mainly involves replacing the suffering joint with artificial prosthesis. Nevertheless, it is reported that the treated joints could hurt again several years later since the implanted prostheses are worn out (2, 33). Moreover, arthroplasty is not a suitable procedure to treat young patients because of their growing skeletons (34). Therefore, exploring an effective approach to treat cartilage defects and overcome the drawbacks of above-mentioned treatments remains a challenge.

1.2 Cartilage Tissue Engineering

Tissue engineering (TE) strategies have been employed with the aim to improve the quality and longevity of repair tissue and long-term patient outcome (35). In articular cartilage tissue engineering (CTE), cells and/or bioactive molecules are delivered to the defect area through a

scaffold to fill and regenerate cartilage lesions (36). Choosing suitable cell sources is important to CTE, especially for bioprinting of engineered cartilage. As the only cell type in cartilage, chondrocyte is a natural choice for CTE. Besides, stem cells have also been explored for application in CTE due to their multipotency (37). Hydrogels are attractive as the scaffolding material because they can provide desirable conditions for embedded cells. Water-swollen polymeric networks of hydrogels mimic native cartilage ECM and provide a favorable 3D microenvironment to maintain the morphology and chondrogenic phenotype of embedded chondrocytes (38, 39). Also, a homogenous cells distribution with high density can be achieved within hydrogels (40-42). Besides, transmitting external stimuli to embedded cells and thus directing the growth and formation of a cartilage tissue is another advantage of hydrogel scaffolds (43, 44). From the material point of view, native cartilage tissue is a cell-laden hydrogel. Different bioactive molecules or growth factors (e.g. bone morphogenetic protein (BMP), insulin-like growth factor 1 (IGF), transforming growth factor beta (TGF-β), fibroblast growth factors (FGF)) have been investigated independently and synergistically for their application in CTE. TGF-β family play an important role in chondrogenesis (45, 46) and cartilage development (47). Both IGF-1 and FGF-2 favors cell proliferation and result in more and accelerated cartilaginous ECM deposition (48-50). BMPs (mainly BMP2 and BMP7) showed positive effects on chondrogenesis and osteogenesis (51, 52), and thus are promising for osteochondral defect regeneration studies since they help engineered osteochondral constructs anchor into the subchondral bone at the implant site (53, 54). Other than growth factors, mechanical stimuli are another kind of stimulating factor for cartilage repair. Various mechanical loading regimes from a single loading to continuous loading have been tried to accelerate and promote cartilage formation. The time, frequency and value of load are usually needed to be optimized according to cell type and scaffold materials (55-57). High-water content of hydrogel makes it attractive as bioactive molecules delivery vehicle and embedded chondrocytes can sense the external stimuli to stimulate the cartilage tissue formation.

1.3 Bioprinting Cartilage Constructs

Bioprinting is an emerging technique that allows for fabrication of complex constructs with control over external shape and internal structure. It allows for accurate positioning of biologics (e.g. cells, biomaterials, bioactive molecules) in a layer-by-layer manner, thus facilitating the

production of customized regenerative cartilage constructs (58). The key to the success of these regenerative constructs is to make them biologically active, which is usually accomplished by incorporating living cells. It has been shown that the extrusion and laser-based bioprinting technologies are promising to incorporate cells with limited harm on the viability or long-term performance of the embedded living cells (59-63). Laser-based bioprinting deposits light energy on photocrosslinkable prepolymers solutions in predefined patterns and thus can be used to print a crosslinked cell-laden hydrogel (64). Extrusion-based bioprinting (EBB) allows for the deposition of cell-laden strands through a nozzle and is thought as the most suitable printing technique for the bioprinting of viable constructs with high cell densities and several centimeters in size (65) Therefore, EBB techniques have been most commonly used in printing cartilage constructs with living cells.

Hydrogels, as cell carriers, can provide many advantages in tissue engineering to create various tissues. A wide range of natural polymers (e.g. alginate, collagen, hyaluronic (HA) acid, and gelatin) as well as synthetic polymers (e.g. polyethylene glycol (PEG), Poly (vinyl alcohol) (PVA)) have been widely used as hydrogel materials for CTE applications(66, 67). Crosslinking can be induced chemically (e.g., with the presence of Ca^{2+}), thermally, or by using ultraviolet (UV) or visible light with photo initiators (methacrylate modified HA). To print a biologically active cartilage construct, bio-inks are employed as printing materials. In bioprinting, cell-laden hydrogels are commonly used and are termed “bio-inks” (65). These bio-inks can facilitate homogeneous cell seeding in a highly hydrated and mechanically stable 3D environment. Further information about applicable cell types and hydrogel polymers for bio-inks are reviewed in Chapter 2 of this thesis.

Bio-inks need to be designed in terms of printability so as to facilitate the layer-by-layer printing process. High viscosity can provide bio-ink with good printability but limit cell migration and matrix deposition. Meanwhile, it is difficult to print low-viscosity bio-inks since they tend to be flattened after deposition and have difficulty maintaining the shape as designed. Bioprinting of biological active cartilage constructs with living cells for CTE is concerned in this thesis.

1.4 Mechanical Properties of Bioprinted Hydrogel-based Cartilage Regenerative Constructs

AC functions to support and transfer loading and allows for rotation between bones. When people are doing exercises or sports, AC usually experiences a force several times higher than body weight, e.g. AC in knee experiences a force 3.5 times bodyweight (68). Loading or deformation exerts a combination of tensile, compressive, and shear stresses to the articular cartilage. As such, more than a single type of mechanical test is typically needed to characterize the mechanical properties of native cartilage. Different mechanical testing and their corresponding testing results of articular cartilage are listed in Table 1.1. These mechanical properties have been discussed and relevant testing protocols for CTE applications have been reviewed previously (69). The mechanical properties of bioprinted hydrogel-based cartilage are largely inferior to natural cartilage, due to the intrinsic weakness of hydrogels. Various strategies have been employed to improve the mechanical properties of 3D printed hydrogels construct; these strategies include co-depositing hydrogels and thermoplastic polymers (70), varying architectural properties (71), mixing with other polymers (72), incorporating micro/nano fibers (73), increasing crosslinking densities (41) and hydrogel precursor concentration (74). This thesis also concerns with the influence of internal design on the mechanical properties of 3D printed hydrogel scaffolds.

Table 1.1 Compressive, tensile, shear and aggregate moduli of human articular cartilage and bioprinted hydrogel-based cartilage constructs.

Mechanical characterization	Human articular cartilage	Bioprinted hydrogel-based cartilage constructs
Compressive Young's modulus	0.45 to 0.85 Megapascal (MPa) (41, 72, 75-80)	0.007-0.250 kilopascal (KPa) (30, 60, 67, 68)
Tensile Young's modulus	5 to 25 MPa (81-84)	0.116-0.230KPa (72)
Shear modulus	0.2 to 2MPa (83, 85)	Not reported
Aggregate modulus	0.5 to 0.9 MPa(86)	Not reported

1.5 The Importance of Calcified Cartilage in Cartilage Regeneration

Calcified cartilage is a layer of articular cartilage that serves as a transition from pliable cartilage to more rigid subchondral bone (87). As a native osteochondral interface, calcified cartilage layer mainly consists of a layer of scarce hypertrophic chondrocytes embedded in the mineralized matrix of Collagen types II and X, as well as proteoglycans (88-90). This layer serves as a functional junction for cartilage-to-bone and allows for pressurization during loading (91).

Notably, current cartilage repair strategies mainly focus on employing tissue-engineered cartilage constructs to treat cartilage defects (92). However, limited research is on engineering a functional and stable osteochondral interface to mimic the functionality of native cartilage, which remains a challenge nowadays. It is also noted that the reported approaches to achieve an osteochondral interface are mostly cell-based (93, 94) and that deep-zone chondrocytes are cultured in a mineralization media and/or on a material substrate containing calcium phosphate. The results illustrate that deep-zone chondrocytes can synthesize mineralized matrix (e.g. hydroxyapatite, a semicrystalline calcium phosphate) (94). As a general requirement, an osteochondral interface should favor chondrocyte viability and facilitate the deposition of calcified cartilage matrix (e.g. Collagen type X and mineralized matrix). This thesis also addresses the issue on the development of such an interface for the regeneration of calcified cartilage.

1.6 Research Objectives

By addressing the aforementioned issues, this thesis aimed to bioprint cartilage constructs that incorporate living cells and characterize them *in vitro* for CTE. The specific objectives of this thesis were set as follows.

The first objective was to fabricate CTE scaffolds based on the bioprinting technique and to study the influence of scaffold design on the mechanical performance. Gelatin and alginate mixtures were synthesized and printed with the help of thermal/submerged ionic crosslinking process, creating porous hydrogel scaffolds. The scaffold geometries, including stand orientation and the spacing between them, were adjusted for bioprinting and their influence on the scaffold mechanical properties were investigated.

The second objective was to develop a 3D bioprinting technique or process supplemented with the submerged cross-linking mechanism to fabricate alginate hydrogel constructs with living cells. To this end, cells and alginate mixture were prepared and bioprinted into pre-treated well of tissue culture plates containing crosslinking medium. *In vitro* biological performance of the printed alginate constructs was evaluated in terms of cell viability, proliferation and secretion of sulfated GAGs and Collagen type II.

The third objective was to test the hypothesis that homogeneously dispersed hydroxyapatite in alginate hydrogel promotes the formation of calcified cartilage matrix. To do so, sodium citrate was used to achieve homogenous mixing of hydroxyapatite within alginate. Cell growth, extracellular matrix (ECM) production, and mineralization potential were evaluated in the presence or absence of hydroxyapatite particles for comparison.

1.7 Organization of the Dissertation

The thesis is organized into 6 chapters. It includes the introduction chapter, four chapters adapted from four manuscripts, and a chapter summarizing the conclusions drawn from this research and the recommendations for future studies.

Chapter 2 presents a literature review on the application of extrusion-based hydrogel bioprinting for cartilage tissue engineering. It reviews applicable cell sources and toolkits of polymer that can be used for bio-ink formulations for CTE, and two bioprinting approaches (i.e., self-supporting hydrogel bioprinting and hybrid bioprinting) and their applications in fabricating chondral, osteochondral, and zonal organized cartilage regenerative constructs. This is followed by the insights on the current limitations and future opportunities of 3D bioprinting of cartilage regenerative constructs.

Chapter 3 addresses the fabrication of scaffolds based on the bioprinting technique and studies the influence of scaffold design on the mechanical performance. With the help of thermal/submerged ionic crosslinking process, porous alginate/gelatin hydrogel scaffolds can be printed. Then, six scaffold geometries are designed and produced by changing the strands orientation and spacing of hydrogel scaffold. The influence of scaffold internal geometry on its mechanical performance is investigated.

Chapter 4 presents the development of a bioprinting technique for fabricating porous chondrocyte-laden hydrogel constructs. The cell viability, cell proliferation, and cartilage ECM

deposition of the printed constructs are investigated. The fabrication technique and the printed scaffolds obtained support high cell viability and the deposition of cartilage ECM, demonstrating their potential for applications in CTE.

Chapter 5 presents a study to test the hypothesis that the addition of hydroxyapatite into alginate hydrogel promotes the biosynthesis of calcified cartilage matrix. First, homogenous mixing of alginate and hydroxyapatite is achieved with the addition of a surfactant. Next, cell growth, biosynthesis, and mineralization potential are evaluated with/without hydroxyapatite. Last, the printability of the composite hydrogel precursors is examined and verified by printing porous scaffolds using a 3D Bioplotter.

Chapter 6 summarizes conclusions drawn from this research and recommendations for future studies.

1.8 Contributions of the Primary Investigator

Manuscripts included in this thesis are co-authored and contributions of all authors are highly appreciated; however, it is the mutual understanding of all authors that Fu You, as the first author, is the primary investigator of the research work.

References

1. Wooley PH, Grimm MJ, Radin EL. The structure and function of joints. Arthritis and Allied Conditions.A Textbook of Rheumatology, Lippincott Williams & Wilkins, Philadelphia. 2005:149-73.

2. Athanasiou KA, Darling EM, Hu JC. Articular cartilage tissue engineering. Synthesis Lectures on Tissue Engineering. 2009;1(1):1-182.

3. Eyre DR, Wu JJ. Collagen structure and cartilage matrix integrity. J Rheumatol Suppl. 1995 Feb;43:82-5.

4. Guilak F, Setton L, Kraus V. Structure and function of articular cartilage. Principles And Practice Of Orthopaedic Sports Medicine.In Principles and Practice of Orthopaedic Sports Medicine.Edited by Garrett WE, et al.Philadelphia, PA: Lippincott Williams & Wilkins. 2000.

5. Choi JB, Youn I, Cao L, Leddy HA, Gilchrist CL, Setton LA, et al. Zonal changes in the three-dimensional morphology of the chondron under compression: the relationship among cellular, pericellular, and extracellular deformation in articular cartilage. J Biomech. 2007;40(12):2596-603.

6. McDevitt CA, Marcelino J, Tucker L. Interaction of intact type VI collagen with hyaluronan. FEBS Lett. 1991;294(3):167-70.

7. Aigner T, Reichenberger E, Bertling W, Kirsch T, Stöss H, Von der Mark K. Type X collagen expression in osteoarthritic and rheumatoid articular cartilage. Virchows Archiv B. 1993;63(1):205.

8. Roughley PJ, Lee ER. Cartilage proteoglycans: structure and potential functions. Microsc Res Tech. 1994;28(5):385-97.

9. Hu JC, Athanasiou KA. Structure and function of articular cartilage. In: Handbook of histology methods for bone and cartilage. Springer; 2003. p. 73-95.

10. Frisbie D, Cross M, McIlwraith C. A comparative study of articular cartilage thickness in the stifle of animal species used in human pre-clinical studies compared to articular cartilage thickness in the human knee. Veterinary and Comparative Orthopaedics and Traumatology (VCOT). 2006;19(3):142-6.

11. Hunziker E, Quinn T, Häuselmann H. Quantitative structural organization of normal adult human articular cartilage. Osteoarthritis and Cartilage. 2002;10(7):564-72.

12. Meachim G, Sheffield SR. Surface ultrastructure of mature adult human articular cartilage. J Bone Joint Surg Br. 1969 Aug;51(3):529-39.
13. Muir H, Bullough P, Maroudas A. The distribution of collagen in human articular cartilage with some of its physiological implications. J Bone Joint Surg Br. 1970 Aug;52(3):554-63.
14. Stockwell RA. The interrelationship of cell density and cartilage thickness in mammalian articular cartilage. J Anat. 1971 Sep;109(Pt 3):411-21.
15. Magnussen RA, Dunn WR, Carey JL, Spindler KP. Treatment of focal articular cartilage defects in the knee. Clin Orthop. 2008;466(4):952-62.
16. Buckwalter JA. Articular cartilage: injuries and potential for healing. Journal of Orthopaedic & Sports Physical Therapy. 1998;28(4):192-202.
17. Beris AE, Lykissas MG, Papageorgiou CD, Georgoulis AD. Advances in articular cartilage repair. Injury. 2005;36(4):S14-23.
18. Fisher MB, Belkin NS, Milby AH, Henning EA, Bostrom M, Kim M, et al. Cartilage repair and subchondral bone remodeling in response to focal lesions in a mini-pig model: implications for tissue engineering. Tissue Engineering Part A. 2014;21(3-4):850-60.
19. Zhang L, Hu J, Athanasiou KA. The role of tissue engineering in articular cartilage repair and regeneration. Critical Reviews™ in Biomedical Engineering. 2009;37(1-2).
20. Jorgensen C, Noel D, Apparailly F, Sany J. Stem cells for repair of cartilage and bone: the next challenge in osteoarthritis and rheumatoid arthritis. Ann Rheum Dis. 2001 Apr;60(4):305-9.
21. Furukawa T, Eyre DR, Koide S, Glimcher MJ. Biochemical studies on repair cartilage resurfacing experimental defects in the rabbit knee. J Bone Joint Surg Am. 1980 Jan;62(1):79-89.
22. Gilbert JE. Current treatment options for the restoration of articular cartilage. Am J Knee Surg. 1998 Winter;11(1):42-6.
23. Johnstone B, Yoo JU. Autologous mesenchymal progenitor cells in articular cartilage repair. Clin Orthop. 1999;367:S156-62.
24. Brittberg M. Cartilage repair: on cartilaginous tissue engineering with the emphasis on chondrocyte transplantation. . 1996.
25. Bombardier C, Hawker G, Mosher D. Arthritis Alliance of Canada. The impact of arthritis in Canada: today and over the next. 2011;30.
26. Woolf AD, Pfleger B. Burden of major musculoskeletal conditions. Bull World Health Organ. 2003;81(9):646-56.

27. Bitton R. The economic burden of osteoarthritis. Am J Manag Care. 2009 Sep;15(8 Suppl):S230-5.
28. Steadman JR, Rodkey WG, Rodrigo JJ. Microfracture: surgical technique and rehabilitation to treat chondral defects. Clin Orthop. 2001;391:S362-9.
29. Knutsen G, Engebretsen L, Ludvigsen TC, Drogset JO, Grontvedt T, Solheim E, et al. Autologous chondrocyte implantation compared with microfracture in the knee. A randomized trial. J Bone Joint Surg Am. 2004 Mar;86-A(3):455-64.
30. Gudas R, Stankevičius E, Monastyreckienė E, Pranys D, Kalesinskas RJ. Osteochondral autologous transplantation versus microfracture for the treatment of articular cartilage defects in the knee joint in athletes. Knee Surgery, Sports Traumatology, Arthroscopy. 2006;14(9):834-42.
31. Brouwer RW, van Raaij TM, Bierma-Zeinstra S, Verhagen AP, Jakma TT, Verhaar JA. Osteotomy for treating knee osteoarthritis. The Cochrane Library. 2007.
32. Amstutz HC, Thomas BJ, Jinnah R, Kim W, Grogan T, Yale C. Treatment of primary osteoarthritis of the hip. A comparison of total joint and surface replacement arthroplasty. J Bone Joint Surg Am. 1984 Feb;66(2):228-41.
33. Katz MM, Hungerford DS, Krackow KA, Lennox DW. Results of total knee arthroplasty after failed proximal tibial osteotomy for osteoarthritis. J Bone Joint Surg Am. 1987 Feb;69(2):225-33.
34. Harrysson OL, Robertsson O, Nayfeh JF. Higher cumulative revision rate of knee arthroplasties in younger patients with osteoarthritis. Clin Orthop. 2004;421:162-8.
35. Nerem RM, Sambanis A. Tissue engineering: from biology to biological substitutes. Tissue Eng. 1995;1(1):3-13.
36. Kuo CK, Li WJ, Mauck RL, Tuan RS. Cartilage tissue engineering: its potential and uses. Curr Opin Rheumatol. 2006 Jan;18(1):64-73.
37. Gao J, Yao J, Caplan AI. Stem cells for tissue engineering of articular cartilage. Proc Inst Mech Eng Part H J Eng Med. 2007;221(5):441-50.
38. Kirchmajer DM, Gorkin III R. An overview of the suitability of hydrogel-forming polymers for extrusion-based 3D-printing. Journal of Materials Chemistry B. 2015;3(20):4105-17.
39. Fedorovich NE, Alblas J, de Wijn JR, Hennink WE, Verbout AJ, Dhert WJ. Hydrogels as extracellular matrices for skeletal tissue engineering: state-of-the-art and novel application in organ printing. Tissue Eng. 2007;13(8):1905-25.

40. Awad HA, Wickham MQ, Leddy HA, Gimble JM, Guilak F. Chondrogenic differentiation of adipose-derived adult stem cells in agarose, alginate, and gelatin scaffolds. Biomaterials. 2004;25(16):3211-22.
41. You F, Wu X, Zhu N, Lei M, Eames BF, Chen X. 3D Printing of porous cell-laden hydrogel constructs for potential applications in cartilage tissue engineering. ACS Biomaterials Science & Engineering. 2016;2(7):1200-10.
42. Nicodemus GD, Bryant SJ. Cell encapsulation in biodegradable hydrogels for tissue engineering applications. Tissue Engineering Part B: Reviews. 2008;14(2):149-65.
43. Yang S, Leong K, Du Z, Chua C. The design of scaffolds for use in tissue engineering. Part I. Traditional factors. Tissue Eng. 2001;7(6):679-89.
44. Bian L, Zhai DY, Zhang EC, Mauck RL, Burdick JA. Dynamic compressive loading enhances cartilage matrix synthesis and distribution and suppresses hypertrophy in hMSC-laden hyaluronic acid hydrogels. Tissue Engineering Part A. 2011;18(7-8):715-24.
45. Hwang NS, Kim MS, Sampattavanich S, Baek JH, Zhang Z, Elisseeff J. Effects of Three-Dimensional Culture and Growth Factors on the Chondrogenic Differentiation of Murine Embryonic Stem Cells. Stem Cells. 2006;24(2):284-91.
46. Iwasaki M, Nakata K, Nakahara H, Nakase T, Kimura T, Kimata K, et al. Transforming growth factor-beta 1 stimulates chondrogenesis and inhibits osteogenesis in high density culture of periosteum-derived cells. Endocrinology. 1993 Apr;132(4):1603-8.
47. Kim SE, Park JH, Cho YW, Chung H, Jeong SY, Lee EB, et al. Porous chitosan scaffold containing microspheres loaded with transforming growth factor-β1: implications for cartilage tissue engineering. J Controlled Release. 2003;91(3):365-74.
48. Gooch KJ, Blunk T, Courter D, Sieminski A, Bursac PM, Vunjak-Novakovic G, et al. IGF-I and mechanical environment interact to modulate engineered cartilage development. Biochem Biophys Res Commun. 2001;286(5):909-15.
49. Veilleux N, Spector M. Effects of FGF-2 and IGF-1 on adult canine articular chondrocytes in type II collagen–glycosaminoglycan scaffolds in vitro. Osteoarthritis and cartilage. 2005;13(4):278-86.
50. Fujisato T, Sajiki T, Liu Q, Ikada Y. Effect of basic fibroblast growth factor on cartilage regeneration in chondrocyte-seeded collagen sponge scaffold. Biomaterials. 1996;17(2):155-62.

51. Hicks DL, Sage AB, Shelton E, Schumacher BL, Sah RL, Watson D. Effect of bone morphogenetic proteins 2 and 7 on septal chondrocytes in alginate. Otolaryngology—Head and Neck Surgery. 2007;136(3):373-9.
52. Kaps C, Bramlage C, Smolian H, Haisch A, Ungethüm U, Burmester G, et al. Bone morphogenetic proteins promote cartilage differentiation and protect engineered artificial cartilage from fibroblast invasion and destruction. Arthritis & Rheumatology. 2002;46(1):149-62.
53. Mason JM, Breitbart AS, Barcia M, Porti D, Pergolizzi RG, Grande DA. Cartilage and bone regeneration using gene-enhanced tissue engineering. Clin Orthop. 2000;379:S171-8.
54. Shim J, Jang K, Hahn SK, Park JY, Jung H, Oh K, et al. Three-dimensional bioprinting of multilayered constructs containing human mesenchymal stromal cells for osteochondral tissue regeneration in the rabbit knee joint. Biofabrication. 2016;8(1):014102.
55. Lee C, Grodzinsky A, Spector M. Biosynthetic response of passaged chondrocytes in a type II collagen scaffold to mechanical compression. Journal of Biomedical Materials Research Part A. 2003;64(3):560-9.
56. Ng KW, Mauck RL, Statman LY, Lin EY, Ateshian GA, Hung CT. Dynamic deformational loading results in selective application of mechanical stimulation in a layered, tissue-engineered cartilage construct. Biorheology. 2006;43(3, 4):497-507.
57. Hunter CJ, Mouw JK, Levenston ME. Dynamic compression of chondrocyte-seeded fibrin gels: effects on matrix accumulation and mechanical stiffness. Osteoarthritis and Cartilage. 2004;12(2):117-30.
58. Di Bella C, Fosang A, Donati DM, Wallace GG, Choong PF. 3D bioprinting of cartilage for orthopedic surgeons: reading between the lines. Frontiers in surgery. 2015;2:39.
59. Visser J, Peters B, Burger TJ, Boomstra J, Dhert WJ, Melchels FP, et al. Biofabrication of multi-material anatomically shaped tissue constructs. Biofabrication. 2013;5(3):035007.
60. Lee W, Lee V, Polio S, Keegan P, Lee J, Fischer K, et al. On-demand three-dimensional freeform fabrication of multi-layered hydrogel scaffold with fluidic channels. Biotechnol Bioeng. 2010;105(6):1178.
61. Schuurman W, Levett PA, Pot MW, van Weeren PR, Dhert WJ, Hutmacher DW, et al. Gelatin-methacrylamide hydrogels as potential biomaterials for fabrication of tissue-engineered cartilage constructs. Macromolecular bioscience. 2013;13(5):551-61.

62. Cui X, Breitenkamp K, Lotz M, D'Lima D. Synergistic action of fibroblast growth factor-2 and transforming growth factor-beta1 enhances bioprinted human neocartilage formation. Biotechnol Bioeng. 2012;109(9):2357-68.
63. Cohen DL, Malone E, Lipson H, Bonassar LJ. Direct freeform fabrication of seeded hydrogels in arbitrary geometries. Tissue Eng. 2006;12(5):1325-35.
64. Billiet T, Vandenhaute M, Schelfhout J, Van Vlierberghe S, Dubruel P. A review of trends and limitations in hydrogel-rapid prototyping for tissue engineering. Biomaterials. 2012;33(26):6020-41.
65. Malda J, Visser J, Melchels FP, Jüngst T, Hennink WE, Dhert WJ, et al. 25th anniversary article: engineering hydrogels for biofabrication. Adv Mater. 2013;25(36):5011-28.
66. Jeon O, Powell C, Ahmed SM, Alsberg E. Biodegradable, photocrosslinked alginate hydrogels with independently tailorable physical properties and cell adhesivity. Tissue Engineering Part A. 2010;16(9):2915-25.
67. Spiller KL, Maher SA, Lowman AM. Hydrogels for the repair of articular cartilage defects. Tissue engineering part B: reviews. 2011;17(4):281-99.
68. Mansour JM. Biomechanics of cartilage. Kinesiology: the mechanics and pathomechanics of human movement. 2003:66-79.
69. Little CJ, Bawolin NK, Chen X. Mechanical properties of natural cartilage and tissue-engineered constructs. Tissue Engineering Part B: Reviews. 2011;17(4):213-27.
70. Izadifar Z, Chang T, Kulyk W, Chen X, Eames BF. Analyzing biological performance of 3D-printed, cell-impregnated hybrid constructs for cartilage tissue engineering. Tissue Engineering Part C: Methods. 2015;22(3):173-88.
71. You F, Wu X, Chen X. 3D printing of porous alginate/gelatin hydrogel scaffolds and their mechanical property characterization. International Journal of Polymeric Materials and Polymeric Biomaterials. 2017;66(6):299-306.
72. Markstedt K, Mantas A, Tournier I, Martínez Ávila H, Hägg D, Gatenholm P. 3D bioprinting human chondrocytes with nanocellulose–alginate bioink for cartilage tissue engineering applications. Biomacromolecules. 2015;16(5):1489-96.
73. Visser J, Melchels FP, Jeon JE, Van Bussel EM, Kimpton LS, Byrne HM, et al. Reinforcement of hydrogels using three-dimensionally printed microfibres. Nature communications. 2015;6.

74. Bertassoni LE, Cardoso JC, Manoharan V, Cristino AL, Bhise NS, Araujo WA, et al. Direct-write bioprinting of cell-laden methacrylated gelatin hydrogels. Biofabrication. 2014;6(2):024105.
75. Demarteau O, Pillet L, Inaebnit A, Borens O, Quinn T. Biomechanical characterization and in vitro mechanical injury of elderly human femoral head cartilage: comparison to adult bovine humeral head cartilage. Osteoarthritis and cartilage. 2006;14(6):589-96.
76. Barker MK, Seedhom BB. The relationship of the compressive modulus of articular cartilage with its deformation response to cyclic loading: does cartilage optimize its modulus so as to minimize the strains arising in it due to the prevalent loading regime? Rheumatology (Oxford). 2001 Mar;40(3):274-84.
77. Schinagl RM, Gurskis D, Chen AC, Sah RL. Depth-dependent confined compression modulus of full-thickness bovine articular cartilage. Journal of Orthopaedic Research. 1997;15(4):499-506.
78. Athanasiou KA, Agarwal A, Dzida F. Comparative study of the intrinsic mechanical properties of the human acetabular and femoral head cartilage. Journal of Orthopaedic Research. 1994;12(3):340-9.
79. Abbadessa A, Blokzijl M, Mouser V, Marica P, Malda J, Hennink W, et al. A thermo-responsive and photo-polymerizable chondroitin sulfate-based hydrogel for 3d printing applications. Carbohydr Polym. 2016;149:163-74.
80. Pescosolido L, Schuurman W, Malda J, Matricardi P, Alhaique F, Coviello T, et al. Hyaluronic acid and dextran-based semi-IPN hydrogels as biomaterials for bioprinting. Biomacromolecules. 2011;12(5):1831-8.
81. Akizuki S, Mow VC, Müller F, Pita JC, Howell DS, Manicourt DH. Tensile properties of human knee joint cartilage: I. Influence of ionic conditions, weight bearing, and fibrillation on the tensile modulus. Journal of Orthopaedic Research. 1986;4(4):379-92.
82. Elliott DM, Guilak F, Parker Vail T, Wang JY, Setton LA. Tensile properties of articular cartilage are altered by meniscectomy in a canine model of osteoarthritis. Journal of Orthopaedic Research. 1999;17(4):503-8.
83. Magnussen RA, Guilak F, Vail TP. Cartilage degeneration in post-collapse cases of osteonecrosis of the human femoral head: Altered mechanical properties in tension, compression, and shear. Journal of orthopaedic research. 2005;23(3):576-83.

84. Kesti M, Eberhardt C, Pagliccia G, Kenkel D, Grande D, Boss A, et al. Bioprinting complex cartilaginous structures with clinically compliant biomaterials. Advanced Functional Materials. 2015;25(48):7406-17.
85. Zhu W, Mow VC, Koob TJ, Eyre DR. Viscoelastic shear properties of articular cartilage and the effects of glycosidase treatments. Journal of Orthopaedic Research. 1993;11(6):771-81.
86. Athanasiou KA, Rosenwasser M, Buckwalter J, Malinin T, Mow V. Interspecies comparisons of in situ intrinsic mechanical properties of distal femoral cartilage. Journal of Orthopaedic Research. 1991;9(3):330-40.
87. Radin EL, Rose RM. Role of subchondral bone in the initiation and progression of cartilage damage. Clin Orthop. 1986;213:34-40.
88. Havelka S, Horn V, Spohrova D, Valouch P. The calcified-noncalcified cartilage interface: the tidemark. Acta Biol Hung. 1984;35(2-4):271-9.
89. Norrdin R, Kawcak C, Capwell B, McIlwraith C. Calcified cartilage morphometry and its relation to subchondral bone remodeling in equine arthrosis. Bone. 1999;24(2):109-14.
90. Boskey AL. Mineral-matrix interactions in bone and cartilage. Clin Orthop. 1992;281:244-74.
91. Khanarian NT, Boushell MK, Spalazzi JP, Pleshko N, Boskey AL, Lu HH. FTIR-I Compositional Mapping of the Cartilage-to-Bone Interface as a Function of Tissue Region and Age. Journal of Bone and Mineral Research. 2014;29(12):2643-52.
92. Chung C, Burdick JA. Engineering cartilage tissue. Adv Drug Deliv Rev. 2008;60(2):243-62.
93. Kandel R, Hurtig M, Grynpas M. Characterization of the mineral in calcified articular cartilagenous tissue formed in vitro. Tissue Eng. 1999;5(1):25-34.
94. Allan K, Pilliar R, Wang J, Grynpas M, Kandel R. Formation of biphasic constructs containing cartilage with a calcified zone interface. Tissue Eng. 2007;13(1):167-77.

Chapter 2: Application of Extrusion-based Hydrogel Bioprinting for Cartilage Tissue Engineering

This chapter has been published as You, F., Eames, B.F., Chen, X. (2017). Application of Extrusion-based Hydrogel Bioprinting for Cartilage Tissue Engineering. International Journal of Molecular Science, 18(7), 1597. According to the Copyright Agreement, "the authors retain the right to include the journal article, in full or in part, in a thesis or dissertation".

2.1 Abstract

Extrusion-based bioprinting (EBB) is a rapidly developing technique that has made substantial progress in the fabrication of constructs for cartilage tissue engineering (CTE) over the past decade. With this technique, cell-laden hydrogels or bio-inks have been extruded onto printing stages, layer-by-layer, to form three-dimensional (3D) constructs with varying sizes, shapes, and resolutions. This paper reviews the cell sources and hydrogels that can be used for bio-ink formulations in CTE application. Also, this paper discusses the important properties of bio-inks to be applied in the EBB technique, including biocompatibility, printability as well as mechanical properties. The printability of a bio-ink is associated with the formation of first layer, ink rheological properties, and crosslinking mechanisms. Further, this paper discusses two bioprinting approaches to build up cartilage constructs, i.e., self-supporting hydrogel bioprinting and hybrid bioprinting, along with their applications in fabricating chondral, osteochondral, and zonally-organized cartilage regenerative constructs. Last, current limitations and future opportunities of EBB in printing cartilage regenerative constructs are reviewed.

Keywords: cartilage tissue engineering; extrusion-based bioprinting; hydrogels; bio-inks; self-supporting hydrogel bioprinting; hybrid bioprinting

2.2 Bioprinting Is Promising Technique to Process Hydrogel for Fabrication of Cartilage Constructs in CTE

Bioprinting of personalized complex tissue grafts is promising for overcoming the current challenges of cartilage tissue engineering (CTE). Cartilage is a highly hydrated and specialized tissue to provide a low-friction, wear-resistant, and load-bearing surface in diarthrodial joints for

efficient joint movement (1). Unfortunately, the structure and function of the cartilage are frequently disrupted or lost with trauma or aging; and there is no sufficient heal response for regeneration as cartilage shows little self-repair tendency. These defects or injuries last for years and eventually lead to arthritis (2). To address this problem, tissue engineering (TE) approaches aiming to engineer constructs to regenerate cartilage defects are under active investigation. Ideally, the tissue-engineered constructs for CTE should fill cartilage defects, resemble extracellular matrix (ECM), hold cells in place, and retain a space for the growing tissue (3, 4). To this end, hydrogel has been illustrated promising due to the fact that it closely mimics native ECM and thus providing a 3D culture microenvironment favorable for encapsulated cells to retain the rounded morphology and chondrogenic phenotype (5-7). Furthermore, hydrogels allow for achieving high cell seeding density and homogenous cell distribution throughout scaffold (6, 8-14), and transmitting external stimuli to embedded cells so as to direct growth and formation of the regenerating cartilage (15, 16). Several disadvantages of hydrogels, however, have also been identified, such as weak mechanical strength and stability. It is also hard to handle and process hydrogels into cartilage regenerative constructs with desired internal structure and external shape. To overcome these problems, the bioprinting technique has been rapidly developing and gaining interest for fabrication of customized cartilage constructs.

Although some reviews on bioprinting of tissues and organs are available, investigation into the EBB cartilage constructs from bio-inks has not been well-documented. This article presents a brief review of the application of EBB for fabricating cartilage constructs from bio-inks, covering its working principles, applicable cell sources and materials, printability, printed cartilage constructs, as well as future perspectives of bioprinting cartilage.

2.3 EBB for CTE

2.3.1 EBB

Rapid prototyping (RP), also known as solid freeform fabrication, refer to a series of techniques that manufacture objects through sequential delivery of energy and/or material in a layer-by-layer manner per computer aided design (CAD) data. The external shape and internal architecture of the scaffold can be defined by either 3D computer models or clinical imaging data (e.g. the defect area of the patient can be scanned by magnetic resonance imaging or computed

tomography) (17, 18). Once the external/internal geometric information is determined, the RP system is programed to fabricate the scaffold as designed.

RP techniques can be divided into three classifications based on their working principles: (i) laser-based; (ii) extrusion-based, and; (iii) printer-based systems. Among various RP techniques, extrusion-based bioprinting (EBB) stands out for its unique advantages. EBB allows for production of 3D tissue constructs from bio-inks by a layer-by-layer deposition process in a designed way (19). EBB also allows for higher cell seeding density, higher printing speed to facilitate scalability, and relatively less process-induced cell damage (20). EBB can print continuous cylindrical filaments from almost all types of bio-inks to high cell density aggregates of a wide range of viscosities. Once the bio-ink is printed, it can be crosslinked by ionic, photo, and/or thermal crosslinking mechanisms (Figure 2.1). Given the complexity of biological tissue, multiple bio-inks are often used to fabricate a tissue construct, which is also achievable by using EBB with multiple printing heads.

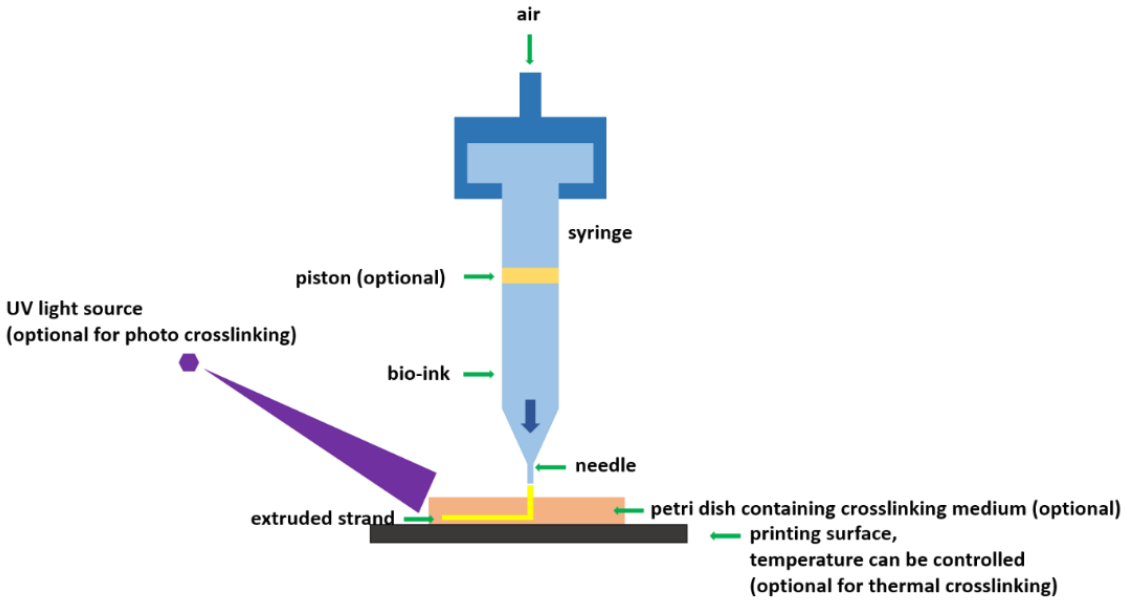

Figure 2.1 Schematic of extrusion-based bioprinting using various crosslinking mechanisms.

2.3.2 Bio-inks

Hydrogel precursors and living cells are two important components of bio-ink formulations. Cell sources and hydrogel types employed for encapsulating chondrogenic cells are reviewed below.

2.3.2.1 Applicable Cell Sources

The choice of cells is a central problem to any modality of tissue engineering. For cartilage bioprinting, several factors need to be taken into consideration when choosing suitable cell sources: i) cells must be robust enough to survive any shear stress and pressure during the printing process; ii) cells must proliferate well; and iii) cells must possess biosynthesis levels (e.g. of proteoglycans, collagen type II) comparable with cartilage cells in vivo so they can maintain their biological functions (21). So far, the use of chondrocytes over stem cells for cartilage bioprinting is predominant (Table 2.1).

Consistent with the distinct zonal structure of native articular cartilage (22), chondrocytes from different zones show different characteristics of biosynthesis levels. Superficial zone has a dense network of collagen fibers that are parallel to the articular surface, while collagen fibers are randomly arranged in the middle region and perpendicular to the subchondral bone in the deep zone (23). The content of the other important component in cartilage, proteoglycan, is lowest in the superficial zone and increases through the middle and deep zones (24). Limited numbers of chondrocytes in articular cartilage make it necessary to expand chondrocytes before use. The monolayer expansion process usually leads to chondrocyte dedifferentiation with decreased GAG synthesis and Collagen type II expression (25, 26). Most studies typically use chondrocyte mixtures from full-thickness cartilage (27-29) to obtain higher cell populations. Recently, more attention has been focused on employing zonal chondrocytes to achieve different purposes. For example, deep zone chondrocytes are utilized to engineer a functional osteochondral interface by coculturing with calcium phosphate (30). Chondrocytes isolated from the superficial layer exhibit increased proteoglycan 4 expression, and thus superficial chondrocytes are promising to be used as the cell source for engineering articular surface (1). Articular chondrocytes provide researchers with a unique opportunity to replicate the native zonal structure by embedding and culturing zonal chondrocytes in different layers of gels, although it is still elusive if this is a promising approach or an overcomplicated strategy (31).

Donor site morbidity during harvesting of joint cartilage further limits the use of articular chondrocytes (32). Therefore, nasoseptal chondrocytes, as another autologous chondrocyte source, is also explored for bioprinting cartilage constructs (33, 34). Another promising cell type is the multipotent mesenchymal stem cell (MSC), which can be derived from multiple tissues, such as bone marrow, adipose tissues, synovium, periosteum, and muscle. These stem cells can be differentiated to undergo chondrogenesis with the supplement of specific growth factors (35, 36), such as transforming growth factor beta family (37) and therefore they have been explored to be used in CTE (38-44).

Table 2.1 Cell sources that have been used in CTE or cartilage bioprinting.

Cell Source	**Features**	**References for Application in CTE**	**References for Application in Bioprinting for CTE**
	Chondrocytes		
Articular	ease of induction, make it easy to replicate native zonal cartilage by using zonal chondrocytes. Invasive harvesting procedure, donor site morbidity, low cell yields, low bioactivity, tend to dedifferentiate during expansion.	(45–51)	(48–51)
Auricular	elastic cartilage, Faster cell proliferation rates than articular chondrocytes, produce more biochemically and histologically similar cartilage than articular chondrocytes when implanted in vivo.	(52–54)	-
Nasoseptal	hyaline cartilage, proliferate faster and less tendency of dedifferentiation than articular chondrocytes when culturing monolayer, capable of producing a cartilage ECM with a high GAG accumulation and collagen II/I.	(33,34,55,56)	(33,34)
	MSC		
Bone marrow	high differentiation potentials and less morbidity during harvesting, chondrogenesis under appropriate culture conditions, involving the supplementation of growth factors such as TGF-β, FGF-2.	(38,57–59)	(58)
Adipose	differentiating into chondrocytes in the presence of TGF-β, ascorbate, and dexamethasone, lower chondrogenesis potential than stem cells from other sources, lower deposition of cartilage ECM than other cell types.	(39,60,61)	-
Muscle	differentiation into various lineages, induction to chondrocytes with the addition of BMP-2, improved healing of cartilage defect with an efficacy equivalent to chondrocytes.	(40,41,62–64)	-
Synovium	greater chondrogenic potential than stem cells from other sources, comparable biosynthesis level with articular chondrocytes in terms of type II collagen, aggrecan.	(62,65–67)	-
Periosteum	good accessibility, proliferate faster that stem cells from other sources, and capability to differentiate into multiple mesenchymal lineages, including bone and cartilage.	(42,68)	-

2.3.2.2 Applicable Hydrogel-forming Polymers for Formulating Bio-inks

Hydrogel cross-linking mechanisms are generally categorized into ‘physical’ crosslinking and ‘chemical’ crosslinking. Physical (thermal (69, 70) ionic (71) and photo (72)) crosslinking include reversible entangled chains, hydrogen bonding, etc. while chemical (enzyme (73) and pH (74)) crosslinking are permanent junctions formed by irreversible, covalent bonds. Hydrogel can be classified into two groups based on their sources: natural hydrogels (e.g. agarose, alginate, cellulose, gelatin, gellan gum, hyaluronic acid, collagen, fibrin) and synthetic hydrogels (e.g. Pluronic® F127, PEG and PVA). Hydrogels that are biocompatible for encapsulating stem cells or chondrogenic cells for CTE are summarized and reviewed (Table 2.2). There are pros and cons to each type of these hydrogels and researchers attempted to modify these polymers to improve their properties like bioactivity, mechanical properties, and printability.

Table 2.2 Toolkit of Bio-ink formulation.

	Crosslinking	Advantages	Disadvantages	Encapsulated Cells	References in Other Techniques	References in Bioprinting
Agarose	thermal crosslinking at 26-30 °C, agarose solidifies when temperature is lower than the thermal crosslinking temperature	simple and non-toxic crosslinking process, good mechanical properties, and stability of printed construct	not degradable, poor cell adhesion, impaired cell viability due to high temperature to dissolve agarose	bone marrow stem cells(BMSC), adipose stem Cells (ASC)	(75–77)	(78)
Alginate	ionic crosslinking with divalent cations	rapid gelation, high printability, biocompatible, good stability, and integrality of printed construct	poor cell adhesion, this disadvantage can be overcome by modifying alginate with RGD, collagen type I or oxygenation	BMSC, ASC, chondrocytes	(79–81)	(82)
Methylcellulose	thermal crosslinking below 37 °C, silanized hydroxypropyl methylcellulose can be synthesized to be crosslinked by changing pH	good printability, biocompatibility	partially degrade when culturing in cell culture media and therefore not suitable for long-term culturing	chondrocytes	(83–85)	(35)
Chitosan	ionic or covalent crosslinking	biocompatibility, antibacterial	slow gelation rate and poor mechanical properties without modification	BMSC	(86–88)	(89)
Gellan gum	thermal crosslinking or ionic crosslinking with divalent cation	biocompatible, high printability	poor cellular adhesion	ASC, nasal chondrocytes	(90–92)	(93,94)
Hyaluronic acid	ionic or covalent crosslinking, functionalized with	promote cell proliferation, fast gelation, high	fast degradation, poor mechanical	BMSC, chondrocytes,fibroblasts	(95–98)	(99)

	methacrylate to be photocrosslinkable	printability with suitable modification, have lubricating properties	properties and stability without modification			
Gelatin	thermal crosslinking, photocrosslinkable polymers can be obtained by functionalization withmethacrylamide side groups to make it stable at 37 °C	biocompatibility, high cell adhesion support cell viability and proliferation	poor mechanical properties and stability, low printability	BMSC, fibroblasts, chondrocytes	(100–102)	(69,72,103)
Collagen	pH crosslinking (7-7.4) at 37 °C or thermal crosslinking	biocompatibility, high cell adhesion, promote cell proliferation and serve as a signal transducer, high printability	low gelation rate, poor mechanical properties and stability	BMSC, fibroblasts, chondrocytes	(104–106)	(107,108)
Fibrin	enzymatic crosslinking, gels when combining fibrinogen, Ca^{2+} and thrombin at room temperature	biocompatibility, high cell adhesion, rapid gelation	limited printability and poor mechanical properties	BMSC, chondrocytes	(109)	(110–112)
Matrigel	irreversible thermal crosslinking at 24-37 °C	biocompatibility, support cell viability, differentiation, printability	slow gelation and poor stability	BMSC, chondrocytes	(113–114)	(115)
Pluronic® F127	thermal crosslinking	biocompatibility, high printability, support cell viability	Weak stability and mechanical properties, fast degradation, slow gelation	BMSC, fibroblasts	(74,116–117)	(118)
Poly(ethylene glycol)	radiation crosslinking or free radical polymerization	biocompatibility, support cell viability, easily modified with various functional groups	poor cellular adhesion, low cell proliferation rate	BMSC, chondrocytes	(119–120)	(121)

2.4 Important Properties of Bio-inks

2.4.1 Biocompatibility

Biocompatibility must be considered before the application of any material for tissue engineering and regenerative medicine. Biocompatibility refers to the ability of a biomaterial to perform its desired function without eliciting any undesirable biological effects (122). For the purposes of this review, a bioprinted hydrogel must be cytocompatible, nonimmunogenic and have nontoxic byproducts of degradation without eliciting any detrimental effects from the time of bioprinting to in vitro maturation and in vivo implantation (123). The main factor that could influence the biocompatibility given the same material lays in the bioprinting process, which means the whole printing process needs to be cytocompatible. In most cases, bio-inks are stored as liquids in a reservoir prior to being dispensed onto the printing surface and a crosslinking process is followed to solidify the bio-inks. The cytompatibility of this process is characterized by the cell viability test using live/dead staining (124). To elevate the cell viability, bio-inks are designed to minimize the stress-induced damage to cells due to the sensitivity of cells encapsulated in the bio-inks. In the cases of printing mechanisms involving the use of heating or pressure, the heating temperatures are kept within the range favoring cell survival and the pressure is maintained as low as possible.

2.4.2 Printability

Printability of a bio-ink, once printed in a layer fashion, is its ability to form and maintain a 3D construct with structural fidelity and integrity. Printability is considered to be associated with surface tension, viscosity, rheological properties, and crosslinking mechanisms. Standardized tests to quantify the printability still do not exist, and an optical examination method is usually adopted to do a geometry comparison (e.g. pore size, fiber diameter) between generated constructs and CAD data (125, 126).

First-layer formation

The printing and formation of the first layer of bio-inks play an important role for fabricating the whole construct, which can be largely determined by the contact angle between the printed strand and the receiving surface. Contact angle, also known as wetting angle, is measured at where a liquid meets a solid surface. It quantifies the wettability of a solid surface

by a liquid. A relatively large contact angle between dispensed bio-inks and the substrate help to maintain the vertical dimension of printed bio-inks and avoid the flattening of the printed hydrogel precursor solution. The interaction between printed bio-inks and substrate is crucial, since suitable interaction helps to anchor the whole bioprinted construct on the printing surface and avoids possible deformation and undesired movement during the layer-by-layer bio-inks deposition process. Unfortunately, most receiving surfaces such as glass or plastic have poor contact angles with bio-inks owing to the materials properties and it is difficult to establish any interaction between receiving surface and dispensed bio-inks. These issues could be addressed by either printing hydrogels in a hydrophobic high-density fluid, such as perfluorotributylamine (78), or coating a thin layer of chemicals, such as 3-(trimethoxysilyl) propyl methacrylate, on the printing surface (127) to enhance their hydrophobicity. Polyethylenimine was used successfully in our group to pre-treat the culture plates to establish an electrostatic interaction between printed cell-laden hydrogel and the receiving surface (128).

Viscosity

Viscosity describes the internal resistance of a fluid to flow upon application of stress. The viscosity of a polymer solution is determined by its concentration, molecular weight, and temperature. Higher polymer concentration and molecular weight are associated with higher viscosity. Typically, sufficient viscosity of bio-inks leads to good printability, since it can help the bio-inks to overcome the surface-tension-driven droplet formation and be drawn to form continuous strands. Sufficient viscosity will also help the dispensed strands to maintain the cylinder shape and keep adjacent strands from merging together, which also explains why thermoplastic polymers are usually printed with higher accuracy and resolution than hydrogels. However, cells thrive best in an aqueous environment, in which their matrix deposition is not limited by the dense crosslinked polymer network (129). Bio-inks with high viscosity require high pressure to expel them out of the dispensing needle; in this case, the embedded cells are exposed to a high shear force, which may impair cell viability (130).

The viscosity of a bio-ink solution is mainly determined by the polymer concentration and molecular weight. Given that bio-inks with high concentrations may not be favorable for cell proliferation/migration and ECM formation (129), it is reasonable to choose low concentrations

of high molecular weight polymers for better printability in bioprinting. This also explains the success of natural polymers in the bioprinting area.

Shear Thinning

Shear thinning is another desirable feature for bio-inks that will help to improve the printability, and it refers to the fact that viscosity decreases as shear rate increases (131). Shear thinning behaviour is more obvious in polymer solutions with higher concentrations. When shear thinning bio-inks are exposed to high shear rates inside a nozzle during bioprinting, a decreased viscosity or shear stress will be present, which favors the survival of embedded cells. Meanwhile, a sudden decrease of shear rates upon deposition causes a sharp increase in viscosity, resulting in a high printing fidelity.

Crosslinking mechanisms

The printability is also influenced by how easily and efficiently materials can be crosslinked. EBB usually requires printing a cell-laden polymer solution followed by initiating gelation immediately after extrusion. The cell-laden polymer solution must be either prepared quite viscous or crosslinked rapidly after dispensing onto the printing surface to achieve good printability and shape fidelity. However, high viscosity is not ideal for its application in tissue engineering and impedes cells survival and proliferation (132, 133). Therefore, a relatively rapid crosslinking process is usually desirable in the printing process. Currently, ionic, photo and thermal crosslinking are most commonly-used crosslinking mechanisms in bioprinting (Table 2.2).

2.4.3 Strategies to Strengthen Mechanical Properties of Engineered Cartilage Construct

Engineered cartilage should maintain sufficient mechanical properties after bioprinting to provide embedded cells with a stable environment for attachment, proliferation, and differentiation. Particularly for cartilage bioprinting in CTE, mechanical properties are crucial because the functions of cartilage mainly rely on their mechanical performance. Mechanical properties of hydrogel are intrinsically weak compared to cartilage (134). Strategies have been developed to strengthen the initial mechanical performance of engineered constructs.

Research has supplemented hydrogel with mineral particles (e.g. hydroxyapatite) to create composite hydrogels, by combining organic and inorganic phases to obtain desirable properties including the improvement of mechanical properties and enhancement of biological properties (135, 136). In CTE, the presence of calcium phosphate has been shown to promote chondrocyte hypertrophy and Collagen type X deposition and thus improve the regeneration of calcified cartilage (30, 137). Moreover, hydroxyapatite would be a good supplement in scaffolding materials in CTE to recruit endogenous cells in vivo to regenerate articular surface without cell transplantation (138).

A novel approach reinforced hydrogel constructs by incorporating printed polycaprolactone (PCL) scaffolds. Hydrogel precursors were poured and perfused into the printed porous PCL scaffold and crosslinked. In this way, the stiffness of the resulting constructs could be tailored to that of native cartilage by reinforcement with high-porosity PCL scaffolds (139). Fabricating cartilage constructs by alternating printing injected-printed hydrogels and electrospun thermoplastic polymer fibers is also feasible (108). It would be a promising technique if electrospun thermoplastic polymer fibers can be incorporated into EBB to print constructs with native mechanical characteristics.

A higher mechanical strength can also be achieved by blending multiple polymers and varying the molar ratio of bio-ink components. From instance, nanocellulose and alginate composite bio-ink was synthesized and printed to fabricate chondrocyte-laden constructs. Increasing the alginate fraction in bio-ink formula would lead to an increase in compressive modulus of printed constructs (34).

Making use of the crosslinking mechanism is also an efficient way to enhance the mechanical properties of the printed constructs. For example, a three-step method was used to crosslink alginate hydrogel for improved elastic stiffness; and the three steps are the primary calcium ionic cross-linking to increase the initial viscosity of alginate, secondary calcium ionic crosslinking to solidify the printed structure, and tertiary barium ionic crosslinking to strengthen elastic stiffness (140).

Another effective way to enhance the mechanical properties is the use of hybrid bioprinting to co-deposit hydrogels and thermoplastic polymers alternately. Cell-laden hydrogels are supported by printed thermoplastic polymers and in this way, these hybrid constructs possess mechanical characteristics that was mainly provided by the printed thermoplastic polymer frame,

which is significantly higher than the hydrogel-only constructs (141). Meanwhile, by designing and changing the architecture of the thermoplastic polymer framework parameters, including molecular weight of polymer, strand size, strand spacing, and strand orientation, the mechanical properties of the construct can be tuned (142). A covalent bonding based on methacrylate groups between thermoplastic polymer methacrylated poly(hydroxymethylglycolide-co-e-caprolactone)/PCL (pMHMGCL/PCL) and gelatin methacrylamide (GelMA) hydrogel can also be established to improve binding in the interface of two materials and further elevate the mechanical performance of the engineered construct (29).

If a scaffold is designed to initially promote engineered tissue formation in vitro prior to implantation *in vivo*, then they are not required to exactly match the mechanical properties of natural cartilage at the initial stage. Thereby many hydrogel-based cartilage bioprinting research still focus on formulating bio-inks to favor the synthesis of cartilaginous ECM instead of their initial mechanical strength with the hope that the ECM generated by the cells *in vitro* provides sufficient mechanical properties upon implantation *in vivo*.

2.5 Cartilage Constructs Bioprinting

Current cartilage constructs are mainly printed based on two approaches: i) direct printing of cartilage constructs from bio-inks (called the self-supporting hydrogel bioprinting) and ii) alternating printing of bio-inks and thermoplastic-polymer network (called the hybrid bioprinting). The advantages of self-supporting hydrogel bioprinting rests on their mild and physiological crosslinking conditions and its relatively-simple process as compared to hybrid bioprinting. However, the self-supporting bioprinting requires a high level of printability of bio-inks and the printed hydrogel constructs typically have week mechanical properties (128). In contrast, the thermoplastic-polymer network printed in hybrid bioprinting can offer a sufficient mechanical support to the subsequently dispensed hydrogel strands for being crosslinked. Therefore, hybrid bioprinting can print a broader range of bio-inks than self-supporting hydrogel bioprinting. Nevertheless, the high temperature for melting thermoplastic polymers in hybrid bioprinting may impair cell viability. Also, hybrid bioprinting may introduce extra printing errors due to its complex process and heating-related stresses within printed constructs (143).

2.5.1 Self-supporting Hydrogel Bioprinting

Self-supporting hydrogel bioprinting approaches form cartilage constructs for CTE application by printing stem cell- or chondrocyte-laden natural and synthetic hydrogels (144). Chondrocytes and stem cells embedded within alginate hydrogels has been demonstrated to be viable and metabolically active (145). Rapid crosslinking makes alginate a commonly-used component in bio-inks to print cartilage constructs. A highly printable bio-ink consisted of alginate and nanocellulose was formulated. The printed constructs supported the culture of human nasoseptal chondrocytes and had the potential to be printed into more complex shapes (34). Alginate has also been sulfated to bind growth factors such as fibroblast growth factor (FGF), transforming growth factor (TGF) without losing its printability (146, 147). A chondrocyte-laden construct consisting of sulfated alginate and nanocellulose still provided good printability and collagen type II deposition (148, 149). Lack of sufficient cell adhesion sites still limits the application of alginate in CTE. By incorporating BioCartilage (cartilage extracellular matrix particles) and gellan in alginate, the bioactivity and printability of the bio-ink was significantly improved and the resulting patient-specific cartilage grafts showed good mechanical property and biological properties (27).

Hyaluronic acid (HA), as an essential component of cartilage ECM, can mediate cellular signaling, wound repair, and ECM organization due to its structural and biological properties (150). More recently, HA is increasingly explored as a "building block" in various bio-inks formulations for cartilage bioprinting in CTE because of its viscoelastic and bioactive properties (151). Nevertheless, one major drawback of unmodified HA for cartilage bioprinting is the poor stability owing to its water solubility. To address the problem of the poor stability of printed HA, the photo-crosslinkable dextran derivate or acrylated Pluronic was added to improve mechanical properties and the printability of the material. Moreover, embedded chondrocytes demonstrated good compatibility with this bio-inks formulation (152, 153).

Although gelatin gel has been shown to support chondrocyte viability and differentiation, its low viscosity and de-crosslinking at 37 ℃ make it hard to print (154). Therefore, gelatin is usually modified to become photo-crosslinkable by a straightforward reaction with an acrylate or methacrylate agent (155, 156). For example, a study (102) explored the functionalization, preparation and use of cell-laden gelatin methacryloyl (GelMA)-based hydrogels as modular tissue culture platforms. For improved printability of gelatin, HA was also incorporated in

GelMA and printed chondrocyte-laden constructs supported the viability of embedded chondrocytes and cartilaginous tissue formation (50).

Acrylation is also commonly used with synthetic hydrogels to facilitate cartilage bioprinting. An example is printing poly (ethylene glycol) dimethacrylate (PEGDMA) together with human chondrocytes to repair defects with osteochondral plugs through a layer-by-layer manner. The printed construct showed a higher mechanical property of 395.73 kPa than most printed natural hydrogels. This study demonstrated that hydrogel bioprinting is a feasible approach of producing cartilage constructs with anatomic characteristics to accurate targeted locations. The embedded human chondrocyte viability was 89% and showed an elevated glycosaminoglycan (GAG) content. Also, printed cartilage constructs firmly attached to the surrounding tissue and showed even greater proteoglycan deposition at the interface of implant and native cartilage (48).

Improving the integrity between the engineered cartilage and subchondral bone remains a challenge. In this regard, a self-supporting hydrogel construct was printed onto the printed bone paste (consisting of demineralized bone matrix and powdered gelatin), to mimic the cartilage and subchondral bone respectively (157). Heterogeneous cell-laden high-viscosity alginate hydrogel constructs were printed with distinct parts for human chondrocytes and osteogenic progenitors for potential use as osteochondral grafts. Embedded cells stayed in their compartment of the printed scaffold for the whole culture period and viability remained high throughout the printing and culture process and cartilage and bone ECM formation were observed both *in vitro* and *in vivo* (158). The reported cartilage constructs fabricated by self-supporting hydrogel bioprinting are summarized in Table 2.3.

To sum up, self-supporting hydrogel bioprinting of cartilage constructs can be processed under cytocompatible conditions and printed constructs are generally shown to support cartilage ECM biosynthesis. Current research emphasis is focused on formulating bio-inks to achieve high printability and improving the mechanical performance of printed constructs. The relatively weak mechanical properties of printed hydrogel-based cartilage constructs limit its application to regenerating focal cartilage defects, where most of exerted force are born by its surrounding tissue. To overcome these issues, hybrid cartilage bioprinting by alternating printing of bio-inks and thermoplastic polymers fibers (hybrid bioprinting) has been brought forwarded.

Table 2.3 Overview of Publications on the self-supporting hydrogel bioprinting of (osteo)chondral and zonally organized cartilage regenerative constructs.

Material (s)	Cell Type (s)	Mechanical Properties	Crosslinking Mechanism (s)	Outcomes	Reference
Hydrogel Bioprinting of Chondral Constructs					
Alginate	ATDC5 chondrogenic cell line and embryonic chick chondrocytes	Unconfined compressive modulus: 20~70 kPa (depending on the culture time and crosslinking densities)	Ionic	~85% cell viability, show cartilage ECM formation in constructs	(128)
Nanocellulose with alginate	Human nasoseptal chondrocytes	Unconfined compressive modulus: 75~250 kPa (depending on the ratio of two materials	Ionic	73~86% cell viability	(34)
Methacrylated chondroitin sulfate (CSMA) with a triblock copolymer poly (N-(2-hydroxypropyl)methacrylamide-mono/dilactate)	ATDC5 chondrogenic cell line	Unconfined compressive modulus: 7~60 kPa (depending on the degree of methacrylation)	Photo	~95% cell viability	(159)
GelMA with gellan gum	ATDC5 chondrogenic cell line	Unconfined compressive modulus: 18~59 kPa (depending on the concentration of gellan gum)	Ionic, photo and thermal	Approximately 50% cell viability in plotted gels due to the supraphysiological temperature of 40~50 °C.	(94,160)
GelMA with gellan gum	Equine articular chondrocytes	Unconfined compressive modulus: 2.7–186 kPa (depending on ratio and content of two components)	Ionic, photo and thermal	Support cartilage matrix production, higher gellan gum contents improves the printability but compromise cartilage ECM, and high total polymer concentrations hamper the distribution of ECM.	(94,160)
Fibroin and gelatin	Human mesenchymal stem cells, Human articular chondrocytes	Not reported	Enzymatic	84~90% cell viability of both cell types during 14 days of culture, supported cartilage ECM deposition and remodeling, minimize hypertrophic differentiation towards development and promote cartilage development.	(73)
Hydroxyethyl methacrylate derivatized dextran (Dex-HEMA) and hyaluronic acid (HA).	Equine articular chondrocytes	Ultimate compressive stress: 100~160 kPa (depending	Photo	Cell viabilities are 94% and 75% after day 1 and day 3	(153)

		on the HA content), uncontained compressive modulus: 26 kPa for different constructs			
Diacrylated Pluronic F127 and methacrylated HA	Bovine articular chondrocytes	Unconfined compressive modulus: 1.5~6.5 kPa (depending on the methacrylated HA content)	Photo	Cell viability is between 60% to 85%.	(152)
GelMA constructs reinforced with methacrylated pHMGCL/PCL	Human articular chondrocytes	Unconfined compressive failure force ~2.7 N and ~7.7 N when covalent bonds between gelMA and methacrylated pHMGCL/PCL are established	Photo	Cartilage ECM network consisting of GAGs and collagen type II are formed after 6 weeks of in vitro culture and Collagen type II production was more pronounced in vivo compared to in vitro	(29)
Gellan, alginate and cartilage extracellular matrix particles	Bovine articular chondrocytes	Tensile modulus ~ 116–230 kPa	Ionic and thermal	Cell viability: 80% and 96%, 60% viable cells are observed in the centre of some samples at day 7. Constructs with cartilage ECM particles increased cartilage ECM formation, but the influence of TGF-β3 on cartilage ECM is more pronounced and constructs with TGF-β3 showed most cartilage ECM formation.	(27)
Methacrylated HA with HA-pNIPAAM	Bovine articular chondrocytes	Not reported	Thermal and photo	Cell viability is negatively influenced by the addition of HA-pNIPAAM.	(28)
Hydrogel Bioprinting of Osteochondral Constructs					
Alginate (cartilage) Gelatin with demineralized bone matrix (bone)	Cell-free	Not reported	Ionic	Directly printing into an osteochondral defect of a bovine femur and showed good geometric fidelity.	(157)
Alginate (cartilage) Alginate with biphasic calcium phosphate particles (bone)	Human articular chondrocytes (cartilage) Human mesenchymal stromal cells (bone)	Unconfined compressive modulus: 4.5–15 kPa (depending on porosity of constructs)	Ionic	Cell viability: ~89% Cartilage and bone ECM formed in designed regions of the constructs after culturing for 3 weeks. In vivo tests showed similar results after 6 weeks of culture	(158)
GelMA with gellan gum	Murine	Unconfined	Photo and	Cell viability: 60–90%	(93)

(cartilage) GelMA, gellan gum and polylactic acid microcarriers (bone)	mesenchymal stromal cells	compressive modulus: ~25–50 kPa (depending on concentration of microcarriers)	ionic		
Hydrogel Bioprinting of Zonally Organized Cartilage Constructs					
Collagen type II	Rabbit articular chondrocytes (2×10^7 cells/mL in superficial zone, 1×10^7 cell/mL in middle zone and 0.5×10^7 cells/mL in deep zone)	Not reported	Thermal	Cell viability: 93% Zonally organized cartilage constructs could be fabricated by bioprinting collagen type II hydrogel constructs with a biomimetic cell density gradient. The cell density gradient distribution resulted in a gradient distribution of ECM.	(49)

2.5.2 Hybrid Bioprinting

A hybrid construct combining advantages of hydrogel and thermoplastics has been brought forward, offering potential for application in CTE (141). Scaffolds made from thermoplastic polymers provide stronger structural properties, and hydrogels provide a biologically favorable, highly hydrated microstructure like native cartilage ECM for chondrocytes. By alternately printing thermoplastic polymer and cell-laden hydrogels, hybrid cartilage constructs are yielded. This mechanism makes a broader range of bio-inks types available for use compared to bioprinting of hydrogels alone, since requirements for viscosity and gelling speed are less stringent (141). Also, engineered cartilage fabricated by hybrid bioprinting technique possess adequate mechanical characteristics, since thermoplastic polymer framework mainly provides mechanical property of the constructs (141).

By applying this state-of-the-art printing technology, human nasoseptal chondrocyte-laden alginate hydrogel with a supportive PCL structure was printed (33). The study demonstrated in vitro and in vivo applications of hybrid constructs encapsulating chondrocytes and growth factors in CTE. Another trial explored the feasibility to use embryonic chick chondrocytes as cell sources for hybrid printing and comprehensively studied biological performance of the embedded chondrocytes. Cell viability, proliferation, and cartilage ECM biosynthesis were all kept at high levels in hybrid constructs, confirming the validity of the hybrid bioprinting for effective CTE (161). Given the bioinert nature of alginate, it is not an ideal material for encapsulating chondrocytes and maintaining their functionality. Therefore, a study printed hybrid tissue analogues by dispensing decellularized extracellular matrix (dECM) instead of alginate in

the abovementioned hybrid bioprinting system. The results showed the versatility and flexibility of hybrid bioprinting process using various tissue-specific dECM bio-inks, including adipose, cartilage and heart tissues, which can provide bioactive cues for embedded cells (143).

Hybrid bioprinting also showed good suitability to fabricate osteochondral constructs, enabling researchers to use different bio-inks in cartilage portion and bone portion. A mechanically stable 3D dual cell-laden construct consisting of osteoblasts and chondrocytes for osteochondral tissue engineering using a multi-head extrusion-based printing system was successfully printed. Two different alginate solutions with encapsulated osteoblasts or chondrocytes were deposited into the previously printed PCL framework (162). A more recent study from the same research group successfully bioprinted a multilayered construct with three distinct layers by varying the hydrogel materials and incorporated growth factors using a similar hybrid printing process and achieved the regeneration of osteochondral defects in the knee joints of rabbits (163). Overviews of hybrid bioprinting for fabricating osteo (chondral) constructs reviewed in Table 2.4.

These studies show the promise of hybrid bioprinting as an advanced fabrication technique for CTE. However, mechanical stimuli exerted on hybrid construct would probably be mainly withstood by the polymeric scaffolds instead of chondrocyte-laden hydrogel because of stress shielding (164). This might be an issue when considering mechanical stimuli can positively mediate chondrocytes biosynthetic behavior (165) and cartilage tissue remodeling (166). Therefore, further studies need to be carried out to determine the influence of mechanical stimuli on the engineered hybrid constructs.

Table 2.4 Overview of Publications on the hybrid bioprinting of osteo (chondral) constructs.

Materials	Cell Types	Mechanical Properties	Crosslinking Mechanism (s)	Outcomes	Reference
Hybrid Bioprinting of Chondral Constructs					
Alginate reinforced with PCL framework	C20A4 human chondrocyte cell line	Unconfined compressive modulus: 6000 kPa	Ionic	Cell viability varies from 70 to 80%. Co-deposition of thermoplastic polymer and hydrogel is firstly introduced for bioprinting of reinforced constructs.	(141)
Alginate reinforced with PCL framework	Human nasoseptal chondrocytes	Not reported	Ionic	85% cell viability, cartilage ECM formation in constructs with the addition of TGF-β after culturing for 4 weeks. Cartilage ECM formation is observed in constructs with after 4 weeks in vivo.	(33)
Alginate reinforced with PCL framework	Embryonic chick chondrocytes	Not reported	Ionic	Cell viability: 77~85%; Cartilage ECM (GAG and collagen type II) is formed in constructs.	(161)
dECM reinforced with PCL framework	Human adipose-derived stem cells (hASCs) and human inferior turbinate-tissue derived mesenchymal stromal cells (hTMSCs)	Not reported	Thermal	Cell viability: >90%. The dECM provided cues for cells survival and long-term functionality. Embedded cell synthesizes cartilage ECM and expressed chondrogenic genes.	(143)
Hybrid Bioprinting of Osteochondral Constructs					
Alginate reinforced with PCL framework	Human nasoseptal chondrocytes (cartilage) Human osteoblasts cell line (MG63)	Not reported	Ionic	Cell viability: ~93.9% for dispensed chondrocytes and ~95.6% for dispensed osteoblasts during 7 days of culture.	(162)
Atelocollagen supplemented with BMP-2 (cartilage) CB(6)-HA supplemented with TGF-β (bone) The whole structure is reinforced with PCL framework	Human turbinate-derived mesenchymal stromal cells (hTMSCs)	Not reported	Thermal and enzymic	Cell viability: 93% for atelocollagen (bone) and 86% CB (6)-HA (cartilage). In vivo results showed neocartilage is formed in cartilage region while new bone is observed in subchondral bone. The constructs are well integrated with surrounding native tissue in vivo.	(163)

2.6 Zonal Cartilage Bioprinting

Zonal cartilage constructs that reflect the native structural depth-dependent characteristics of articular cartilage could have advantages over homogeneous constructs. A zonal cartilage construct can be achieved by the following strategies i) using zonal chondrocyte subpopulations from different zones of cartilage; ii) using a single cell source combined with the correct biochemical and/or biomechanical cues; and iii) using different biomaterials and smart scaffold designs. Zonal chondrocyte subpopulations from different zones of cartilage tissue can be harvested (1, 167, 168), but donor site morbidity, dedifferentiation during expansion, and limited availability are the drawbacks of this strategy. Meanwhile, there is still a debate if zonal chondrocytes can maintain their phenotype after being isolated from their original biomechanical and biochemical environment (31). Comparing with Strategy I, Strategy ii might be an easier and more practical technique based on using only one cell source combined with the suitable biochemical and/or biomechanical cues. BMSCs have been induced to differentiate into zonal chondrogenic cells by co-culturing with various molecules (169-171). This method shows great promise since it would be easier to carry out and potentially could solve the problems associated with direct isolating zonal chondrocytes from cartilage. A good example of Strategy iii was reported by Wise et al (172). They successfully mimicked the cells and ECM organization found in the superficial zone by culturing BMSCs on electrospun and oriented PCL scaffolds. Bio-inks can be formulated based on these strategies for the fabrication of complex zonal structures. Technically, zonal cartilage bioprinting can be realized either by self-supporting hydrogel bioprinting or hybrid bioprinting (Figure 2.2). It has been reported that zonal engineered cartilage could be fabricated by bioprinting collagen type II hydrogel constructs with a biomimetic cell density gradient (49). Even though, zonal cartilage bioprinting is still a challenging task probably because of the complexity of fabrication process, involving multiple bio-inks preparation, frequent switching between dispensing heads, complicated real-time calibration.

2.7 Current Limitations and Recommendations for Future Research

EBB is a convenient and promising technique that can print porous tissue-engineered constructs with structural and biological properties from a wide range of bio-inks. It still has several limitations, including limited biomaterials for bio-ink formulation, cell death during

printing, low resolution as well as insufficient mechanical properties. Bio-inks formulation is restricted by limited printable biomaterials, which makes up only a small portion of biomaterials applied in tissue engineering. To alleviate this problem, development of new biomaterials for bio-ink formulation is needed. When formulating and processing new bio-inks, the properties discussed in Section 3 should be considered and/or compromised for a given CTE application. Further, for clinic application, bio-inks must also satisfy the requirements and regulations as set in standards and norms. Unfortunately, such standards and norms are few nowadays and even none are directly related to bioprinted implants for tissue engineering, which raises a great need for such standards and norms (173). Cell death during the printing process is usually caused by the process-induced forces, such as shear stress, exerted on cells (174, 175). This happens especially when the bio-ink is highly viscous, in which cells would experience significantly higher shear stress (176). Meanwhile, high viscosity possibly induces clogging of the nozzle tip, leading to disturbance of the printing process (177-179). However, relatively high viscosity is essential for the bio-inks to be dispensed into undisrupted strands with higher resolution and printing accuracy. A recent study printed hydrogels in liquid nitrogen to fabricate scaffolds with high resolution and precisely defined dimensions (180). But it impaired the cell viability when printing with cell-laden hydrogels. Therefore, a compromise is usually needed to be made among these factors. Future studies should also focus on new approaches to improve the printability of bio-inks without negatively influencing the cell behavior. Research should also be implemented on developing new techniques to process bio-inks prior to printing to improve printability. For example, increased mixing of alginate and cross-linker solutions actually improved geometric fidelity, mechanical properties and cell viability of printed constructs (181-183).

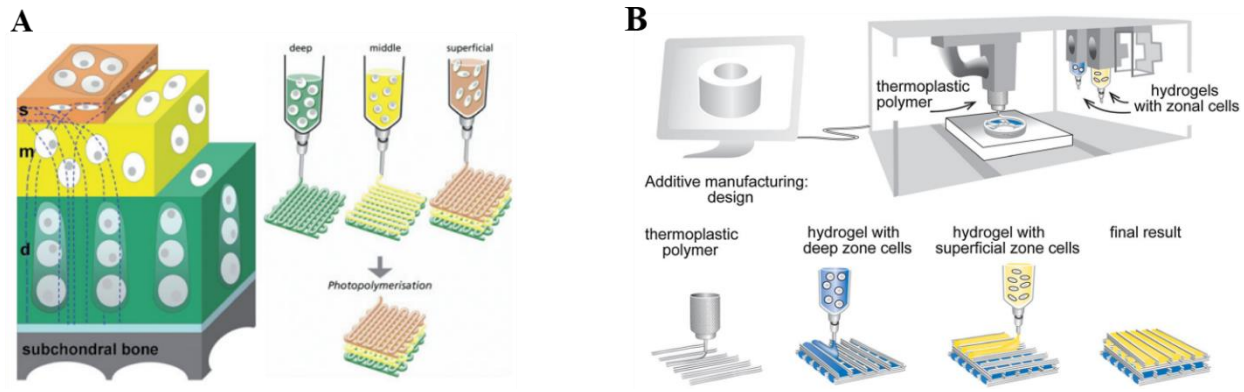

Figure 2.2 (A) Schematic of self-supporting hydrogel bioprinting for fabrication of zonal cartilage constructs. Zonal constructs are printed with chondrocytes from the superficial, middle, and deep zones incorporated in distinct hydrogel precursors in defined geometries. Reproduced with permission. Copyright 2009, Wiley Online Library (145); (B) Schematic of hybrid bioprinting for fabrication of zonal cartilage constructs. Alternating steps of printing polymer and zonal cell-laden hydrogels are performed to obtain zonal constructs Reproduced with permission. Copyright 2015, Wiley Online Library (32).

Other printing parameters, including printing pressure, nozzle geometry and diameter, and bio-ink concentration, have also been shown to influence cell viability within bio-inks (72, 130). Manipulating and optimizing these process parameters can potentially address these issues and challenges to some extent. Recent finding also demonstrated the influence of these printing parameters on printing accuracy (184). Therefore, we urge that future studies should indicate these parameters when investigating new bio-inks to improve consistency and repeatability.

To fabricate functional cartilage construct, suitable cell sources, biological cues, and construct organization are still needed to be determined for successful cartilage regeneration. Most present studies only focus on evaluating cell viability in different bioprinted hydrogels, while functionality of the engineered cartilage is not very well characterized. As such, we also urge that, for bioprinted engineered cartilage constructs, research should also emphasize the overall chondrogenesis within the constructs, either qualitatively (e.g., Alcian Blue and Safranin O histology) or quantitatively (e.g., collagen and glycosaminoglycan content, or aggrecan and collagen II gene expression). Moreover, given that the mechanical performance of cartilage engineered from hydrogel is usually inferior to native cartilage, research on mechanical properties is also required for future cartilage bioprinting studies. Notably, current mechanical characterization of engineered cartilage constructs is mainly performed based on a single

mechanical test (Table 2.4 and 2.5). But a single acceptable mechanical test result does not sufficiently prove the engineered constructs can perform its biomechanical functions as good as native cartilage tissue. Therefore, a series of mechanical tests (e.g., compression, tensile, and shear tests) are needed to be done to comprehensively characterize the mechanical performance of bioprinted cartilage constructs (185).

Theoretically, the shape of scaffolds fabricated by bioprinting techniques can match personalized defects in vivo. Notably, current in vivo research is usually based on man-made regular defects, which can be made fitting with a bioprinted scaffold with exact shape and dimension. It could be difficult for the in vitro printed material to match perfectly with the defect that needs to be regenerated. Printed construct could deform during in vitro culture and defects may expand while waiting for implantation. Although defined defects can be created in clinic, this is not desirable since it further increases the area that needs to be regenerated. Therefore, the concept of "In situ" bioprinting has been performed to directly print alginate hydrogels into a defect on an explanted articular surface from a calf (157). This strategy avoids laboratory-based constructs culture and multiple surgical intervention and would represent the future of tissue engineering using bioprinting techniques for cartilage regeneration.

Issues facing CTE is the inability to translate technologies into the clinic and lack of clinic standards of materials for human tissue bioprinting. (186). To move bioprinted living cartilage implants into clinic application, bio-inks also must satisfy the requirements and regulations on safety, sterility, and reproducibility. To ensure safety of bioprinted living implants for clinical application and to help researchers qualify and validate the bioprinting process and bio-ink formulations, consistent standards are required. Additive manufacturing standards have been published by American Society for Testing and Materials (ASTM) F2792. Meanwhile, standards for tissue-engineered constructs have been approved by the ASTM international committee F04, the International Organization for Standardization technical committee 150/SCZ, and the British Standards Institute. Nevertheless, there are no standards is currently available for bioprinted implants applied in tissue engineering field (173). To ensure sterility throughout bioprinting, the process has to be incorporated in a Good Manufacturing Practice facility, and all components of bioprinter should be sterile and can be operated in a sterile environment. Moreover, the whole bioprinting process should involve minimal manual handling and operation. Therefore, skilled operators are needed to monitor the printing process. Automated, reliable quality control during

the printing process will promote the translation of printers into clinics. Having an integrated bioreactor system with bioprinters to allow in vitro culture before implantation is also an efficient way to avoid undesirable handling of the printed construct and to improve the sterility and reproducibility. However, a proven bioprinter-bioreactor setup is not commercially available yet.

2.8 Conclusion

EBB is an advanced fabrication technique to produce customized cell-laden hydrogel-based constructs for CTE to mimic chondral, osteochondral and zonal organization of articular cartilage. Despite the advantages and opportunities provided by hydrogel-based EBB for cartilage bioprinting, there are still multiple challenges that need to be addressed. Bio-inks for EBB need to be synthesized and optimized in terms of their biocompatibility, formulation, processing, printability, and optimal cell sources. Self-supporting hydrogel bioprinting and hybrid bioprinting are two common approaches to fabricate cartilage constructs. The former technique provides a cell-friendly printing environment but limited mechanical strength, while the latter brings elevated mechanical properties but the stress shielding may disable external mechanical stimuli. Tackling the challenges revolving around bio-inks and mechanical performance of resulting cartilage constructs will foster biologically active and living bioprinted implants for future clinical applications.

References

1. Klein T, Schumacher B, Schmidt T, Li K, Voegtline M, Masuda K, et al. Tissue engineering of stratified articular cartilage from chondrocyte subpopulations. Osteoarthritis and cartilage. 2003;11(8):595-602.

2. O'Driscoll SW. The healing and regeneration of articular cartilage. J Bone Joint Surg Am. 1998 Dec;80(12):1795-812.

3. Drury JL, Mooney DJ. Hydrogels for tissue engineering: scaffold design variables and applications. Biomaterials. 2003;24(24):4337-51.

4. Hutmacher DW. Scaffolds in tissue engineering bone and cartilage. Biomaterials. 2000;21(24):2529-43.

5. Fedorovich NE, Alblas J, de Wijn JR, Hennink WE, Verbout AJ, Dhert WJ. Hydrogels as extracellular matrices for skeletal tissue engineering: state-of-the-art and novel application in organ printing. Tissue Eng. 2007;13(8):1905-25.

6. Hoffman AS. Hydrogels for biomedical applications. Adv Drug Deliv Rev. 2012;64:18-23.

7. Kirchmajer DM, Gorkin III R. An overview of the suitability of hydrogel-forming polymers for extrusion-based 3D-printing. Journal of Materials Chemistry B. 2015;3(20):4105-17.

8. Awad HA, Wickham MQ, Leddy HA, Gimble JM, Guilak F. Chondrogenic differentiation of adipose-derived adult stem cells in agarose, alginate, and gelatin scaffolds. Biomaterials. 2004;25(16):3211-22.

9. Benoit DS, Schwartz MP, Durney AR, Anseth KS. Small functional groups for controlled differentiation of hydrogel-encapsulated human mesenchymal stem cells. Nature materials. 2008;7(10):816-23.

10. Chenite A, Chaput C, Wang D, Combes C, Buschmann M, Hoemann C, et al. Novel injectable neutral solutions of chitosan form biodegradable gels in situ. Biomaterials. 2000;21(21):2155-61.

11. Nicodemus GD, Bryant SJ. Cell encapsulation in biodegradable hydrogels for tissue engineering applications. Tissue Engineering Part B: Reviews. 2008;14(2):149-65.

12. Schmedlen RH, Masters KS, West JL. Photocrosslinkable polyvinyl alcohol hydrogels that can be modified with cell adhesion peptides for use in tissue engineering. Biomaterials. 2002;23(22):4325-32.

13. Masters KS, Shah DN, Leinwand LA, Anseth KS. Crosslinked hyaluronan scaffolds as a biologically active carrier for valvular interstitial cells. Biomaterials. 2005;26(15):2517-25.
14. Matsusaki M, Yoshida H, Akashi M. The construction of 3D-engineered tissues composed of cells and extracellular matrices by hydrogel template approach. Biomaterials. 2007;28(17):2729-37.
15. Yang S, Leong K, Du Z, Chua C. The design of scaffolds for use in tissue engineering. Part I. Traditional factors. Tissue Eng. 2001;7(6):679-89.
16. Bian L, Zhai DY, Zhang EC, Mauck RL, Burdick JA. Dynamic compressive loading enhances cartilage matrix synthesis and distribution and suppresses hypertrophy in hMSC-laden hyaluronic acid hydrogels. Tissue Engineering Part A. 2011;18(7-8):715-24.
17. Peltola SM, Melchels FP, Grijpma DW, Kellomäki M. A review of rapid prototyping techniques for tissue engineering purposes. Ann Med. 2008;40(4):268-80.
18. Mohan Pandey P, Venkata Reddy N, Dhande SG. Slicing procedures in layered manufacturing: a review. Rapid prototyping journal. 2003;9(5):274-88.
19. Mironov V, Trusk T, Kasyanov V, Little S, Swaja R, Markwald R. Biofabrication: a 21st century manufacturing paradigm. Biofabrication. 2009;1(2):022001.
20. Ozbolat IT, Hospodiuk M. Current advances and future perspectives in extrusion-based bioprinting. Biomaterials. 2016;76:321-43.
21. Murphy SV, Atala A. 3D bioprinting of tissues and organs. Nat Biotechnol. 2014;32(8):773-85.
22. Sophia Fox AJ, Bedi A, Rodeo SA. The basic science of articular cartilage: structure, composition, and function. Sports health. 2009;1(6):461-8.
23. Speer DP, Dahners L. The Collagenous Architecture of Articular Cartilage: Correlation of Scanning Electron Microscopy and Polarized Light Microscopy Observations. Clin Orthop. 1979;139:267-75.
24. Poole AR, Kojima T, Yasuda T, Mwale F, Kobayashi M, Laverty S. Composition and structure of articular cartilage: a template for tissue repair. Clin Orthop. 2001;391:S26-33.
25. Ma B, Leijten J, Wu L, Kip M, van Blitterswijk C, Post J, et al. Gene expression profiling of dedifferentiated human articular chondrocytes in monolayer culture. Osteoarthritis and cartilage. 2013;21(4):599-603.

26. Caron M, Emans P, Coolsen M, Voss L, Surtel D, Cremers A, et al. Redifferentiation of dedifferentiated human articular chondrocytes: comparison of 2D and 3D cultures. Osteoarthritis and Cartilage. 2012;20(10):1170-8.
27. Kesti M, Eberhardt C, Pagliccia G, Kenkel D, Grande D, Boss A, et al. Bioprinting complex cartilaginous structures with clinically compliant biomaterials. Advanced Functional Materials. 2015;25(48):7406-17.
28. Kesti M, Müller M, Becher J, Schnabelrauch M, D'Este M, Eglin D, et al. A versatile bioink for three-dimensional printing of cellular scaffolds based on thermally and photo-triggered tandem gelation. Acta biomaterialia. 2015;11:162-72.
29. Boere KW, Visser J, Seyednejad H, Rahimian S, Gawlitta D, Van Steenbergen MJ, et al. Covalent attachment of a three-dimensionally printed thermoplast to a gelatin hydrogel for mechanically enhanced cartilage constructs. Acta biomaterialia. 2014;10(6):2602-11.
30. Khanarian NT, Haney NM, Burga RA, Lu HH. A functional agarose-hydroxyapatite scaffold for osteochondral interface regeneration. Biomaterials. 2012;33(21):5247-58.
31. Schuurman W, Klein T, Dhert W, Weeren P, Hutmacher D, Malda J. Cartilage regeneration using zonal chondrocyte subpopulations: a promising approach or an overcomplicated strategy? Journal of tissue engineering and regenerative medicine. 2015;9(6):669-78.
32. Chung C, Burdick JA. Engineering cartilage tissue. Adv Drug Deliv Rev. 2008;60(2):243-62.
33. Kundu J, Shim J, Jang J, Kim S, Cho D. An additive manufacturing ‐ based PCL–alginate–chondrocyte bioprinted scaffold for cartilage tissue engineering. Journal of tissue engineering and regenerative medicine. 2015;9(11):1286-97.
34. Markstedt K, Mantas A, Tournier I, Martínez Ávila H, Hägg D, Gatenholm P. 3D bioprinting human chondrocytes with nanocellulose–alginate bioink for cartilage tissue engineering applications. Biomacromolecules. 2015;16(5):1489-96.
35. DiCarlo B, Hu J, Gross T, Vago R, Athanasiou K. Biomaterial effects in articular cartilage tissue engineering using polyglycolic acid, a novel marine origin biomaterial, IGF-I, and TGF-β1. Proc Inst Mech Eng Part H J Eng Med. 2009;223(1):63-73.
36. MacBarb RF, Makris EA, Hu JC, Athanasiou KA. A chondroitinase-ABC and TGF-β1 treatment regimen for enhancing the mechanical properties of tissue-engineered fibrocartilage. Acta biomaterialia. 2013;9(1):4626-34.

37. Hunziker E, Driesang I, Morris E. Chondrogenesis in cartilage repair is induced by members of the transforming growth factor-beta superfamily. Clin Orthop. 2001;391:S171-81.
38. Li W, Tuli R, Okafor C, Derfoul A, Danielson KG, Hall DJ, et al. A three-dimensional nanofibrous scaffold for cartilage tissue engineering using human mesenchymal stem cells. Biomaterials. 2005;26(6):599-609.
39. Guilak F, Awad HA, Fermor B, Leddy HA, Gimble JM. Adipose ' derived adult stem cells for cartilage tissue engineering. Biorheology. 2004;41(3-4):389-99.
40. Andriamanalijaona R, Duval E, Raoudi M, Lecourt S, Vilquin J, Marolleau J, et al. Differentiation potential of human muscle-derived cells towards chondrogenic phenotype in alginate beads culture. Osteoarthritis and Cartilage. 2008;16(12):1509-18.
41. Kuroda R, Usas A, Kubo S, Corsi K, Peng H, Rose T, et al. Cartilage repair using bone morphogenetic protein 4 and muscle ' derived stem cells. Arthritis & Rheumatism. 2006;54(2):433-42.
42. Mara CSd, Sartori AR, Duarte AS, Andrade ALL, Pedro MAC, Coimbra IB. Periosteum as a source of mesenchymal stem cells: the effects of TGF-β3 on chondrogenesis. Clinics. 2011;66(3):487-92.
43. Kramer J, Hegert C, Guan K, Wobus AM, Müller PK, Rohwedel J. Embryonic stem cell-derived chondrogenic differentiation in vitro: activation by BMP-2 and BMP-4. Mech Dev. 2000;92(2):193-205.
44. Vats A, Bielby RC, Tolley N, Dickinson SC, Boccaccini AR, Hollander AP, et al. Chondrogenic differentiation of human embryonic stem cells: the effect of the micro-environment. Tissue Eng. 2006;12(6):1687-97.
45. Connelly JT, Wilson CG, Levenston ME. Characterization of proteoglycan production and processing by chondrocytes and BMSCs in tissue engineered constructs. Osteoarthritis and cartilage. 2008;16(9):1092-100.
46. Meretoja VV, Dahlin RL, Wright S, Kasper FK, Mikos AG. The effect of hypoxia on the chondrogenic differentiation of co-cultured articular chondrocytes and mesenchymal stem cells in scaffolds. Biomaterials. 2013;34(17):4266-73.
47. Saha S, Kirkham J, Wood D, Curran S, Yang XB. Informing future cartilage repair strategies: a comparative study of three different human cell types for cartilage tissue engineering. Cell Tissue Res. 2013;352(3):495-507.

48. Cui X, Breitenkamp K, Finn M, Lotz M, D'Lima DD. Direct human cartilage repair using three-dimensional bioprinting technology. Tissue Engineering Part A. 2012;18(11-12):1304-12.
49. Ren X, Wang F, Chen C, Gong X, Yin L, Yang L. Engineering zonal cartilage through bioprinting collagen type II hydrogel constructs with biomimetic chondrocyte density gradient. BMC Musculoskeletal Disorders. 2016;17(1):1.
50. Schuurman W, Levett PA, Pot MW, van Weeren PR, Dhert WJ, Hutmacher DW, et al. Gelatin ' methacrylamide hydrogels as potential biomaterials for fabrication of tissue ' engineered cartilage constructs. Macromolecular bioscience. 2013;13(5):551-61.
51. Cohen DL, Malone E, Lipson H, Bonassar LJ. Direct freeform fabrication of seeded hydrogels in arbitrary geometries. Tissue Eng. 2006;12(5):1325-35.
52. van Osch GJ, Mandl EW, Jahr H, Koevoet W, Nolst ' Trenité G, Verhaar JA. Considerations on the use of ear chondrocytes as donor chondrocytes for cartilage tissue engineering. Biorheology. 2004;41(3-4):411-21.
53. Yamaoka H, Asato H, Ogasawara T, Nishizawa S, Takahashi T, Nakatsuka T, et al. Cartilage tissue engineering using human auricular chondrocytes embedded in different hydrogel materials. Journal of Biomedical Materials Research Part A. 2006;78(1):1-11.
54. Panossian A, Ashiku S, Kirchhoff CH, Randolph MA, Yaremchuk MJ. Effects of cell concentration and growth period on articular and ear chondrocyte transplants for tissue engineering. Plast Reconstr Surg. 2001 Aug;108(2):392-402.
55. Kafienah W, Jakob M, Démarteau O, Frazer A, Barker MD, Martin I, et al. Three-dimensional tissue engineering of hyaline cartilage: comparison of adult nasal and articular chondrocytes. Tissue Eng. 2002;8(5):817-26.
56. Hicks DL, Sage AB, Schumacher BL, Sah RL, Watson D. Growth and phenotype of low-density nasal septal chondrocyte monolayers. Otolaryngology—Head and Neck Surgery. 2005;133(3):417-22.
57. Kafienah W, Mistry S, Dickinson SC, Sims TJ, Learmonth I, Hollander AP. Three ' dimensional cartilage tissue engineering using adult stem cells from osteoarthritis patients. Arthritis & Rheumatism. 2007;56(1):177-87.
58. Costantini M, Idaszek J, Szöke K, Jaroszewicz J, Dentini M, Barbetta A, et al. 3D bioprinting of BM-MSCs-loaded ECM biomimetic hydrogels for in vitro neocartilage formation. Biofabrication. 2016;8(3):035002.

59. Longobardi L, O'Rear L, Aakula S, Johnstone B, Shimer K, Chytil A, et al. Effect of IGF ' I in the chondrogenesis of bone marrow mesenchymal stem cells in the presence or absence of TGF ' β signaling. Journal of Bone and Mineral Research. 2006;21(4):626-36.
60. Zuk PA, Zhu M, Ashjian P, De Ugarte DA, Huang JI, Mizuno H, et al. Human adipose tissue is a source of multipotent stem cells. Mol Biol Cell. 2002 Dec;13(12):4279-95.
61. Huang JI, Kazmi N, Durbhakula MM, Hering TM, Yoo JU, Johnstone B. Chondrogenic potential of progenitor cells derived from human bone marrow and adipose tissue: A patient ' matched comparison. Journal of Orthopaedic Research. 2005;23(6):1383-9.
62. Bauge C, Boumediene K. Use of Adult Stem Cells for Cartilage Tissue Engineering: Current Status and Future Developments. Stem Cells Int. 2015;2015:438026.
63. Nawata M, Wakitani S, Nakaya H, Tanigami A, Seki T, Nakamura Y, et al. Use of bone morphogenetic protein 2 and diffusion chambers to engineer cartilage tissue for the repair of defects in articular cartilage. Arthritis & Rheumatism. 2005;52(1):155-63.
64. Adachi N, Sato K, Usas A, Fu FH, Ochi M, Han CW, et al. Muscle derived, cell based ex vivo gene therapy for treatment of full thickness articular cartilage defects. J Rheumatol. 2002 Sep;29(9):1920-30.
65. Sakaguchi Y, Sekiya I, Yagishita K, Muneta T. Comparison of human stem cells derived from various mesenchymal tissues: superiority of synovium as a cell source. Arthritis & Rheumatism. 2005;52(8):2521-9.
66. Park Y, Sugimoto M, Watrin A, Chiquet M, Hunziker EB. BMP-2 induces the expression of chondrocyte-specific genes in bovine synovium-derived progenitor cells cultured in three-dimensional alginate hydrogel. Osteoarthritis and cartilage. 2005;13(6):527-36.
67. Sampat SR, O'Connell GD, Fong JV, Alegre-Aguarón E, Ateshian GA, Hung CT. Growth factor priming of synovium-derived stem cells for cartilage tissue engineering. Tissue Engineering Part A. 2011;17(17-18):2259-65.
68. Iwasaki M, Nakahara H, Nakata K, Nakase T, Kimura T, Ono K. Regulation of proliferation and osteochondrogenic differentiation of periosteum-derived cells by transforming growth factor-beta and basic fibroblast growth factor. J Bone Joint Surg Am. 1995 Apr;77(4):543-54.
69. You F, Wu X, Chen X. 3D Printing of Porous Alginate/gelatin Hydrogel Scaffolds and Their Mechanical Property Characterization. International Journal of Polymeric Materials and Polymeric Biomaterials. 2016(just-accepted).

70. Duarte Campos DF, Blaeser A, Korsten A, Neuss S, Jäkel J, Vogt M, et al. The stiffness and structure of three-dimensional printed hydrogels direct the differentiation of mesenchymal stromal cells toward adipogenic and osteogenic lineages. Tissue Engineering Part A. 2014;21(3-4):740-56.
71. Rajaram A, Schreyer DJ, Chen DX. Use of the polycation polyethyleneimine to improve the physical properties of alginate–hyaluronic acid hydrogel during fabrication of tissue repair scaffolds. Journal of Biomaterials Science, Polymer Edition. 2015;26(7):433-45.
72. Billiet T, Gevaert E, De Schryver T, Cornelissen M, Dubruel P. The 3D printing of gelatin methacrylamide cell-laden tissue-engineered constructs with high cell viability. Biomaterials. 2014;35(1):49-62.
73. Chameettachal S, Midha S, Ghosh S. Regulation of Chondrogenesis and Hypertrophy in Silk Fibroin-Gelatin-Based 3D Bioprinted Constructs. ACS Biomaterials Science & Engineering. 2016;2(9):1450-63.
74. Smith CM, Stone AL, Parkhill RL, Stewart RL, Simpkins MW, Kachurin AM, et al. Three-dimensional bioassembly tool for generating viable tissue-engineered constructs. Tissue Eng. 2004;10(9-10):1566-76.
75. Roach BL, Nover AB, Ateshian GA, Hung CT. Agarose Hydrogel Characterization for Regenerative Medicine Applications: Focus on Engineering Cartilage. Biomaterials from Nature for Advanced Devices and Therapies. 2016:258.
76. Kao JM, Rose R, Yousef M, Hunter SK, Rodgers V. In vivo biocompatibility evaluation of Cibacron blue-agarose. J Biomed Mater Res. 1999;47(4):537-42.
77. Hunt NC, Grover LM. Cell encapsulation using biopolymer gels for regenerative medicine. Biotechnol Lett. 2010;32(6):733-42.
78. Campos DFD, Blaeser A, Weber M, Jäkel J, Neuss S, Jahnen-Dechent W, et al. Three-dimensional printing of stem cell-laden hydrogels submerged in a hydrophobic high-density fluid. Biofabrication. 2012;5(1):015003.
79. Augst AD, Kong HJ, Mooney DJ. Alginate hydrogels as biomaterials. Macromolecular bioscience. 2006;6(8):623-33.
80. Wang Z, Goh J, De SD, Ge Z, Ouyang H, Chong JSW, et al. Efficacy of bone marrow-derived stem cells in strengthening osteoporotic bone in a rabbit model. Tissue Eng. 2006;12(7):1753-61.

81. Diekman BO, Estes BT, Guilak F. The effects of BMP6 overexpression on adipose stem cell chondrogenesis: Interactions with dexamethasone and exogenous growth factors. Journal of Biomedical Materials Research Part A. 2010;93(3):994-1003.
82. Jia J, Richards DJ, Pollard S, Tan Y, Rodriguez J, Visconti RP, et al. Engineering alginate as bioink for bioprinting. Acta biomaterialia. 2014;10(10):4323-31.
83. Sannino A, Demitri C, Madaghiele M. Biodegradable cellulose-based hydrogels: design and applications. Materials. 2009;2(2):353-73.
84. Thirumala S, Gimble JM, Devireddy RV. Methylcellulose based thermally reversible hydrogel system for tissue engineering applications. Cells. 2013;2(3):460-75.
85. Vinatier C, Magne D, Weiss P, Trojani C, Rochet N, Carle G, et al. A silanized hydroxypropyl methylcellulose hydrogel for the three-dimensional culture of chondrocytes. Biomaterials. 2005;26(33):6643-51.
86. Berger J, Reist M, Mayer JM, Felt O, Peppas N, Gurny R. Structure and interactions in covalently and ionically crosslinked chitosan hydrogels for biomedical applications. European Journal of Pharmaceutics and Biopharmaceutics. 2004;57(1):19-34.
87. Rinaudo M. Chitin and chitosan: properties and applications. Progress in polymer science. 2006;31(7):603-32.
88. Hong Y, Song H, Gong Y, Mao Z, Gao C, Shen J. Covalently crosslinked chitosan hydrogel: properties of in vitro degradation and chondrocyte encapsulation. Acta biomaterialia. 2007;3(1):23-31.
89. Ye K, Felimban R, Traianedes K, Moulton SE, Wallace GG, Chung J, et al. Chondrogenesis of infrapatellar fat pad derived adipose stem cells in 3D printed chitosan scaffold. PloS one. 2014;9(6):e99410.
90. Coutinho DF, Sant SV, Shin H, Oliveira JT, Gomes ME, Neves NM, et al. Modified Gellan Gum hydrogels with tunable physical and mechanical properties. Biomaterials. 2010;31(29):7494-502.
91. Oliveira JT, Gardel LS, Rada T, Martins L, Gomes ME, Reis RL. Injectable gellan gum hydrogels with autologous cells for the treatment of rabbit articular cartilage defects. Journal of Orthopaedic Research. 2010;28(9):1193-9.

92. Oliveira JT, Martins L, Picciochi R, Malafaya P, Sousa R, Neves N, et al. Gellan gum: a new biomaterial for cartilage tissue engineering applications. Journal of biomedical materials research Part A. 2010;93(3):852-63.
93. Levato R, Visser J, Planell JA, Engel E, Malda J, Mateos-Timoneda MA. Biofabrication of tissue constructs by 3D bioprinting of cell-laden microcarriers. Biofabrication. 2014;6(3):035020.
94. Mouser VH, Melchels FP, Visser J, Dhert WJ, Gawlitta D, Malda J. Yield stress determines bioprintability of hydrogels based on gelatin-methacryloyl and gellan gum for cartilage bioprinting. Biofabrication. 2016;8(3):035003.
95. Park JY, Choi J, Shim J, Lee J, Park H, Kim SW, et al. A comparative study on collagen type I and hyaluronic acid dependent cell behavior for osteochondral tissue bioprinting. Biofabrication. 2014;6(3):035004.
96. Jeon O, Song SJ, Lee K, Park MH, Lee S, Hahn SK, et al. Mechanical properties and degradation behaviors of hyaluronic acid hydrogels cross-linked at various cross-linking densities. Carbohydr Polym. 2007;70(3):251-7.
97. Skardal A, Zhang J, McCoard L, Xu X, Oottamasathien S, Prestwich GD. Photocrosslinkable hyaluronan-gelatin hydrogels for two-step bioprinting. Tissue Engineering Part A. 2010;16(8):2675-85.
98. Bian L, Hou C, Tous E, Rai R, Mauck RL, Burdick JA. The influence of hyaluronic acid hydrogel crosslinking density and macromolecular diffusivity on human MSC chondrogenesis and hypertrophy. Biomaterials. 2013;34(2):413-21.
99. Ouyang L, Highley CB, Rodell CB, Sun W, Burdick JA. 3D Printing of shear-thinning hyaluronic acid hydrogels with secondary crosslinking. ACS Biomaterials Science & Engineering. 2016.
100. Yamamoto M, Ikada Y, Tabata Y. Controlled release of growth factors based on biodegradation of gelatin hydrogel. Journal of Biomaterials Science, Polymer Edition. 2001;12(1):77-88.
101. Loessner D, Meinert C, Kaemmerer E, Martine LC, Yue K, Levett PA, et al. Functionalization, preparation and use of cell-laden gelatin methacryloyl-based hydrogels as modular tissue culture platforms. Nature protocols. 2016;11(4):727-46.

102. Tabata Y, Ikada Y. Vascularization effect of basic fibroblast growth factor released from gelatin hydrogels with different biodegradabilities. Biomaterials. 1999;20(22):2169-75.
103. Das S, Pati F, Choi Y, Rijal G, Shim J, Kim SW, et al. Bioprintable, cell-laden silk fibroin–gelatin hydrogel supporting multilineage differentiation of stem cells for fabrication of three-dimensional tissue constructs. Acta biomaterialia. 2015;11:233-46.
104. Peng H, Poovaiah N, Forrester M, Cochran E, Wang Q. Ex vivo culture of primary intestinal stem cells in collagen gels and foams. ACS Biomaterials Science & Engineering. 2014;1(1):37-42.
105. Nims RJ, Cigan AD, Durney KM, Jones BK, O'Neill JD, Law WA, et al. Constrained cage culture improves engineered cartilage functional properties by enhancing collagen network stability. Tissue Engineering Part A. 2017.
106. Makris E, Hu J, Athanasiou K. Hypoxia-induced collagen crosslinking as a mechanism for enhancing mechanical properties of engineered articular cartilage. Osteoarthritis and cartilage. 2013;21(4):634-41.
107. Rhee S, Puetzer JL, Mason BN, Reinhart-King CA, Bonassar LJ. 3D bioprinting of spatially heterogeneous collagen constructs for cartilage tissue engineering. ACS Biomaterials Science & Engineering. 2016;2(10):1800-5.
108. Xu T, Binder KW, Albanna MZ, Dice D, Zhao W, Yoo JJ, et al. Hybrid printing of mechanically and biologically improved constructs for cartilage tissue engineering applications. Biofabrication. 2012;5(1):015001.
109. Ahmed TA, Dare EV, Hincke M. Fibrin: a versatile scaffold for tissue engineering applications. Tissue Engineering Part B: Reviews. 2008;14(2):199-215.
110. Gao G, Cui X. Three-dimensional bioprinting in tissue engineering and regenerative medicine. Biotechnol Lett. 2016;38(2):203-11.
111. Ozbolat IT. Bioprinting scale-up tissue and organ constructs for transplantation. Trends Biotechnol. 2015;33(7):395-400.
112. Lee Y, Polio S, Lee W, Dai G, Menon L, Carroll RS, et al. Bio-printing of collagen and VEGF-releasing fibrin gel scaffolds for neural stem cell culture. Exp Neurol. 2010;223(2):645-52.

113. Novikova LN, Mosahebi A, Wiberg M, Terenghi G, Kellerth J, Novikov LN. Alginate hydrogel and matrigel as potential cell carriers for neurotransplantation. Journal of Biomedical Materials Research Part A. 2006;77(2):242-52.
114. Kleinman HK, Martin GR. Matrigel: basement membrane matrix with biological activity. Seminars in cancer biology; Elsevier; 2005.
115. Snyder J, Hamid Q, Wang C, Chang R, Emami K, Wu H, et al. Bioprinting cell-laden matrigel for radioprotection study of liver by pro-drug conversion in a dual-tissue microfluidic chip. Biofabrication. 2011;3(3):034112.
116. Fedorovich NE, De Wijn JR, Verbout AJ, Alblas J, Dhert WJ. Three-dimensional fiber deposition of cell-laden, viable, patterned constructs for bone tissue printing. Tissue Engineering Part A. 2008;14(1):127-33.
117. Khattak SF, Bhatia SR, Roberts SC. Pluronic F127 as a cell encapsulation material: utilization of membrane-stabilizing agents. Tissue Eng. 2005;11(5-6):974-83.
118. Wu W, DeConinck A, Lewis JA. Omnidirectional printing of 3D microvascular networks. Adv Mater. 2011;23(24).
119. Hwang NS, Varghese S, Li H, Elisseeff J. Regulation of osteogenic and chondrogenic differentiation of mesenchymal stem cells in PEG-ECM hydrogels. Cell Tissue Res. 2011;344(3):499-509.
120. Bryant SJ, Bender RJ, Durand KL, Anseth KS. Encapsulating chondrocytes in degrading PEG hydrogels with high modulus: engineering gel structural changes to facilitate cartilaginous tissue production. Biotechnol Bioeng. 2004;86(7):747-55.
121. Hockaday L, Kang K, Colangelo N, Cheung P, Duan B, Malone E, et al. Rapid 3D printing of anatomically accurate and mechanically heterogeneous aortic valve hydrogel scaffolds. Biofabrication. 2012;4(3):035005.
122. Williams DF. On the mechanisms of biocompatibility. Biomaterials. 2008;29(20):2941-53.
123. Atala A, Yoo JJ. Essentials of 3D biofabrication and translation. Academic Press; 2015.
124. Li J, Chen M, Fan X, Zhou H. Recent advances in bioprinting techniques: approaches, applications and future prospects. Journal of Translational Medicine. 2016;14(1):271.
125. Ballyns JJ, Cohen DL, Malone E, Maher SA, Potter HG, Wright T, et al. An optical method for evaluation of geometric fidelity for anatomically shaped tissue-engineered constructs. Tissue Engineering Part C: Methods. 2009;16(4):693-703.

126. Trachtenberg JE, Placone JK, Smith BT, Piard CM, Santoro M, Scott DW, et al. Extrusion-based 3D printing of poly (propylene fumarate) in a full-factorial design. ACS Biomaterials Science & Engineering. 2016;2(10):1771-80.
127. Nikkhah M, Eshak N, Zorlutuna P, Annabi N, Castello M, Kim K, et al. Directed endothelial cell morphogenesis in micropatterned gelatin methacrylate hydrogels. Biomaterials. 2012;33(35):9009-18.
128. You F, Wu X, Zhu N, Lei M, Eames BF, Chen X. 3D Printing of porous cell-laden hydrogel constructs for potential applications in cartilage tissue engineering. ACS Biomaterials Science & Engineering. 2016;2(7):1200-10.
129. Malda J, Visser J, Melchels FP, Jüngst T, Hennink WE, Dhert WJ, et al. 25th anniversary article: engineering hydrogels for biofabrication. Adv Mater. 2013;25(36):5011-28.
130. Li M, Tian X, Schreyer DJ, Chen X. Effect of needle geometry on flow rate and cell damage in the dispensing ' based biofabrication process. Biotechnol Prog. 2011;27(6):1777-84.
131. Guvendiren M, Lu HD, Burdick JA. Shear-thinning hydrogels for biomedical applications. Soft Matter. 2012;8(2):260-72.
132. Nichol JW, Koshy ST, Bae H, Hwang CM, Yamanlar S, Khademhosseini A. Cell-laden microengineered gelatin methacrylate hydrogels. Biomaterials. 2010;31(21):5536-44.
133. Phelps EA, Enemchukwu NO, Fiore VF, Sy JC, Murthy N, Sulchek TA, et al. Maleimide cross ' linked bioactive peg hydrogel exhibits improved reaction kinetics and cross ' linking for cell encapsulation and in situ delivery. Adv Mater. 2012;24(1):64-70.
134. Izadifar Z, Chen X, Kulyk W. Strategic design and fabrication of engineered scaffolds for articular cartilage repair. Journal of functional biomaterials. 2012;3(4):799-838.
135. Zhang L, Rodriguez J, Raez J, Myles AJ, Fenniri H, Webster TJ. Biologically inspired rosette nanotubes and nanocrystalline hydroxyapatite hydrogel nanocomposites as improved bone substitutes. Nanotechnology. 2009;20(17):175101.
136. Chang C, Peng N, He M, Teramoto Y, Nishio Y, Zhang L. Fabrication and properties of chitin/hydroxyapatite hybrid hydrogels as scaffold nano-materials. Carbohydr Polym. 2013;91(1):7-13.
137. Khanarian NT, Jiang J, Wan LQ, Mow VC, Lu HH. A hydrogel-mineral composite scaffold for osteochondral interface tissue engineering. Tissue Engineering Part A. 2011;18(5-6):533-45.

138. Lee CH, Cook JL, Mendelson A, Moioli EK, Yao H, Mao JJ. Regeneration of the articular surface of the rabbit synovial joint by cell homing: a proof of concept study. The Lancet. 2010;376(9739):440-8.
139. Visser J, Melchels FP, Jeon JE, van Bussel EM, Kimpton LS, Byrne HM, et al. Reinforcement of hydrogels using three-dimensionally printed microfibres. Nature communications. 2015;6.
140. Tabriz AG, Hermida MA, Leslie NR, Shu W. Three-dimensional bioprinting of complex cell laden alginate hydrogel structures. Biofabrication. 2015;7(4):045012.
141. Schuurman W, Khristov V, Pot M, Van Weeren P, Dhert W, Malda J. Bioprinting of hybrid tissue constructs with tailorable mechanical properties. Biofabrication. 2011;3(2):021001.
142. Olubamiji AD, Izadifar Z, Si JL, Cooper DM, Eames BF, Chen DX. Modulating mechanical behaviour of 3D-printed cartilage-mimetic PCL scaffolds: influence of molecular weight and pore geometry. Biofabrication. 2016;8(2):025020.
143. Pati F, Jang J, Ha D, Kim SW, Rhie J, Shim J, et al. Printing three-dimensional tissue analogues with decellularized extracellular matrix bioink. Nature Communications. 2014;5.
144. Klein TJ, Rizzi SC, Reichert JC, Georgi N, Malda J, Schuurman W, et al. Strategies for zonal cartilage repair using hydrogels. Macromolecular bioscience. 2009;9(11):1049-58.
145. Khalil S, Sun W. Bioprinting endothelial cells with alginate for 3D tissue constructs. J Biomech Eng. 2009;131(11):111002.
146. Arlov Ø, Aachmann FL, Sundan A, Espevik T, Skjåk-Bræk G. Heparin-like properties of sulfated alginates with defined sequences and sulfation degrees. Biomacromolecules. 2014;15(7):2744-50.
147. Freeman I, Kedem A, Cohen S. The effect of sulfation of alginate hydrogels on the specific binding and controlled release of heparin-binding proteins. Biomaterials. 2008;29(22):3260-8.
148. Müller M, Öztürk E, Arlov Ø, Gatenholm P, Zenobi-Wong M. Alginate Sulfate–Nanocellulose Bioinks for Cartilage Bioprinting Applications. Ann Biomed Eng. 2016:1-14.
149. Öztürk E, Arlov Ø, Aksel S, Li L, Ornitz DM, Skjåk ' Bræk G, et al. Sulfated hydrogel matrices direct mitogenicity and maintenance of chondrocyte phenotype through activation of fgf signaling. Advanced Functional Materials. 2016;26(21):3649-62.
150. Prestwich GD. Hyaluronic acid-based clinical biomaterials derived for cell and molecule delivery in regenerative medicine. J Controlled Release. 2011;155(2):193-9.

151. Burdick JA, Prestwich GD. Hyaluronic acid hydrogels for biomedical applications. Adv Mater. 2011;23(12).
152. Müller M, Becher J, Schnabelrauch M, Zenobi-Wong M. Nanostructured Pluronic hydrogels as bioinks for 3D bioprinting. Biofabrication. 2015;7(3):035006.
153. Pescosolido L, Schuurman W, Malda J, Matricardi P, Alhaique F, Coviello T, et al. Hyaluronic acid and dextran-based semi-IPN hydrogels as biomaterials for bioprinting. Biomacromolecules. 2011;12(5):1831-8.
154. Wang X, Mäkitie AA, Partanen J, Tuomi J, Paloheimo K, Yliperttula M. The integrations of biomaterials and rapid prototyping techniques for intelligent manufacturing of complex organs. INTECH Open Access Publisher; 2013.
155. Ifkovits JL, Burdick JA. Review: photopolymerizable and degradable biomaterials for tissue engineering applications. Tissue Eng. 2007;13(10):2369-85.
156. Billiet T, Gevaert E, De Schryver T, Cornelissen M, Dubruel P. The 3D printing of gelatin methacrylamide cell-laden tissue-engineered constructs with high cell viability. Biomaterials. 2014;35(1):49-62.
157. Cohen DL, Lipton JI, Bonassar LJ, Lipson H. Additive manufacturing for in situ repair of osteochondral defects. Biofabrication. 2010;2(3):035004.
158. Fedorovich NE, Schuurman W, Wijnberg HM, Prins H, van Weeren PR, Malda J, et al. Biofabrication of osteochondral tissue equivalents by printing topologically defined, cell-laden hydrogel scaffolds. Tissue Engineering Part C: Methods. 2011;18(1):33-44.
159. Abbadessa A, Blokzijl M, Mouser V, Marica P, Malda J, Hennink W, et al. A thermo-responsive and photo-polymerizable chondroitin sulfate-based hydrogel for 3D printing applications. Carbohydr Polym. 2016;149:163-74.
160. Melchels FP, Dhert WJ, Hutmacher DW, Malda J. Development and characterisation of a new bioink for additive tissue manufacturing. Journal of Materials Chemistry B. 2014;2(16):2282-9.
161. Izadifar Z, Chang T, Kulyk W, Chen X, Eames BF. Analyzing biological performance of 3D-printed, cell-impregnated hybrid constructs for cartilage tissue engineering. Tissue Engineering Part C: Methods. 2015.

162. Shim J, Lee J, Kim JY, Cho D. Bioprinting of a mechanically enhanced three-dimensional dual cell-laden construct for osteochondral tissue engineering using a multi-head tissue/organ building system. J Micromech Microengineering. 2012;22(8):085014.
163. Shim J, Jang K, Hahn SK, Park JY, Jung H, Oh K, et al. Three-dimensional bioprinting of multilayered constructs containing human mesenchymal stromal cells for osteochondral tissue regeneration in the rabbit knee joint. Biofabrication. 2016;8(1):014102.
164. Deng D, Liu W, Cheema U, Mudera V, Hadjipanayi E, Brown RA. Less is more: New biomimetic approach to control spatial and temporal cell loading for tissue engineering. Journal of Biomedical Materials Research Part A. 2014;102(11):4108-17.
165. Kim Y, Sah RL, Grodzinsky AJ, Plaas AH, Sandy JD. Mechanical regulation of cartilage biosynthetic behavior: physical stimuli. Arch Biochem Biophys. 1994;311(1):1-12.
166. Grodzinsky AJ, Levenston ME, Jin M, Frank EH. Cartilage tissue remodeling in response to mechanical forces. Annu Rev Biomed Eng. 2000;2(1):691-713.
167. Kim T, Sharma B, Williams C, Ruffner M, Malik A, McFarland E, et al. Experimental model for cartilage tissue engineering to regenerate the zonal organization of articular cartilage. Osteoarthritis and cartilage. 2003;11(9):653-64.
168. Sharma B, Williams CG, Kim TK, Sun D, Malik A, Khan M, et al. Designing zonal organization into tissue-engineered cartilage. Tissue Eng. 2007;13(2):405-14.
169. Coates EE, Riggin CN, Fisher JP. Matrix molecule influence on chondrocyte phenotype and proteoglycan 4 expression by alginate ' embedded zonal chondrocytes and mesenchymal stem cells. Journal of Orthopaedic Research. 2012;30(12):1886-97.
170. Nguyen LH, Kudva AK, Guckert NL, Linse KD, Roy K. Unique biomaterial compositions direct bone marrow stem cells into specific chondrocytic phenotypes corresponding to the various zones of articular cartilage. Biomaterials. 2011;32(5):1327-38.
171. Nguyen LH, Kudva AK, Saxena NS, Roy K. Engineering articular cartilage with spatially-varying matrix composition and mechanical properties from a single stem cell population using a multi-layered hydrogel. Biomaterials. 2011;32(29):6946-52.
172. Wise JK, Yarin AL, Megaridis CM, Cho M. Chondrogenic differentiation of human mesenchymal stem cells on oriented nanofibrous scaffolds: engineering the superficial zone of articular cartilage. Tissue Engineering Part A. 2008;15(4):913-21.

173. Chhaya MP, Poh PS, Balmayor ER, van Griensven M, Schantz J, Hutmacher DW. Additive manufacturing in biomedical sciences and the need for definitions and norms. Expert review of medical devices. 2015;12(5):537-43.
174. Chen X. Dispensed-Based Bio-Manufacturing Scaffolds for Tissue Engineering Applications. International Journal on Engineering Applications (IREA). 2014;2(1):10-9.
175. Li M, Tian X, Zhu N, Schreyer DJ, Chen X. Modeling process-induced cell damage in the biodispensing process. Tissue Engineering Part C: Methods. 2009;16(3):533-42.
176. Yu Y, Zhang Y, Martin JA, Ozbolat IT. Evaluation of cell viability and functionality in vessel-like bioprintable cell-laden tubular channels. J Biomech Eng. 2013;135(9):091011.
177. Sarker M, Chen X. Modeling the Flow Behavior and Flow Rate of Medium Viscosity Alginate for Scaffold Fabrication With a Three-Dimensional Bioplotter. Journal of Manufacturing Science and Engineering. 2017;139(8):081002.
178. Chen X. Modeling and control of fluid dispensing processes: a state-of-the-art review. The International Journal of Advanced Manufacturing Technology. 2009;43(3):276-86.
179. Chen X, Li M, Ke H. Modeling of the flow rate in the dispensing-based process for fabricating tissue scaffolds. Journal of manufacturing science and engineering. 2008;130(2):021003.
180. Adamkiewicz M, Rubinsky B. Cryogenic 3D printing for tissue engineering. Cryobiology. 2015;71(3):518-21.
181. Cohen DL, Lo W, Tsavaris A, Peng D, Lipson H, Bonassar LJ. Increased mixing improves hydrogel homogeneity and quality of three-dimensional printed constructs. Tissue engineering Part C: methods. 2010;17(2):239-48.
182. Ning L, Xu Y, Chen X, Schreyer DJ. Influence of mechanical properties of alginate-based substrates on the performance of Schwann cells in culture. Journal of Biomaterials science, Polymer edition. 2016;27(9):898-915.
183. Cao N, Chen X, Schreyer D. Influence of calcium ions on cell survival and proliferation in the context of an alginate hydrogel. ISRN Chemical Engineering. 2012;2012.
184. He Y, Yang F, Zhao H, Gao Q, Xia B, Fu J. Research on the printability of hydrogels in 3D bioprinting. Sci Rep. 2016 Jul 20;6:29977.
185. Little CJ, Bawolin NK, Chen X. Mechanical properties of natural cartilage and tissue-engineered constructs. Tissue Engineering Part B: Reviews. 2011;17(4):213-27.

186. Huang BJ, Hu JC, Athanasiou KA. Cell-based tissue engineering strategies used in the clinical repair of articular cartilage. Biomaterials. 2016;98:1-22.

Chapter 3: 3D Printing of Porous Alginate/gelatin Hydrogel Scaffolds and Their Mechanical Property Characterization

This chapter has been published as You, F., Wu, X., Chen, X. (2017). 3D printing of porous alginate/gelatin hydrogel scaffolds and their mechanical property characterization. International Journal of Polymeric Materials and Polymeric Biomaterials, 66(6), 299-306. According to the Copyright Agreement, "the authors retain the right to include the journal article, in full or in part, in a thesis or dissertation".

3.1 Abstract

Hydrogel scaffolds with well-defined internal structure and interconnected porosity are important for tissue engineering. 3D Bioplotting technique supplemented with thermal/submerged ionic crosslinking process was used to fabricate hydrogel scaffolds. Six scaffold geometries were fabricated and their influence on mechanical performance was investigated. 0/90-0.8 group with the lowest porosity showed the highest Young's modulus while the Shift group showed the lowest Young's modulus. Same trend has also been observed for the dynamic modulus of each group. Results demonstrated that the mechanical performance of hydrogel scaffolds can be tuned by changing the internal structure parameters including strands orientation and spacing between strands.

3.2 Introduction

Hydrogels are water-swollen polymeric networks, making them an ideal class of materials for applications in tissue engineering and drug delivery (1, 2). Due to their high-water content, hydrogels could mimic soft tissue better more than other type of polymeric biomaterials. They are also attractive for cell delivery and encapsulation as they are able to overcome the shortcomings of the traditional post-processing cell seeding, including poor cell-seeding efficiency and non-controllable cell distribution (3, 4, 5). As scaffolding materials, hydrogels need interconnecting porous structure to ensure continuous and sufficient supply of nutrients and removal of metabolites, which is of vital importance for the cell functions of encapsulated cells. Although the insoluble cross-linked network generally exhibits permeability for oxygen, nutrients, and other water-soluble biomolecules to some extent, it is not good enough for many

tissue engineering applications (6). Currently, various rapid prototyping techniques have been reported to process hydrogel precursors into porous hydrogel scaffolds (7, 8) and among them, three-dimensional (3D) Bioplotting has shown to be a promising technique. By using the 3D Bioplotter, the biomaterial solution is dispensed onto a platform through a layer-by-layer manner, forming 3D porous scaffolds.

Alginate has been widely used to fabricate hydrogel scaffolds for tissue engineering application (9). It is a biocompatible and biodegradable natural polysaccharide and its gelation can be induced through multivalent cationic transfer. However, alginate lacks adhesion sites for cells, thus limiting cell adhesion and cell functions (10). For improvement, cell-recognition peptides (e.g., RGD peptides) (11) and/or other biomaterials can be added or mixed into alginate hydrogel to enhance cell adhesion. Gelatin (12) is a naturally-derived biopolymer from collagen, which contains motifs such as RGD sequences, thus being able to improve the cellular behavior. As a biopolymer, gelatin is also known for its suitability for hydrogel printing due to its easy preparation and manipulation (13). Therefore, it is rationale to develop a composite hydrogel precursor consisting of alginate and gelatin to fabricate porous hydrogel scaffolds, as reported in the present study.

To fabricate hydrogel scaffolds by mean of 3D Bioplotting, the liquid hydrogel precursor is loaded into the dispensing head, dispensed by pressurized air and cross-linked immediately after dispensing. Two methods of crosslinking are typically employed for the bioprinting of alginate hydrogel, which are (i) aerosol spraying crosslinking (14) and (ii) submerged crosslinking (15). The former is usually followed by a submerged crosslinking process to strengthen the cross-linked network (16). Utilizing aerosol spraying crosslinking may cause the issue that the printed hydrogel precursor sinks and designed porous structure collapsed. On the other hand, instantaneous crosslinking can be achieved by submerged crosslinking process and help to maintain the shape of the printed hydrogel strand and contribute to a more accurate porous structure. Therefore, the 3D biolpotting technique supplemented with a submerged crosslinking process will be used to produce porous hydrogel scaffolds with the aim to resolve the above-mentioned issues.

It is known that a common disadvantage of porous hydrogel scaffolds is their relatively weak mechanical properties, which may result in a failure to match the targeted tissue. Previous studies showed that the mechanical properties can be altered and adjusted by varying the internal

structures of scaffolds (17, 18). Notably, these studies focused on synthetic polymer or inorganic biomaterials, yet the influence of scaffold structure on the mechanical properties of hydrogel scaffolds has not been well known and documented. Therefore, in this study, with the help of the submerged/thermal crosslinking supplemented 3D Bioplotting technique, various internal structures were designed into the porous hydrogel scaffolds aim to tune and enhance their mechanical performance.

3.3 Materials and Methods

3.3.1 Preparation and Rheology of Hydrogel Precursor

Type A gelatin from porcine skin (Sigma Aldrich) and low viscosity sodium alginate derived from brown algae (Sigma Aldrich) were dissolved in PBS, respectively. The alginate solution was then mixed with the gelatin solution, at concentrations of 6% (w/v) gelatin and 3% (w/v) alginate, under constant stirring, which was kept at 37°C for 2 h to remove remaining air bubbles. Rheological properties of the hydrogel precursor (n=3) were characterized using a rheometer (Brookfield, USA). Specifically, the shear stress was measured at the shear rates varying from 0 to 100 s^{-1} with the temperature fixed at 37 °C; while the storage modulus (G') and loss modulus (G") were assessed by applying 5% strain within the linear viscoelastic region over a frequency range between 1 and 100 rad s^{-1}. The gel temperature of the composite hydrogel precursor was tested over a temperature ramp starting from 45 °C then decreased to 15 °C (AR G2 rheometer, TA Instruments, USA). The rate of temperature change was 1 °C min^{-1}, the oscillation frequency was 1 Hz and the constant shear amplitude was 50 Pa. The gel point describes the temperature of a material when it solidifies, which is defined by the intersection of the storage modulus G' curve and the loss modulus G" curve during temperature decrease at an oscillatory measurement.

3.3.2 Scaffold Fabrication

Petri dishes used as plotting platforms were treated with sterile 0.1% (w/v) polyethylenimine (PEI, Alfa Aesar, Mw: 60000) in phosphate buffered saline (PBS) and incubated overnight at 37 °C. The PEI-coated surfaces were washed with double distilled water prior to use. 3D porous scaffolds were produced by sequential strand deposition using the Bioplotter pneumatic dispensing system (EnvisionTec, Germany). The designed structure is

specified and programed by the CAD/CAM software and then translated into numerical codes by the Bioplotter software for the layer-by-layer scaffold fabrication. A 27-gauge plastic dispense tip (EFD Nordson, Switzerland) with an inner tip diameter of 200μm was used in this study. The composite hydrogel precursor was plotted into the crosslinking medium containing 100mM calcium chloride (Sigma Aldrich), 0.1% (w/v) PEI on the cooling platform (Figure 3.1). Six internal structures were designed and fabricated, which are 1) each layer adhered to the underlying layer perpendicularly to form a 0°/90° with a strand spacing of 0.8 mm (0/90-0.8); 2) each layer adhered to the underlying layer to form a 0°/90° with a strand spacing of 1 mm (0/90-1); 3) the second layer adhered to the underlying layer 0°/45° and the third layer adhered to the first layer 0°/135° with a strand spacing of 1 mm (0/45/135-1); 4) each layer adhered to the underlying layer perpendicularly to form a 0°/45° with a strand spacing of 1 mm (0/45-1); 5) gradient scaffolds exhibiting distinct strand spacing variation with depth (Grad); 6) scaffolds with shifted pattern (Shift, means there is a shift between adjacent printed strands along X or Y axis). The illustration of these designed structures is presented in Figure 3.5, along with their characterization.

3.3.3 Characterization of Hydrogel Scaffolds

Hydrogel scaffold swelling was assessed by measuring the scaffold weight over the first 3 days upon their immersion in PBS. Two experimental setups were analyzed with the hydrogel scaffolds. For the first setup, hydrogel scaffolds were freshly printed and their swelling behavior at 21°C were assessed immediately after crosslinking. In the second setup, the samples were freshly printed but kept at 37 °C during the experiment. The property of swelling is characterized and reported by using a ratio of the hydrogel weight over its initial weight.

The FTIR spectra were scanned under a room temperature with the IlluminatIR II inVia Reflex (Smiths Detection) equipped with an ATR objective. The scanning range is from 650 to 4000 cm^{-1} with a resolution of 4 cm^{-1}. Scaffolds were freeze-dried and grinded into powder before examination. The top images and cross-sectional images of hydrogel scaffolds with different structures were taken with a microscope (Leica, Switzerland). The compressive moduli of scaffolds (with a size of 10×10×5 mm) were tested using a Biodynamic testing machine (Bose) at a cross-head speed of 0.01 mm/s. The Young's modulus was calculated from the linear region of the stress-strain curve for all samples. Creep recovery measurements were performed at

37 °C for 24 h in PBS after a 50% deformation. Then, the stress was removed and the samples could recover for 24 h. The values reported are the average of five specimens. The percentage recovery was calculated using the equation, i.e., Recovery (%) = scaffold height after 24 h recovery/initial scaffold height×100%. Dynamic testing was performed by applying 15% sinusoidal deformation at 1.0 Hz (19). The dynamic modulus was determined from a ratio of the stress amplitude over the strain amplitude after a steady-state response of more than 20 cycles (20).

3.3.4 Statistics

For quantitative analysis, Student's t tests were used to assess differences between two groups and multiple comparisons were performed via one-way ANOVA test using SPSS. P values <0.05 were considered statistically significant. Data are expressed as the mean values ±standard deviation (SD).

3.4 Results and Discussion

3.4.1 Hydrogel Crosslinking

The fabrication of porous alginate/gelatin hydrogel scaffolds was a combination of physical and chemical crosslinking processes (Figure 3.1), where the alginate/gelatin hydrogel in a liquid form at 37°C solidified with the temperature decreased due to the temperature-dependent hysteresis behavior of gelatin and meanwhile, alginate was cross-linked with the presence of calcium ions. The fabrication platform (Figure 3.1D) of the 3D bioplotter (Figure 3.1C) was connected to a cooling tube (Figure 3.1E) for the control of platform temperature. By adjusting the platform temperature below the gel temperature, cross-linking took place in the hydrogel precursor Based on the results showed in Figure 3.2C, the gel temperature of the hydrogel precursor was found as 22.3°C, and thus the temperature of the plotting platform was set at 10 °C to ensure the adequate thermal gelation of the composite hydrogel.

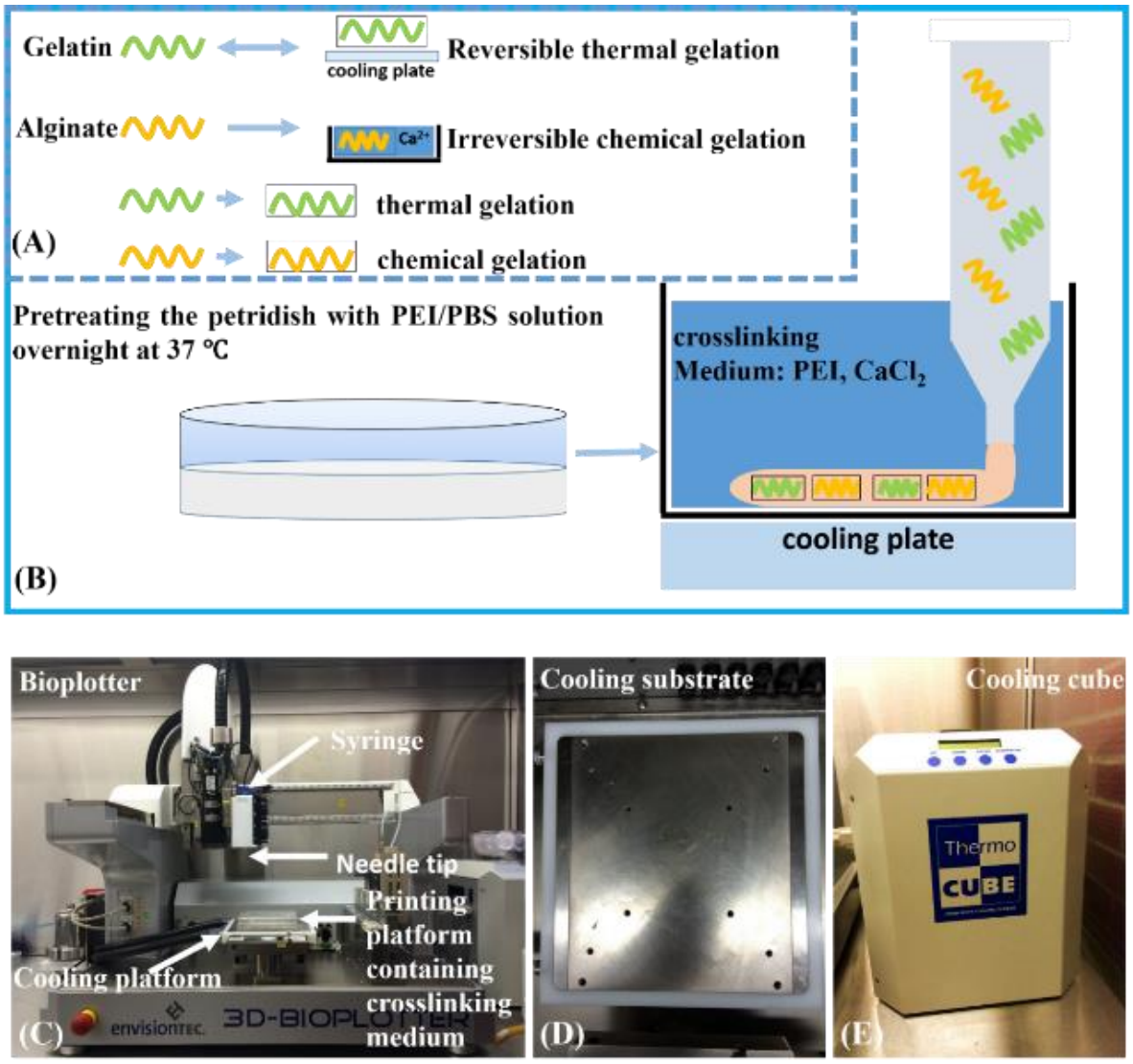

Figure 3.1 (A) Underlying mechanism; (B) Schematics of the hydrogel gelation mechanism based on reversible thermal gelation of gelatin and irreversible chemical gelation of alginate. Instantaneous gelation of gelatin and alginate due to the low temperature of the cooling substrate as well as the $CaCl_2$ bath; Details of the 3D Bioplotter hardware (C-E): (C) 3D Bioplotter; (D) cooling substrate; (E) Cooling tube.

3.4.2 Hydrogel Characterization

3.4.2.1 Viscosity

The viscosity of hydrogel precursor affects the printing process mainly via its flow through the dispense tip, where the major pressure drop is caused. Hydrogel precursor with a high viscosity would probably clog the dispensing needle tip, thus disturbing the subsequent printing

process. In the other hand, if the viscosity of hydrogel precursors is too low, the printed strands tend to spread, thus causing the merge of two adjacent strands of the first layer or collapse of the other layers. As such, the viscosity of hydrogel precursor must be properly selected and formed prior to its bioprinting. As shown in Figure 3.2, at the shear rate near to of 0 s^{-1}, the viscosity has its maximum value about 1765 mPa·s; and as the shear rate increases, the viscosity decreases in a non-linear fashion, reaching a value of 768 mPa·s at a shear rate of 100 s^{-1} (Figure 3.2A). The curves of the viscosity and shear stress versus the shear rate (Figure 3.2A) illustrate the hydrogel precursor is shear-thinning. The curves of storage modulus (G') and loss modulus (G") of the hydrogel precursor versus the frequency is shown in Figure 3.2B. It is seen that the viscous component (loss modulus, G") is higher than the elastic component (storage modulus, G') over the frequency varying from 1 to 100 rad/s at 37°C, which suggests the hydrogel precursor is not crosslinked prior to its printing. A representative of the gel-point determination is shown in Figure 3.2C, where the temperature at which the sol-to-gel transition occurs (G'=G") is determined by the intersection storage modulus G' and loss modulus G"(13). The gel temperature is used as a reference temperature for adjusting the temperature of the fabrication platform.

3.4.2.2 Swelling

Swelling ratio at 21°C experienced an increase in hydrogel weight caused by PBS uptake of the hydrogel scaffold, with a 1.2 to 1.4-fold increase started from fresh hydrogel scaffold. Hydrogels equilibrium was reached after 24 h and the fold increase remained between 1.4-1.5. Experimental conditions at 37°C led to a swelling ratio of 1.4 after 3 h, but for longer incubation the weight dropped to approximate 79% of the original weight (Figure 3.3). Hydrogels are known for their swelling behavior, which is important for 3D bioprinting since it changes the printed strand size and resulting construct in culture. From the storage and loss modulus of hydrogel precursors (Figure 3.2C), hydrogel precursor showed liquid behavior at 37°C. Due to the thermal reversible crosslinking of gelatin component, the liquid state of gelatin at 37°C accelerates hydrogel degradation, while not similar changes were observed for samples at 21°C where gelatin component was still in a solid state.

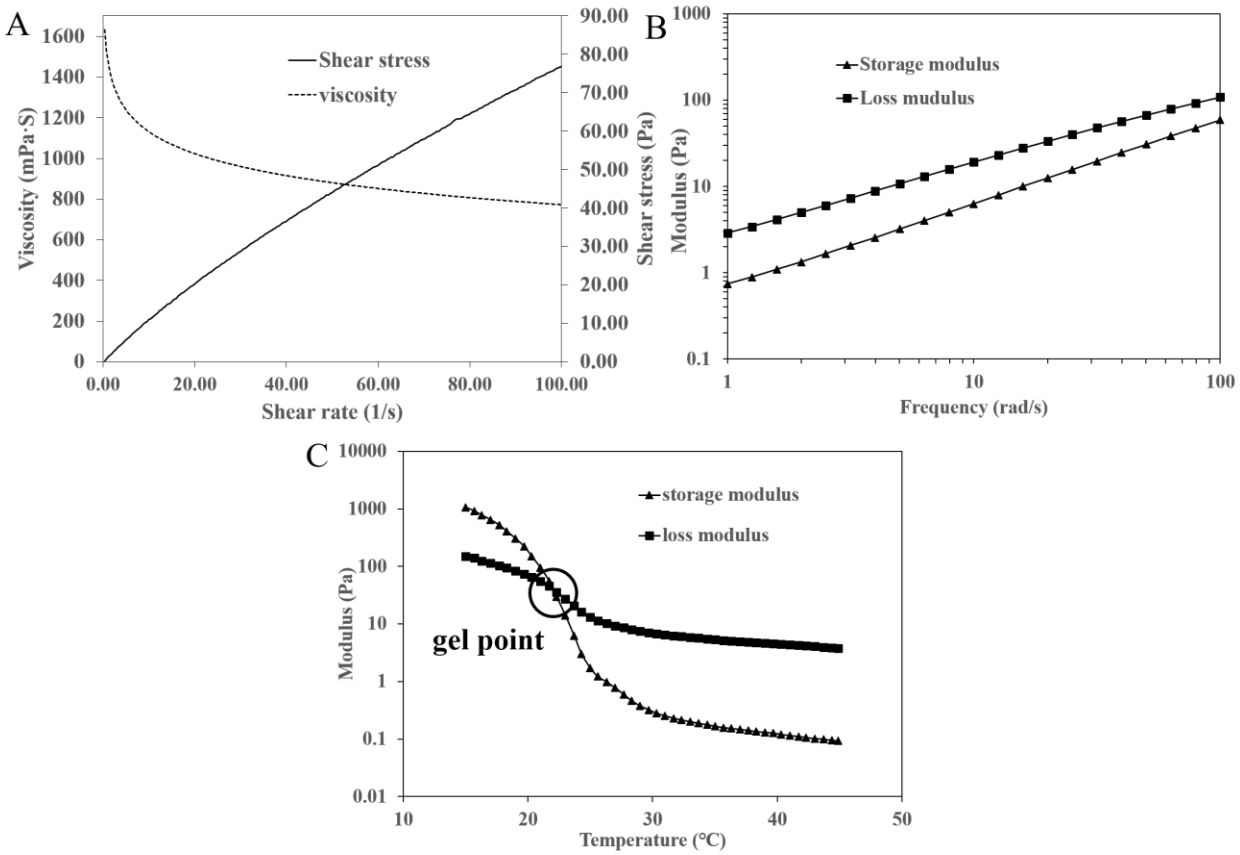

Figure 3.2 Rheological properties of hydrogel composites. (A) Viscosity and shear stress are plotted over a shear rate from 0.0001 to 100 S^{-1}; (B) Storage modulus G' and loss modulus G'' of the composite hydrogel precursor over a frequency from 1 to 100 rad/s ;(C) Representative image of determining the gel point, which is defined as the intersection of storage modulus G' and loss modulus G'' during cooling from 45°C to 15°C.

3.4.2.3 FTIR Analysis

FTIR spectra of alginate/gelatin composite hydrogel is shown in Figure 3.4. The spectrum demonstrates the characteristic absorption bands of the polysaccharide structure of alginate including 1319 cm^{-1} (C–O stretching), 1021 cm^{-1}, (C–O–C stretching). The absorption bands at around 1557 cm^{-1} are the stretching peaks of carboxylate salt groups of alginates. The absorption peaks at 1621 and 1557 cm^{-1} represent the vibration of C=N of gelatin indicating the formation of Schiff's base. Notably, a strong peak of amide II at 1543 cm^{-1}, a characteristic of gelatin, is absent in the composite hydrogel spectrum, suggesting the involvement of this group in the crosslinking reaction (21).

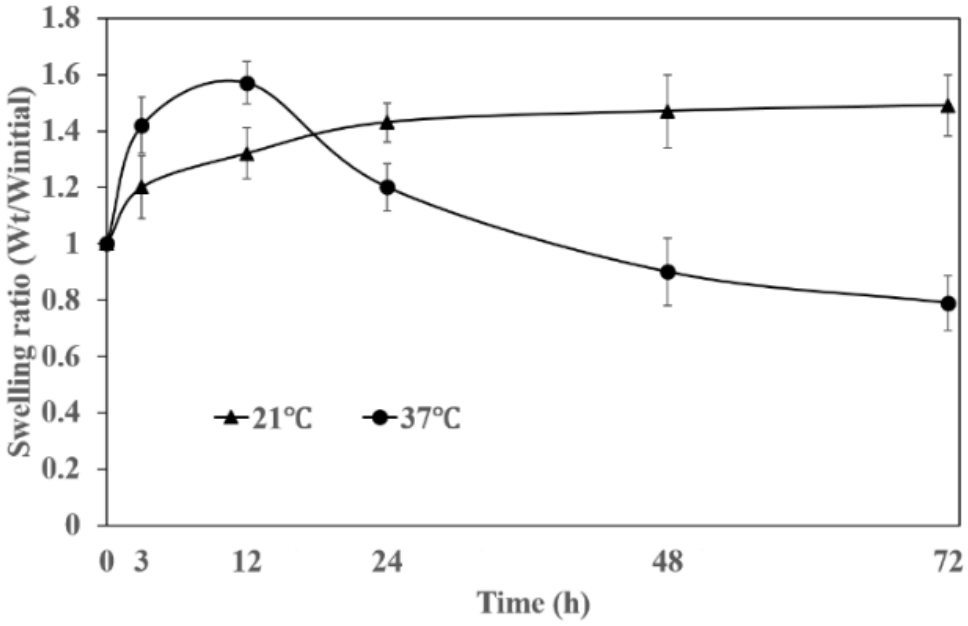

Figure 3.3 Swelling of hydrogel scaffolds over 3 days at two experimental conditions. At each time point, statistical difference ($p<0.05$, $n=4$) was observed between two groups.

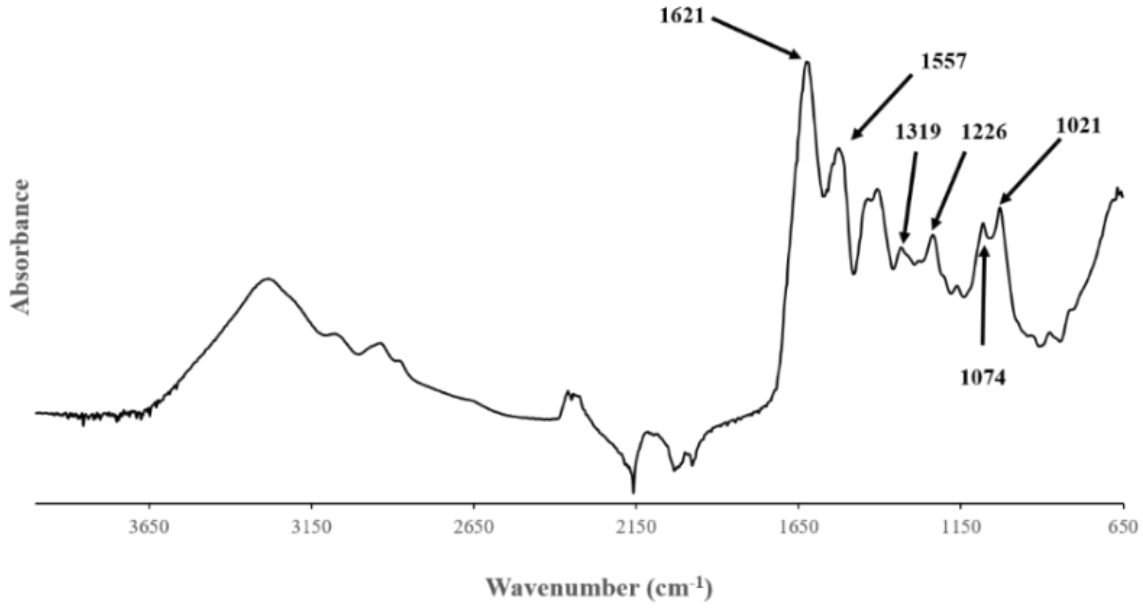

Figure 3.4 ATR-FTIR spectra of sodium alginate/gelatin composite hydrogel.

3.4.2.4 Scaffolds Morphology and Architecture

Hydrogel scaffolds with different internal architecture were successfully fabricated. Different internal architecture was designed and fabricated by changing the strand/fiber orientation and spacing. The CAD 3D models, 2D sections and the morphology of each scaffold group are shown in Figure 3.5. Microscopic images of scaffolds show a well-defined geometry compared with the CAD models. Both 0/90-0.8 and 0/90-1 scaffold groups have no strand distance offset between consecutive layers and the strand deposition angle of 0°/90° created quadrangular pores, the only difference between these two groups is the strand spacing. Grad scaffold group has a continuous offset (0.1 mm) between consecutive layers. The Shift scaffold group owns a shifted pattern, with a constant strand spacing offset of 0.5 mm every other layer. By changing the strand orientation in successive layers, 0/45-1 and 0/45/135-1 scaffold groups were generated, forming polygonal pores.

3.4.3 Mechanical Analysis

Characterization of the mechanical characteristics of the scaffolds is of vital importance in many tissue engineering applications. Mechanical properties of each scaffold group are shown in Figure 3.6. It is evident that 0/90-0.8 group, which has the smallest strand spacing of all groups, owning the highest Young's modulus (92.36±15.83 KPa) and dynamic modulus (798.0±25.8 KPa) among all groups. This is because the 0/90-0.8 scaffold group has the lowest porosity. When increasing the strand spacing to 1 mm (0/90-1 scaffold group), both of its Young's modulus (53.8±2.9 KPa) and dynamic modulus (423.0±87.6 KPa) demonstrate a significant decrease. Bigger strand spacing lowers the mechanical performance, indicating the expected relationship between porosity of the scaffolds and the corresponding mechanical properties. When changing the strand with 45° angle steps between two successive layers (0/45-1), its Young's modulus (77.1±44KPa) and dynamic modulus (614.4± 23.0KPa) are significantly higher than that of 0/90-1 group which has the same strand spacing. This is probably because this angular design of scaffolds affords more contact area between the strands from adjacent layers, which offers more mechanical strength. (Figure 3.7B) (22) However, successively changing the orientation of plotting strands in adjacent layers (0/45/135-1) will further reduce the effective contact area (Figure 3.7C) and thus weakening its mechanical performance.

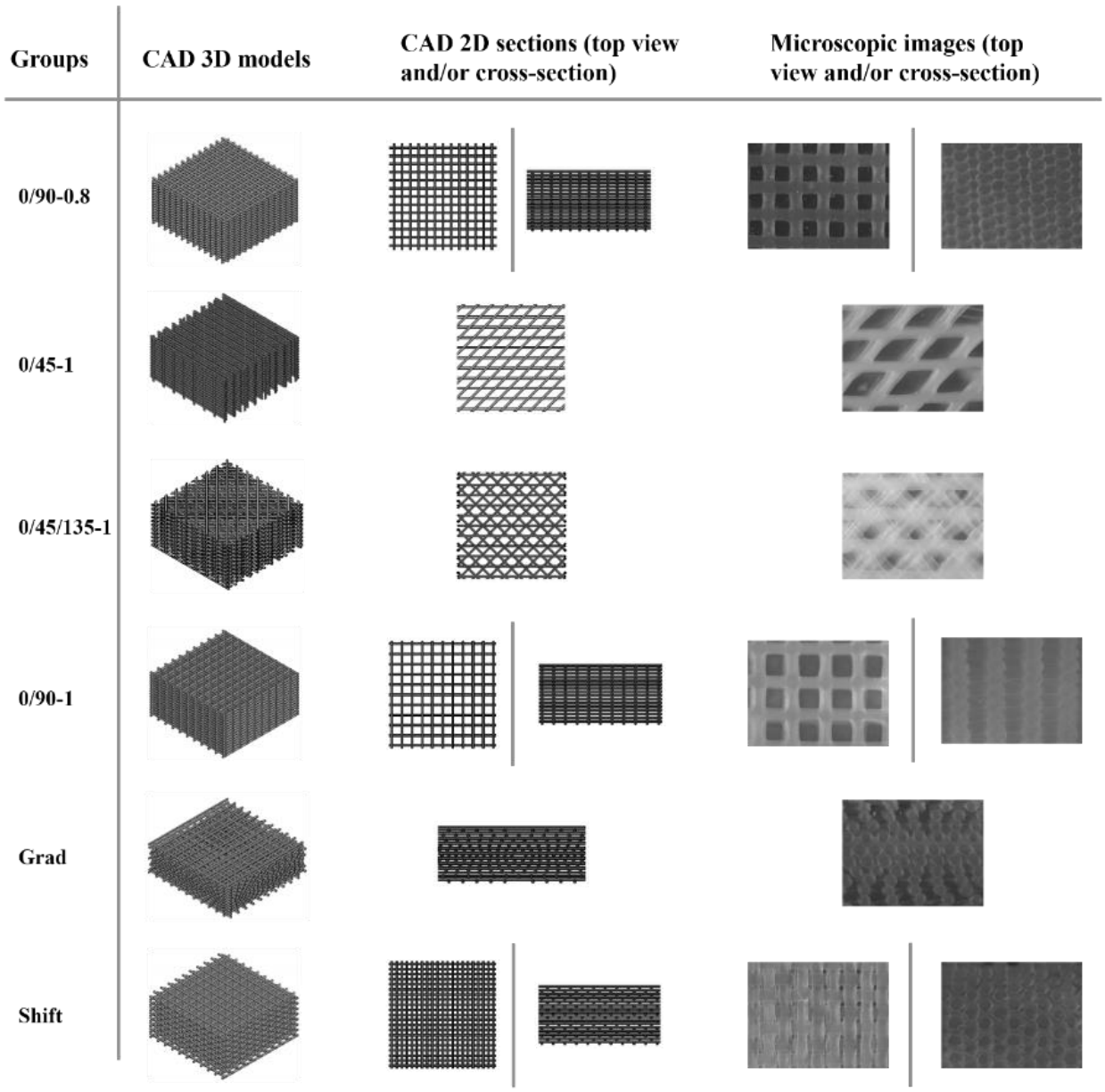

Figure 3.5 CAD 2D sections, 3D models and microscopic pictures for scaffolds designed and produced by 3D plotting techniques for this study.

When changing the strand spacing distribution (Grad and Shift group), the mechanical moduli of the scaffolds are impaired compared with 0/90-1 scaffold group which rigorously repeats the exactly same pattern. This indicated that the relative positioning of the strands from each layer also plays a key role in determining the final mechanical performance. Shift scaffold group showed the lowest Young's modulus (20.3 ±8.0 KPa) and dynamic modulus (103.3±25.0 KPa) among all scaffold groups, which is likely attributable to the structure of its shifted pattern.

A large proportion of the 15% strain probably is mainly counteracted by the deformation of internal pores due to its unique shifted structure. (Figure 3.7D) According to the design, it is obvious that the Grad scaffold group has the second lowest porosity among all groups, which means its mechanical properties probably rank second only to the 0/90-0.8 group. However, it turns out that Grad group does not show an elevated mechanical performance as expected, indicating that it is the internal structure rather than porosity or strands contact area that determines the mechanical properties for the Grad group. The principle behind this is similar with Shift scaffold group. Most of 15% strain is likely to be absorbed by the internal pores due to the strands offsets and thus reducing the ability of scaffolds to resist compression.

Therefore, scaffolds porosity, contact area between strands and spacing variation are believed to be three key factors that influence the mechanical performance of scaffolds. Mechanical difference between the 0/90-1 scaffold and 0/90-0.8 scaffold can be explained by their different porosities. Effective contact area between strands illustrate why 0/45-1 scaffold group exhibited higher modulus in comparison with 0/90-1 and 0/45/135-1 groups. Strands spacing variation (Grad and Shift scaffolds) lead to an inferior mechanical performance to 0/90-1 group.

Scaffold resilience upon deformation is also very important for applications in tissue engineering. The influence of architecture of a scaffold on its resilience was characterized by a recovery experiment and shown in Figure 3.6C. 0/90-0.8 scaffolds recovered approximately 63% of their initial height after a deformation of 50%, while the 0/90-1 scaffolds recovered 64%. 0/45-1, 0/45/135-1, Grad and Shift scaffolds groups recovered 68%, 73%, 80% and 82.5% of their initial height, respectively. Interestingly, greater stiffness is associated with the lower recovery ability. For instance, the 0/90-0.8 group has a compressive modulus of 92KPa, which is the highest of all groups, yet showed the lowest recovery of 71%. Shift scaffold group own the lowest Young's modulus while it has the highest recovery ability among all groups. This is probably because that given a fixed compression deformation, the groups with higher stiffness would experience higher stress, which may result in a less recovery. Recovery is also related to the internal structure. When most deformation is absorbed by the internal pores of scaffolds (Shift and Grad scaffold group), its ability to recover increases.

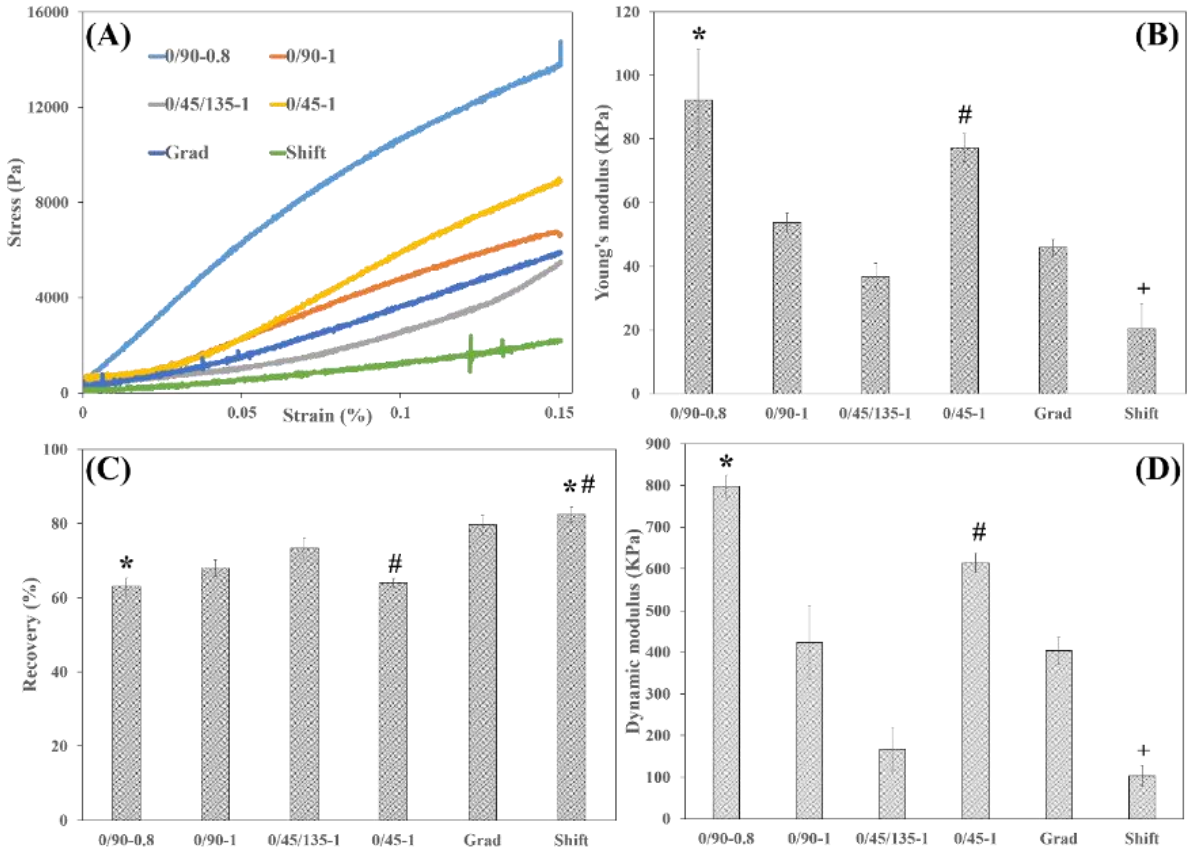

Figure 3.6 (A) Representative strain-stress curves for each group; (B) Young's modulus (*: $p<0.05$ compared with other groups, #: $p<0.05$ compared with other groups, +: $p<0.05$ compared with other groups, n=3); (C) recovery rate (*, #: $p<0.05$, n=3) and (D) dynamic modulus of each scaffold group (*: $p<0.05$ compared with other groups, #: $p<0.05$ compared with other groups, +: $p<0.05$ compared with other groups, n=3).

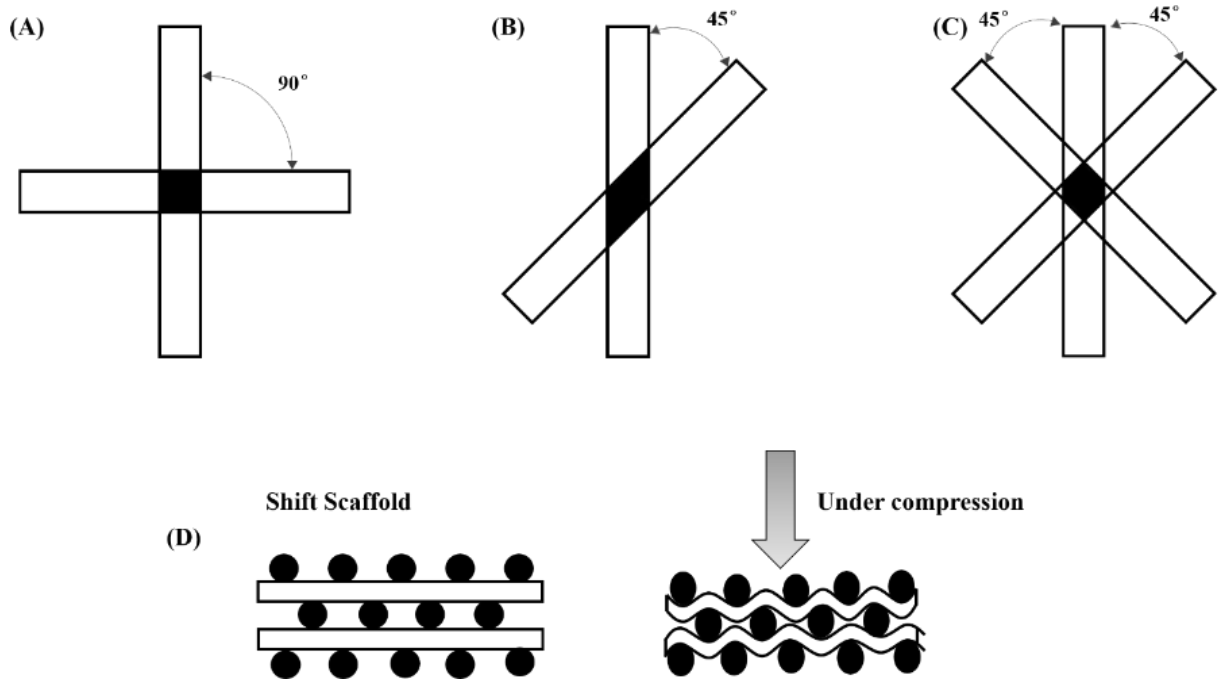

Figure 3.7 The contact area (in black) of the strands with angular design: (A) 0/90-1; (B) 0/45-1; (C) 0/45/135-1. (D) The deformation of internal pores is responsible for the initial strain of Shift scaffolds.

Representative curves for stress vs time and strain vs time of each scaffold group are shown in Figure 3.8. For solid materials, the applied force would result in the instantaneous strain without lags, in this case, the phase angle is 0°. For ideal liquid, the strain lags behind the stress by 90° (23). Because of the viscoelasticity of the porous hydrogel scaffolds, the stress-strain response of all scaffold groups exhibited a phase lag between 0° and 90°.

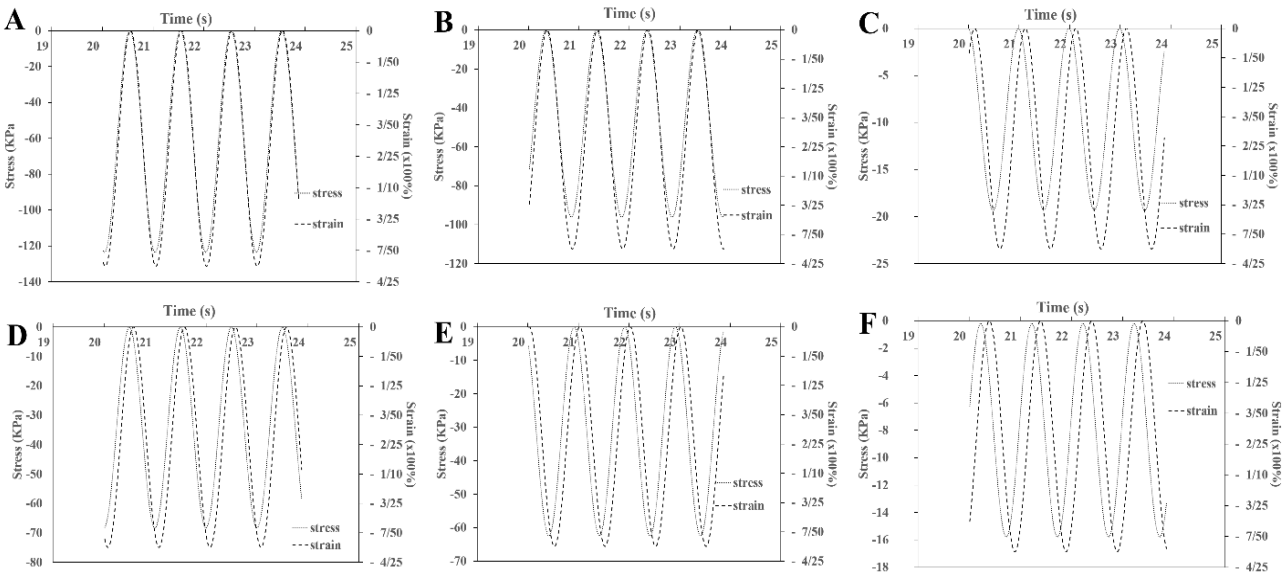

Figure 3.8 Stress vs time and strain vs time for groups of (A) 0/90-0.8, (B) 0/90-1, (C) 0/45/135-1, (D) 0/45-1, (E) Grad, (F) Shift at the loading frequency of 1.0 Hz.

Notably, the fact that the compressive modulus of each scaffold group is much lower than the dynamic moduli at physiological loading frequency suggests that static moduli are not sufficiently representative of the functional response of the viscoelastic materials. This is especially relevant in tissue engineering studies aiming to achieve a functional tissue substitute. Though many researchers used the unconfined compression modulus of tissue constructs as a measure of matrix elaboration (24, 25), the present findings indicate that it is also important to report the dynamic unconfined compression modulus as it may be more close to physiological conditions and thus more representative for tissue engineering application (26).

Most commercially available polymeric materials maintain structural integrity by applying cytotoxic chemicals or high cure temperatures and lack sufficient mechanical stability during printing process. Moreover, the material needs to be kept in liquid state as well as a relative low viscosity while in the dispensing syringe to avoid possible clogging of needle tip, but must be solidified immediately after contacting the platform or dispensing into crosslinking medium to maintain the desired geometry. Therefore, developing a biomaterial suitable for 3D bioprinting is still challenging. The hydrogel composite and fabrication technique reported in this study fulfill these requirements. Compared with previous work of our lab (15), the difference is the gelatin

component, which was included in the material presented in this study. The addition of gelatin induced immediate gelation of the preheated hydrogel precursors when contacting the cooled substrate due to the thermoreversibility of gelatin, which is good for maintaining the geometry of the dispensed strands. Although the chemical crosslinking of alginate component is slower and irreversible compared with physical crosslinking process of gelatin, it makes the scaffold stable under culture conditions and facilitates long-term stability. Ahn et al. (16) prepared alginate hydrogel scaffolds using an aerosol spraying cross-linking technique, which is achieved by an aerosol humidifier spraying a cross-linking agent ($CaCl_2$) mist to cross-link the dispensed alginate strands. Dispensed strands are usually not sufficiently cross-linked by this technique, resulting in the undesired movement during fabrication and loss of porous structure. In the present study, simultaneous crosslinking after dispensing is attained by the supplement of the thermoreversible gelatin component and a submerged ionic cross-linking process.

3.5 Conclusions

In this study, porous alginate/gelatin hydrogel scaffolds were fabricated by the 3D Bioplotting technique supplemented with thermal crosslinking and submerged ionic crosslinking processes. Various internal structures were designed into the scaffolds by changing the orientation and spacing of plotting strands and their influence on the mechanical properties were investigated. Porosity, contact area between strands and spacing variation are believed to be three key factors that influence the mechanical performance of scaffolds. Notably, dynamic modulus of each scaffold was generally much higher than their Young's modulus suggesting that it is also important to characterize the dynamic compression modulus in future study since it may be closer to physiological conditions and thus more representative for tissue engineering application.

References

1. Kopeček J. Hydrogel biomaterials: a smart future? Biomaterials. 2007;28(34):5185-92.

2. Slaughter BV, Khurshid SS, Fisher OZ, Khademhosseini A, Peppas NA. Hydrogels in regenerative medicine. Adv Mater. 2009;21(32-33):3307-29.

3. Awad HA, Wickham MQ, Leddy HA, Gimble JM, Guilak F. Chondrogenic differentiation of adipose-derived adult stem cells in agarose, alginate, and gelatin scaffolds. Biomaterials. 2004;25(16):3211-22.

4. Martin I, Wendt D, Heberer M. The role of bioreactors in tissue engineering. Trends Biotechnol. 2004;22(2):80-6.

5. Hollister SJ. Porous scaffold design for tissue engineering. Nature materials. 2005;4(7):518-24.

6. Gaetani R, Doevendans PA, Metz CH, Alblas J, Messina E, Giacomello A, et al. Cardiac tissue engineering using tissue printing technology and human cardiac progenitor cells. Biomaterials. 2012;33(6):1782-90.

7. Billiet T, Vandenhaute M, Schelfhout J, Van Vlierberghe S, Dubruel P. A review of trends and limitations in hydrogel-rapid prototyping for tissue engineering. Biomaterials. 2012;33(26):6020-41.

8. Landers R, Mülhaupt R. Desktop manufacturing of complex objects, prototypes and biomedical scaffolds by means of computer-assisted design combined with computer-guided 3D plotting of polymers and reactive oligomers. Macromolecular Materials and Engineering. 2000;282(1):17-21.

9. Schloßmacher U, Schröder HC, Wang X, Feng Q, Diehl-Seifert B, Neumann S, et al. Alginate/silica composite hydrogel as a potential morphogenetically active scaffold for three-dimensional tissue engineering. RSC Advances. 2013;3(28):11185-94.

10. Fonseca KB, Maia FR, Cruz FA, Andrade D, Juliano MA, Granja PL, et al. Enzymatic, physicochemical and biological properties of MMP-sensitive alginate hydrogels. Soft Matter. 2013;9(12):3283-92.

11. Liu X, Peng W, Wang Y, Zhu M, Sun T, Peng Q, et al. Synthesis of an RGD-grafted oxidized sodium alginate–N-succinyl chitosan hydrogel and an in vitro study of endothelial and osteogenic differentiation. Journal of Materials Chemistry B. 2013;1(35):4484-92.

12. Young S, Wong M, Tabata Y, Mikos AG. Gelatin as a delivery vehicle for the controlled release of bioactive molecules. J Controlled Release. 2005;109(1):256-74.
13. Billiet T, Gevaert E, De Schryver T, Cornelissen M, Dubruel P. The 3D printing of gelatin methacrylamide cell-laden tissue-engineered constructs with high cell viability. Biomaterials. 2014;35(1):49-62.
14. Ahn S, Lee H, Kim G. Functional cell-laden alginate scaffolds consisting of core/shell struts for tissue regeneration. Carbohydr Polym. 2013;98(1):936-42.
15. Rajaram A, Schreyer DJ, Chen DX. Use of the polycation polyethyleneimine to improve the physical properties of alginate–hyaluronic acid hydrogel during fabrication of tissue repair scaffolds. Journal of Biomaterials Science, Polymer Edition. 2015;26(7):433-45.
16. Ahn S, Lee H, Bonassar LJ, Kim G. Cells (MC3T3-E1)-laden alginate scaffolds fabricated by a modified solid-freeform fabrication process supplemented with an aerosol spraying. Biomacromolecules. 2012;13(9):2997-3003.
17. Wu C, Luo Y, Cuniberti G, Xiao Y, Gelinsky M. Three-dimensional printing of hierarchical and tough mesoporous bioactive glass scaffolds with a controllable pore architecture, excellent mechanical strength and mineralization ability. Acta biomaterialia. 2011;7(6):2644-50.
18. Sobral JM, Caridade SG, Sousa RA, Mano JF, Reis RL. Three-dimensional plotted scaffolds with controlled pore size gradients: effect of scaffold geometry on mechanical performance and cell seeding efficiency. Acta Biomaterialia. 2011;7(3):1009-18.
19. Armstrong CG, Bahrani AS, Gardner DL. In vitro measurement of articular cartilage deformations in the intact human hip joint under load. J Bone Joint Surg Am. 1979 Jul;61(5):744-55.
20. Huang AH, Stein A, Tuan RS, Mauck RL. Transient exposure to transforming growth factor beta 3 improves the mechanical properties of mesenchymal stem cell–laden cartilage constructs in a density-dependent manner. Tissue Engineering Part A. 2009;15(11):3461-72.
21. Sarker B, Papageorgiou DG, Silva R, Zehnder T, Gul-E-Noor F, Bertmer M, et al. Fabrication of alginate–gelatin crosslinked hydrogel microcapsules and evaluation of the microstructure and physico-chemical properties. Journal of Materials Chemistry B. 2014;2(11):1470-82.

22. Farzadi A, Solati-Hashjin M, Asadi-Eydivand M, Osman NAA. Effect of layer thickness and printing orientation on mechanical properties and dimensional accuracy of 3D printed porous samples for bone tissue engineering. . 2014.
23. Jones DS. Dynamic mechanical analysis of polymeric systems of pharmaceutical and biomedical significance. Int J Pharm. 1999;179(2):167-78.
24. Luo Y, Lode A, Akkineni AR, Gelinsky M. Concentrated gelatin/alginate composites for fabrication of predesigned scaffolds with a favorable cell response by 3D plotting. RSC Advances. 2015;5(54):43480-8.
25. You F, Li Y, Zou Q, Zuo Y, Lu M, Chen X, et al. Fabrication and Osteogenesis of a Porous Nanohydroxyapatite/Polyamide Scaffold with an Anisotropic Architecture. ACS Biomaterials Science & Engineering. 2015;1(9):825-33.
26. Park S, Hung C, Ateshian G. Mechanical response of bovine articular cartilage under dynamic unconfined compression loading at physiological stress levels. Osteoarthritis and cartilage. 2004;12(1):65-73.

Chapter 4: 3D Printing of Porous Cell-laden Hydrogel Constructs for Potential Applications in Cartilage Tissue Engineering

Reprinted with permission from You, F., Wu, X., Zhu, N., Lei, M., Eames, B. F., & Chen, X. (2016). 3D Printing of porous cell-laden hydrogel constructs for potential applications in cartilage tissue engineering. ACS Biomaterials Science & Engineering, 2(7), 1200-1210.

4.1 Abstract

Hydrogels are particularly attractive as scaffolding materials for cartilage tissue engineering because their high-water content closely mimics the native extracellular matrix (ECM). Hydrogels can also provide a three-dimensional (3D) microenvironment for homogenously suspended cells that retains their rounded morphology and thus facilitates chondrogenesis in cartilage tissue engineering. However, fabricating hydrogel scaffolds or cell-laden hydrogel constructs with a predesigned external shape and internal structure that does not collapse remains challenging due to the low viscosity and high-water content of hydrogel precursors. Here, we present a study on the fabrication of (cell-laden) alginate hydrogel constructs using a 3D Bioplotting system supplemented with a submerged cross-linking process. Swelling, mechanical properties and protein release profiles were examined and tuned by controlling the initial cross-linking density. Porous cell-laden alginate hydrogel constructs were also fabricated and cell viability, cell proliferation, and cartilaginous ECM deposition were investigated. The fabrication technique and the hydrogel scaffolds obtained supported high cell viability and the deposition of cartilaginous ECM, demonstrating their potential for applications in the field of cartilage tissue engineering.

4.2 Introduction

Hydrogels are three-dimensional (3D) polymeric networks composed of cross-linked hydrophilic polymer chains that can absorb and retain large amounts of water. The high water content environment makes hydrogels especially attractive for cell delivery and encapsulation (1-3) as they bypass the issues that occur with post-processing cell seeding (4, 5), such as insufficient cell seeding and non-uniform cell distribution (6-8). The resulting cross-linked

polymeric networks closely mimic native ECM and, as such, hydrogels can provide a 3D culture microenvironment favorable for encapsulated cells (8-10); for instance, a 3D culture of dedifferentiated chondrocytes in hydrogels can restore the expression of cartilaginous markers (11). Therefore, encapsulating cells in hydrogels is a promising method for providing sufficient cell seeding, homogeneous cell distribution and a suitable 3D microenvironment for encapsulated cells. Cell encapsulation in hydrogels has been successfully achieved (12-17) and several promising techniques, including bioprinting (18), photolithography (19) and laser-assisted printing (20) have been developed to fabricate cell-laden hydrogels.

For cartilage tissue engineering applications, cell-laden hydrogel constructs should be highly porous. Porous structure of scaffolds plays a pivotal role in cell growth and migration. Larger pores and pore interconnectivity can allow effective mass transfer of nutrients and waste (21, 22) but can also result in insufficient cell embedding and intracellular signaling. Smaller pores have the opposite challenges (23); also, cell sheets thicker than 100μm may be unable to provide sufficient pathways for nutrient perfusion and waste removal, leading to necrosis in the center of engineered tissue (24). The viability of porous cell-laden constructs can be around 40% greater than non-porous cell-laden constructs (25). Notably, Griffon et al.(26) found that chondrocytes proliferation and metabolic activity improved with a pore size range of 70-120μm, while Lien et al. reported that scaffolds with pore sizes between 250 and 500μm optimized cartilaginous ECM secretion (27). Designing and fabricating 3D cell-laden hydrogels with an internal architecture of appropriate pore size and porosity is therefore critical for hydrogel-based tissue engineering applications.

However, the production of porous cell-laden hydrogel constructs remains challenging and is mainly limited by hydrogel processing techniques. 3D printing, in which the biomaterial is printed layer by layer, has been widely utilized to fabricate porous hydrogel scaffolds with a predesigned internal porous structure and external shape (28). However, two issues remain with respect to the fabrication of porous cell-laden hydrogel constructs. First, producing a mechanically stable porous hydrogel scaffold that does not collapse is a significant challenge (29-31), usually caused by the low viscosity of the hydrogel precursor. Although the viscosity of the hydrogel can be increased by increasing the polymer concentration and cross-linking density (32, 33), these changes have not achieved shape fidelity while printing and are not desirable for cell viability (34). Cells tend to thrive best in a relatively aqueous environment, in which their

migration and ECM deposition is not limited by a dense polymer network. Our technique enables the fabrication of porous cell-laden hydrogel constructs from a hydrogel precursor with relatively low polymer concentrations, which could be more favorable for encapsulated cells (35). Second, dispensing or printing conditions (e.g., pressure, temperature, nozzle type) may lead to the loss of cell viability (36).

Previous researchers fabricated hydrogel constructs using an aerosol spraying cross-linking process (37). An aerosol humidifier was used to spray a cross-linking agent ($CaCl_2$) to achieve the surface gelation of dispensed alginate strands. However, this method cannot sufficiently cross-link the dispensed hydrogel strands, which may lead to movement between layers and structural collapse during the dispensing process. Loss of pores between strands is the result of insufficient cross-linking. Moreover, the aerosol spray cross-linking was followed by a second process: immersing the scaffolds in the cross-linking solution to further solidify the scaffold structure. In the present study, a one-step submerged cross-linking process is employed to maintain the porous structure of the printed scaffolds and subsequently fabricate cell-laden hydrogel constructs with tunable properties (including swelling, mechanical properties, and protein release profile, etc.) for applications in cartilage tissue engineering. The scaffolds are fabricated based on a Bioplotting system (38) supplemented with a submerged cross-linking technique to allow simultaneous cell encapsulation and pore generation inside the hydrogels (39). The current method employed to fabricate cell-laden alginate hydrogel constructs, which has several advantages as follows: 1) one-step submerged crosslinking process is effective and time saving; 2) this method favors the formation and preservation of printed porous structure, especially good for the preservation of the pores between strands because of the buoyancy provided by the crosslinking solution.

Sodium alginate (SA) was selected as a base hydrogel material. This natural polysaccharide can be ionically cross-linked to become a hydrogel in the presence of calcium ions and can support chondrogenic differentiation to regenerate cartilage (1, 40). Using a 3D Bioplotter, SA solution or cell-impregnated SA was dispensed and fabricated into porous scaffolds on pretreated culture plates containing a tailor-made cross-linking medium (Figure 4.1). *In vitro* results show that the porous cell-laden hydrogel constructs obtained support the survival, proliferation, and ECM deposition of chondrogenic cells. Therefore, this fabrication technique and the hydrogel

scaffolds obtained have great potential for applications within the field of cartilage tissue engineering.

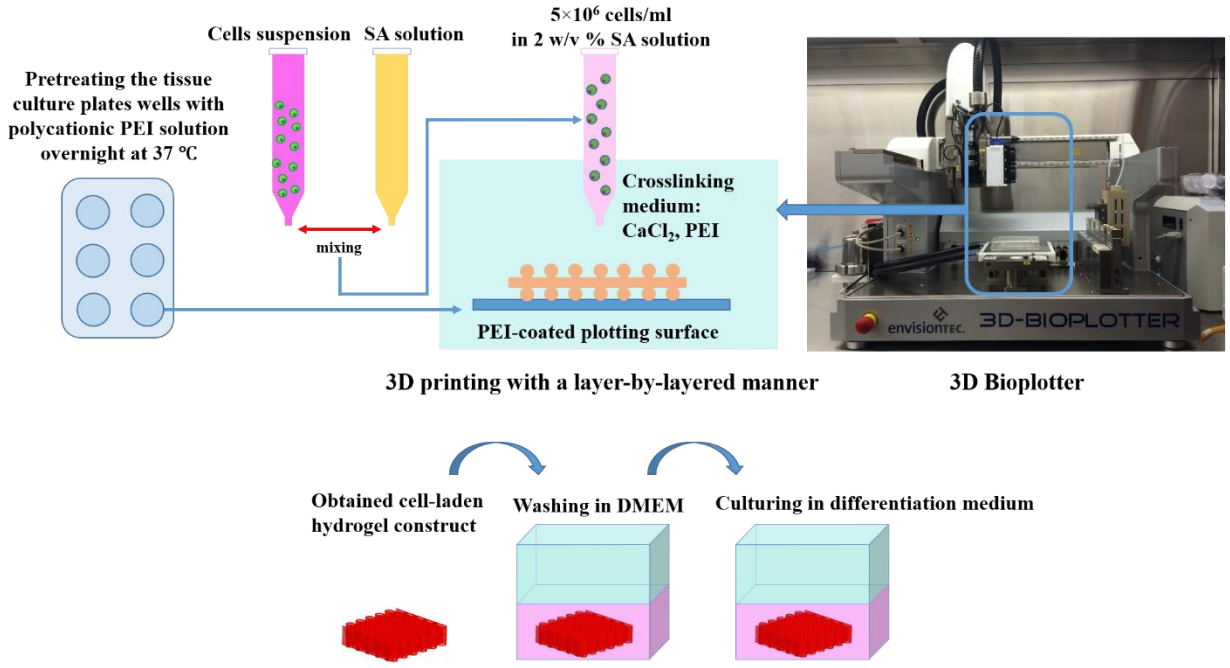

Figure 4.1 Schematic of the printing process using a 3D Bioplotting technique supplemented with a submerged cross-linking process.

4.3 Materials and Methods

4.3.1 Polyethylenimine (PEI) Coating and Contact Angle Measurements

Linear PEI with a low molecular weight has shown great potential for use in the field of tissue engineering and regenerative medicine (41, 42). Tissue culture plates used as plotting platforms were treated with sterile 0.1 w/v % PEI (Alfa Aesar, MW: 60000) in phosphate buffered saline (PBS) and incubated overnight at 37 °C. Contact angles were tested to investigate the influence of the PEI coating process on the plotting surface. Single droplets of 2wt % SA (A2033, medium viscosity, Sigma Aldrich) solution were printed on PEI-coated surfaces.

Four different situations were evaluated:

(1) water droplets printed on a non-coated surface, (2) water droplets printed on a PEI-coated surface, (3) alginate droplets printed on a non-coated surface, and (4) alginate droplets printed on a PEI-coated surface. The static water and SA solution contact angles of single droplets were measured at room temperature. Contact angles from the images obtained by a PGX goniometer

were measured using Image J image processing software (Open Source) containing the contact angle plug in.

4.3.2 Preparation of SA Hydrogel Scaffolds

3D porous scaffolds were produced by sequential strand deposition using a Bioplotter pneumatic dispensing system (EnvisionTec, Germany). Briefly, the Bioplotter is a three-axis dispensing machine that pneumatically deposits (cell-laden) hydrogel precursors on a stationary platform. The structural design is programmed in CAD/CAM software, translated into a numerical code by the Bioplotter software, and contains information for the layer-by-layer build-up of the scaffold.

To validate the influence of PEI on the printing process, different conditions were applied: 1) dispensing hydrogel precursors into PEI-free cross-linking medium on a non-coated plotting surface; 2) dispensing hydrogel precursors into cross-linking medium containing PEI on a non-coated plotting surface; 3) dispensing hydrogel precursors into PEI-free cross-linking medium on a PEI-coated plotting surface; and 4) dispensing hydrogel precursors into a cross-linking medium containing PEI on a PEI-coated plotting surface. The PEI-coated surfaces were washed with double distilled water (DDW) prior to use. SA was dissolved in DDW at a final concentration of 2wt%. The SA strands were plotted into a cross-linking medium containing calcium chloride (Sigma Aldrich; 50, 100, or 200mM $CaCl_2$) and 0.1 % w/v PEI using a plotting speed of 7.5, 6.5, or 5.5 mm/s, respectively, under a pressure of 0.1 bar through a 200μm conical needle. Each layer adhered to the underlying layer perpendicularly to form a 0°/90° strut structure. In this way, scaffolds of 10 (length) ×10 (width) ×5 (height) mm with 1 mm strand spacing were created.

4.3.3 Compressive Mechanical Testing

The Young's modulus of each scaffold was determined by applying unconfined compression with a universal testing machine (Texture Technologies, MA, USA) at a rate of 0.01 mm/s. The Young's modulus was calculated from the slope of the stress-strain curve at a target strain of 10%, which is within the physiological range for articular cartilage (43). Compressive testing was conducted on three samples from each group to facilitate statistical analysis.

4.3.4 Swelling Behavior and *In Vitro* Mass Loss

The hydrogel scaffolds obtained were lyophilized and dry weights (W_0) were measured. Dried hydrogel samples were immersed in 2 mL of DDW and incubated at 37°C. The medium was replaced every other day. At scheduled time points (week 0, 1, 2, 3, 4), the specimens were retrieved and blotted on a Kimwipe® tissue and then weighed (W_t). The swelling ratio was defined as $(W_t-W_0)/W_0\times100\%$. The specimens were then lyophilized and weighed to obtain their dry weights (W_d). Mass loss was calculated using the formula $(W_0-W_d)/W_0\times100\%$.

4.3.5 Morphological Examination

The printed strands and the top and cross-section view of fabricated scaffolds were examined using light microscopy (Leica). The morphologies of the freeze-dried hydrogel scaffolds were examined using a scanning electron microscope (SEM; Phenom G2). The samples were lyophilized in a freeze-dryer for 24 h and coated with gold using a sputter coater prior to examination.

4.3.6 3D Imaging of Porous Hydrogel Scaffolds Structure Via Synchrotron Radiation Based X-ray

The porous hydrogel scaffolds were imaged at the BioMedical Imaging & Therapy facility (BMIT) at the Canadian Light Source (CLS) by means of synchrotron radiation based X-ray inline phase contrast imaging-computed tomography (SR-inline-PCI-CT). Porous hydrogel scaffolds were placed in a sample holder and positioned on the rotating scanning stage for imaging. The projected images were recorded at a photon energy of 30 keV by means of a beam monitor AA-60 (Hamamatsu) coupled to a camera (Hamamatsu ORCA Flash 4.0) with an effective pixel sizes of 12.8 µm. 3D reconstruction was done by Avizo software (FEI, USA).

4.3.7 Protein Release

To characterize the release of a model protein from the SA hydrogel scaffolds, 2 mg/mL bovine serum albumin (BSA) was dissolved in the SA solutions prior to fabrication. Scaffolds were then produced as per the methods mentioned above. After fabrication, the protein-loaded scaffolds were further cross-linked in 3mL cross-linking medium containing PEI for another 20 min. Five µL of the crosslinking medium was taken and treated with 250 µL of Bradford reagent

(Sigma Aldrich, Canada) and measured at 595 nm in a microplate reader subtracting blank control values. BSA concentration in the above-mentioned cross-linking solutions was used to ascertain the encapsulation efficiency and further *in vitro* release was then performed in fresh PBS. The release profile of BSA was evaluated by incubating the SA hydrogel scaffolds in 3 mL PBS at 37°C. At each time point (0.5, 1, 2, 3, 4, 6, 12, 24, 48, 72 and 120 h), five µL of release medium from each sample were treated with 250µL of Bradford reagent and measured at 595 nm in a microplate reader subtracting blank control values. After analysis for each time point, 3 mL of fresh PBS was added to replace the medium. The BSA concentration in the unknown samples was measured using a calibration curve created from standard BSA solutions (44).

4.3.8 Fabrication of Culturing of Cell-laden Constructs

The ATDC5 cell line is derived from mouse teratocarcinoma cells and characterized as a chondrogenic cell line that undergoes a process analogous to chondrocyte differentiation. Therefore, it is considered a promising *in vitro* model to investigate the factors that influence cell behaviors during chondrogenesis (45). ATDC5 cells were grown in polystyrene dishes and cultured in maintenance medium consisting of a 1:1 mixture of Dulbecco's modified Eagle's medium (DMEM) and Ham's F-12 medium (Invitrogen) supplemented with 5% fetal bovine serum (FBS), 1% penicillin/streptomycin, 1% glutamine, and 1% ascorbate 2-phosphate. The cells were harvested at confluence by trypsinization and collected by centrifugation at 1200 g for 5 min, followed by counting the cell number using a haemocytometer. The cell suspensions were homogenously mixed with SA solution using three-way stopcocks to reach the final cell density of 5×10^6 cells/ml and final SA concentration of 2 w/v%. The mixture was transferred into a syringe and loaded into the Bioplotter and then printed to fabricate cell-laden hydrogel constructs by means of the procedures described above. The scaffolds were then each washed with DMEM for 5 min, followed by culturing in differentiation medium (maintenance medium supplemented with 1× ITS premix (insulin, 10 µg/mL; transferrin, 5.5 µg/mL; and selenium, 5 ng/mL) for 1, 14, or 28 days to induce chondrocyte differentiation (Figure 4.1). The maintenance or differentiation media were changed every other day for the duration of the experiment.

Primary chondrocytes were also used as a cell source to fabricate cell-laden hydrogel constructs. Primary chick chondrocytes were isolated from cartilaginous sternums of 14-day-old chick embryos (46). Briefly, the sternums of chick embryos were carefully excised, chopped and

placed in digestion medium consisting of 0.2% collagenase and 0.25% trypsin in Hank's Balanced Salt Solution (HBSS) at 37°C and 5% CO_2 for 2 h with one gentle pipetting at 90 min. The digestion was terminated by adding DMEM supplemented with 10% FBS. The resulting cell suspension was filtered through a 70 µm sterile Nitex filter and centrifuged at 200 g for 10 min. The cell pellets collected were suspended and cultured in culture medium containing DMEM, 10% FBS, 2mM glutamine, 0.1 mg/mL kanamycin, 1% AA (100U/mL penicillin, 0.1mg/mL streptomycin, 0.25µg/mL amphotericin B), and 0.01mg/mL ascorbate. Primary chick chondrocytes-laden hydrogel constructs were fabricated following the procedures described above.

4.3.9 Cell Viability Using Live/Dead Assay

Cell viability studies were conducted using a calcein AM and ethidium bromide (EthD-1) solution. (live/dead viability kit, Invitrogen) according to the manufacturer's instructions. The cell-laden hydrogel scaffolds were incubated for 30 min at 37 °C in the live/dead solution. To visualize the live and dead encapsulated cells in the SA hydrogel scaffolds, images were obtained with a fluorescent microscope (Olympus). To quantitatively determine the cell viability in the cell-laden constructs, the stained cells were released by incubating the constructs in 300µL 50mM EDTA (diluted in DMEM) at 37 °C. By gentle pipetting, the medium was dispersed to obtain an even cell suspension mixture. Samples (n=3) were taken from the cell mixture of each construct and imaged under a coverslip on a standard glass microscope slide at random locations for counting live and dead cells. Cell viability was calculated using the following equation, number of live cells/ (number of live cells + number of dead cells) ×100%. A haemocytometer was used to count the cell number in these cell suspensions (n=3) over the culture period.

4.3.10 Histological Analysis and Immunohistochemistry

ATDC5 cell-laden hydrogel constructs were fixed with 4% paraformaldehyde in Tris-buffered saline (TBS) for 20 min. The scaffolds were then embedded in OCT embedding compound at -80°C for 30 min. Frozen sections (10-µm thick) were prepared with a freezing microtome (Leica, Germany).

Alcian blue staining

To visualize the accumulation of sulfated glycosaminoglycan (GAG), frozen sections were stained with 0.25% Alcian blue in 0.1 M HCl for 30 min at room temperature. The accumulation of GAG was assessed using light microscopy.

Immunocytochemistry

Frozen sections were permeabilized with 0.5% Triton X-100 in PBS (PBS-T), followed by pretreatment to block nonspecific reactions with blocking buffer (4% goat serum and 2% sheep serum in PBS-T). For collagen staining, the primary immunoreaction was carried out with a mouse monoclonal antibody (1:100) against Collagen type II (DSHB), followed by rinsing with blocking buffer. The secondary immunoreaction was carried out with Alexa 488-conjugated goat anti-mouse IgG (1:1000, Invitrogen) in blocking buffer, followed by rinsing with PBS-T. Fluorescent images were recorded with a fluorescence microscope (Nikon).

An MTT (3-(4, 5-dimethylthiazol-2-yl)-2, 5-diphenyltetrazolium bromide) assay was conducted to characterize the primary chondrocytes-laden hydrogel constructs. Briefly, MTT solution (5 mg/mL) was added to each well and the plate incubated again for 5 h. The medium was then aspirated and dimethyl sulfoxide added to solubilize the formazan reaction product at 37 °C for 15 min. The absorbance of each well was measured at 540 nm with a reference at 650 nm using a micro-plate reader. Alcian blue staining was used to detect sulfated GAG accumulation. Briefly, the printed constructs were washed with DMEM and fixed in acetone and methanol solution (1:1) on ice for 15 min and then stained with 0.01 % Alcian blue in 3% acetic acid solution overnight. The stained constructs were washed with 25% ethanol in 3% acetic acid and with 50% ethanol in 3% acetic acid successively, and imaged using light microscopy. Immunofluorescent staining was performed on the printed samples to detect the deposition of Collagen type II according to methods described above.

4.3.11 Statistics

For quantitative analysis, Student's t tests were used to assess differences between two groups and multiple comparisons were performed via one-way ANOVA using SPSS software. Data are expressed as mean values ± standard deviation (SD), with p values <0.05 considered statistically significant.

4.4 Results

4.4.1 Influence of PEI Coating on the Contact Angles of the Plotting Surface

To dispense strands and hydrogel scaffolds with high stability and good reproducibility, the resolution and precision of the entire process must be considered. To this end, the contact angles of droplets printed on both coated and non-coated surfaces were measured. Different contact angles were obtained for water or SA droplets printed on PEI-coated or non-coated surfaces (Figure 4.2). Contact angles for water droplets printed on non-coated and PEI-coated platforms were 34.4±2.1º and 35.3 ±1.7º while for SA droplets were 88.2±1.5º and 68.5 ±4.4º. Notably, the contact angles for SA droplets on the non-coated surface are significant higher than SA droplets on the PEI-coated surface, which means the wettability between the SA solution and platform increased with the PEI coating process.

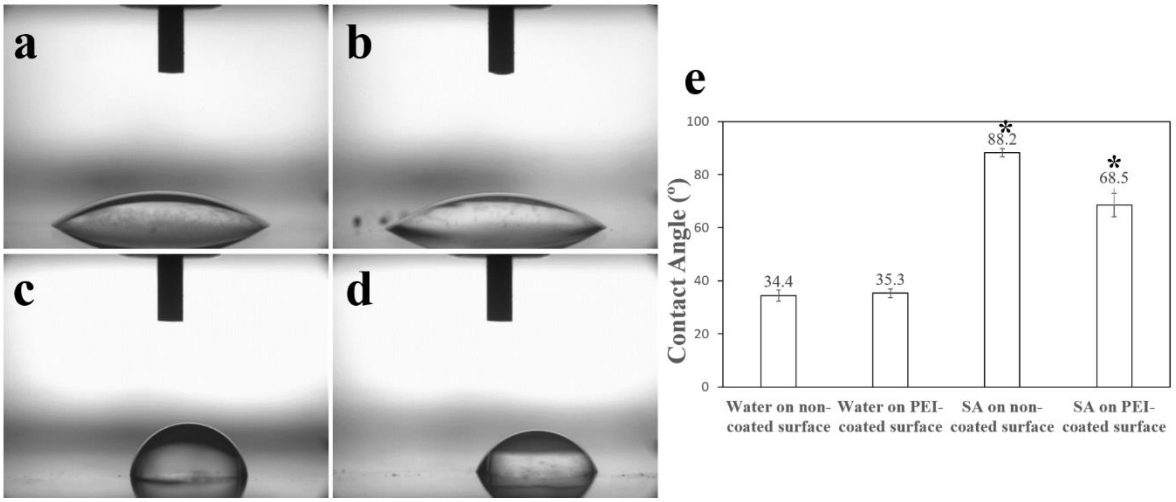

Figure 4.2 (a) Water droplets printed on a non-coated surface, (b) water droplets printed on a PEI-coated surface, (c) SA droplets printed on a non-coated surface, (d) SA droplets printed on a PEI-coated surface, and (e) contact angle measurements for the four different situations. Error bars represent mean ± SD for n=10. *represents significant difference (*$p<0.05$) between the contact angles of (c) and (d).

4.4.2 Scaffold Fabrication

SA strands dispensed in the presence and absence of polycationic PEI were compared (Figure 4.3). The first layer of strands cannot form without a PEI coating process (Figure 4.3a, b). However, the first layer can be printed when dispensing the SA hydrogel precursor onto a

PEI-coated plotting surface (Figure 4.3c), likely because an electrostatic interaction between the dispensed strands and the PEI-coated plotting surface was established. However, the upper layers did not arrange as designed (Figure 4.3d). Only when the SA hydrogel precursor solution is dispensed into cross-linking medium containing PEI on the PEI-coated plotting surface (Figure 4.3e) can the desired structure be obtained. Porous hydrogel scaffolds were then successfully fabricated by a layer-by-layer strand deposition process (Figure 4.3f). Overall, PEI was required both as a coating on culture plates and in the crosslinking medium for successful fabrication of porous scaffolds.

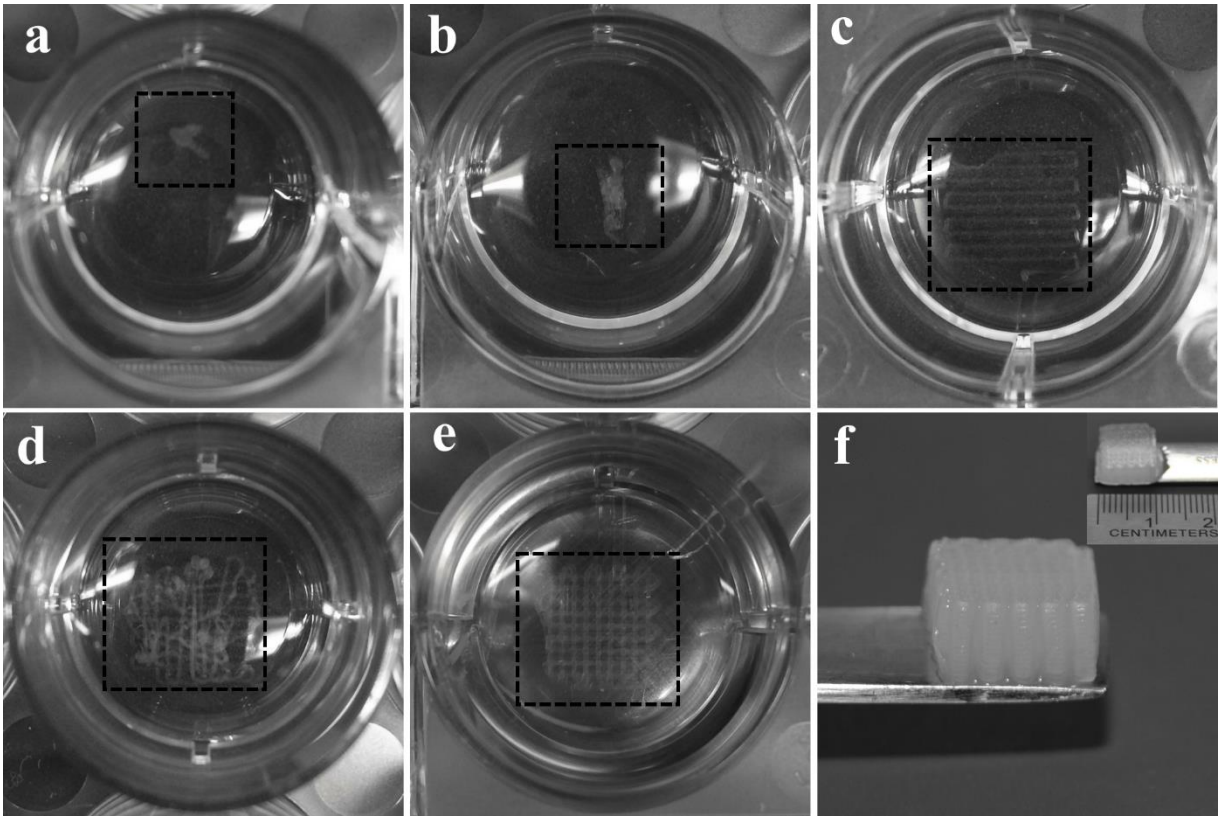

Figure 4.3 (a) Dispensing SA strands into PEI-free cross-linking medium on a non-coated plotting surface, (b) dispensing SA strands into cross-linking medium containing PEI on a non-coated surface, (c) first layer of dispensing SA strands into PEI-free cross-linking medium on a PEI-coated plotting surface, (d) upper layers of dispensing SA strands into PEI-free cross-linking medium on a PEI-coated plotting surface, (e) dispensing SA strands into cross-linking medium with PEI on a PEI-coated plotting surface, and (f) a fabricated porous hydrogel scaffold.

During the fabrication process, strand size is an important design factor that influences the final fabricated 3D structure. Therefore, the dispensed SA strand size for various plotting speeds was measured (Figure 4.4). For a conical needle size of 200μm and a dispensing pressure of 0.1 bar, the SA strand diameter decreased significantly with increasing plotting speed and Ca^{2+} concentration in the cross-linking medium (Figure 4.4b). For the 100mM group, a dispensing speed of 6.5 mm/s was chosen because the diameter of the dispensed strand was close to the 200μm needle size. A dispensing speed of 5.5 mm/s was chosen for the 200mM $CaCl_2$ group for the same reason. For the 50mM $CaCl_2$ group, a dispensing speed of 7.5 mm/s was chosen because: 1) low deposition speed (lower than 7.5 mm/s) resulted in a too wide strand diameter because of the weak cross-linking efficacy caused by the low calcium concentration; and 2) higher dispensing speed (high than 7.5 mm/s) would result in the interruptive and unstable deposition process.

By adjusting the Ca^{2+} concentration (50, 100, or 200mM) in the crosslinking medium, three groups of hydrogel scaffolds were obtained (SA-50mM, SA-100mM, SA-200mM) and their morphology observed using SEM. With increasing Ca^{2+} concentration, the dimensions of the freeze-dried strands decreased (Figure 4.5), which is consistent with previous reports of high cross-linking density resulting in a denser cross-linked structure (47).

Because of the high-water content and low density of the hydrogel, characterizing and visualizing the scaffolds by conventional techniques is challenging. Synchrotron-based phase contrast imaging techniques were used to characterize the porous hydrogel scaffolds. The 3D reconstruction images obtained show the scaffold morphology features a porous structure and a highly interconnected pore network (Figure 4.6a,b). Microscopic images show the porous structure from top (Figure 4.6c) and cross-section view (Figure 4.6d). The top-view images (Figure 4.6b,c) show the pores in the scaffold are completely interconnected with channels extending uninterrupted from the top and bottom. The cross-sectional view (Figure 4.6d) shows small pores between strands indicating that the pore structure of the scaffold was well maintained.

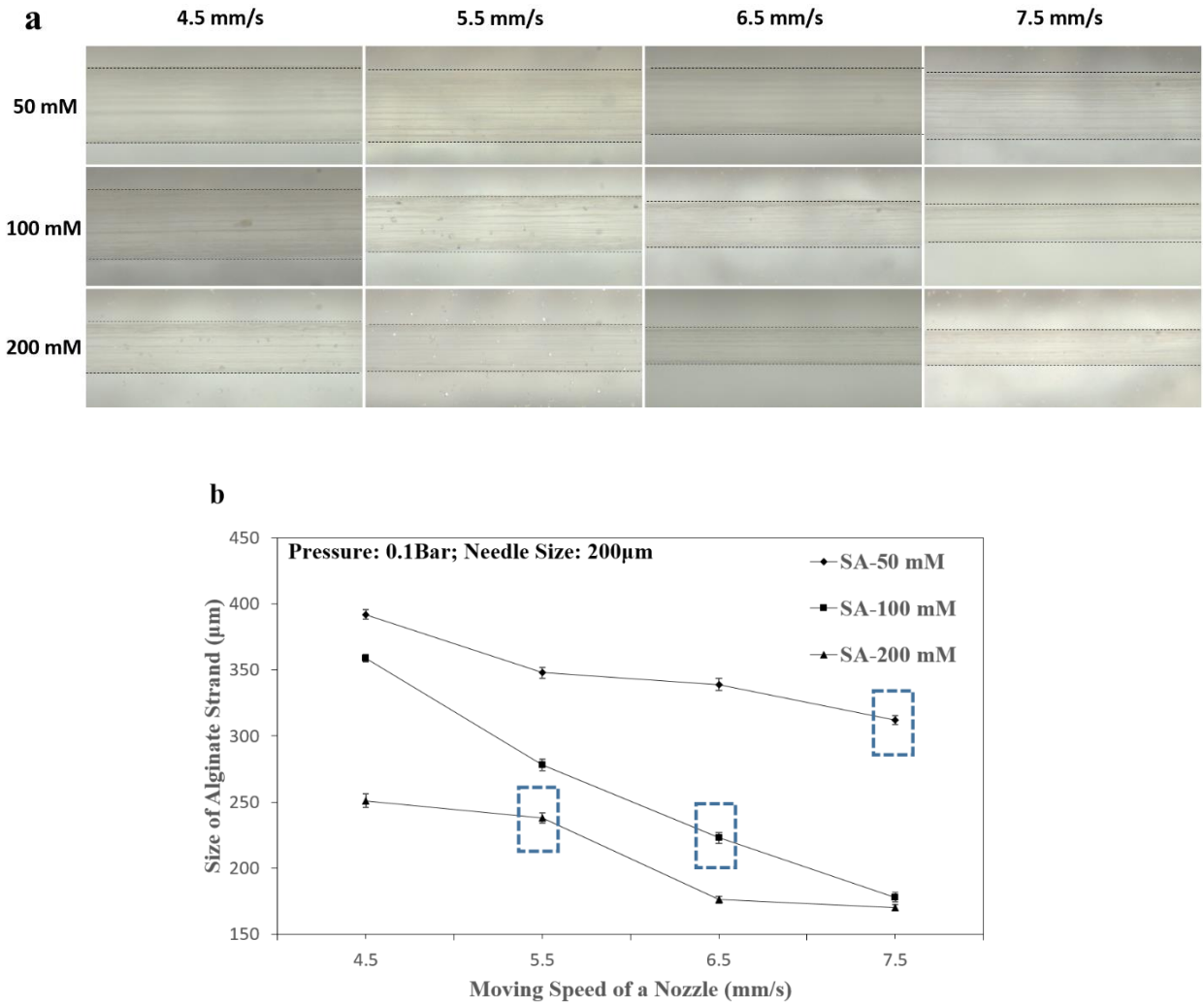

Figure 4.4 (a) Representative images of dispensing SA strands into cross-linking medium containing 50, 100, and 200mM $CaCl_2$ at various plotting speeds (4.5, 5.5, 6.5, 7.5 mm/s) with a needle (200µm) under a dispensing pressure of 0.1 bar; (b) SA strand size at various plotting speeds (n=10). The dashed blue frame in (b) indicates the plotting speed adopted to fabricate scaffolds for each group. Scale bar=200µm.

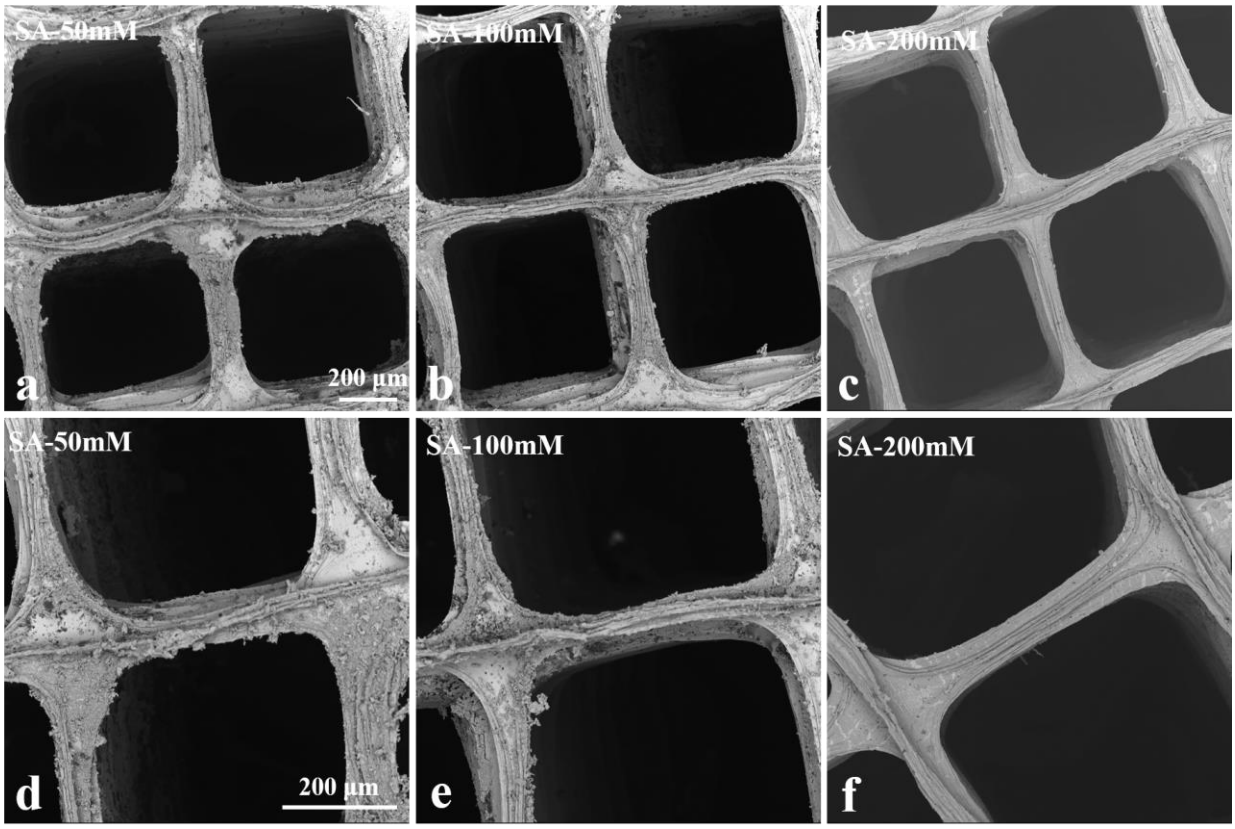

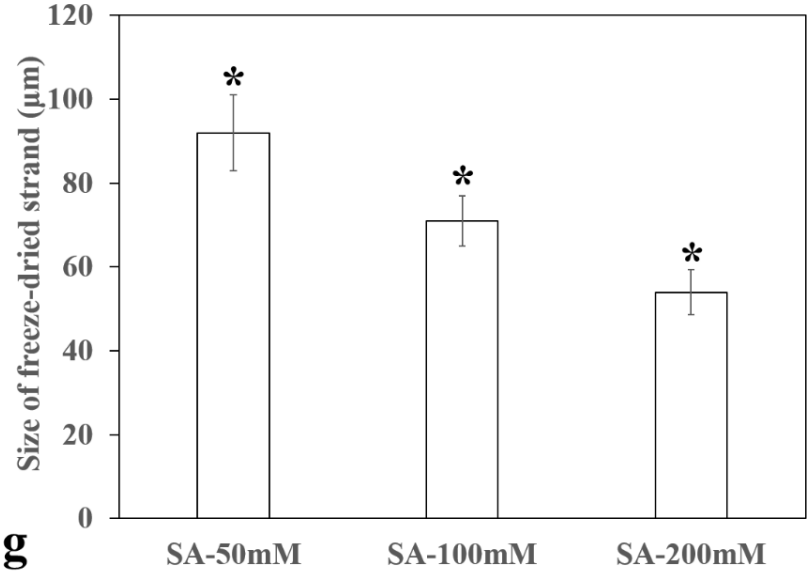

Figure 4.5 SEM images of SA-50mM (a, d), SA-100mM (b, e), and SA-200mM (c, f) scaffolds and the size of freeze-dried strands (g). (n=10, *$p<0.05$)

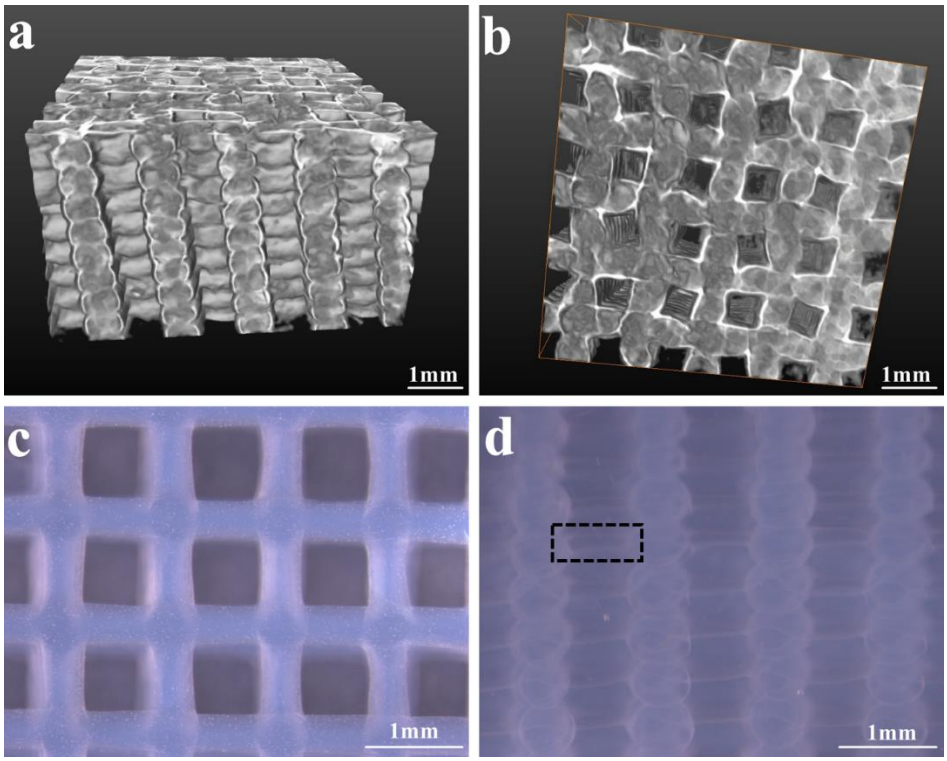

Figure 4.6 SR-inline-PCI-CT-based 3D reconstruction of porous hydrogel scaffolds (SA-100mM): cross-section (a) and top view (b); microscopic images of porous hydrogel scaffolds (SA-100mM): top view (c) and cross-section (d). Black frame in (d) indicates the pores between deposited layers.

4.4.3 Swelling Behavior and *In Vitro* Mass Loss

All three groups attained their maximum swelling ratio at week 1 (Figure 4.7a). The SA-50mM and SA-100mM groups then experienced varying downward trends. The swelling ratio of the SA-200mM group remained stable for the first three weeks, then decreased at week 4. The *in vitro* mass loss of the SA hydrogel scaffolds is shown in Figure 4.7b. The mass loss for each group increased with time, to 46.5, 44, and 33% after 4 weeks for SA-50mM, SA-100mM, and SA-200mM, respectively.

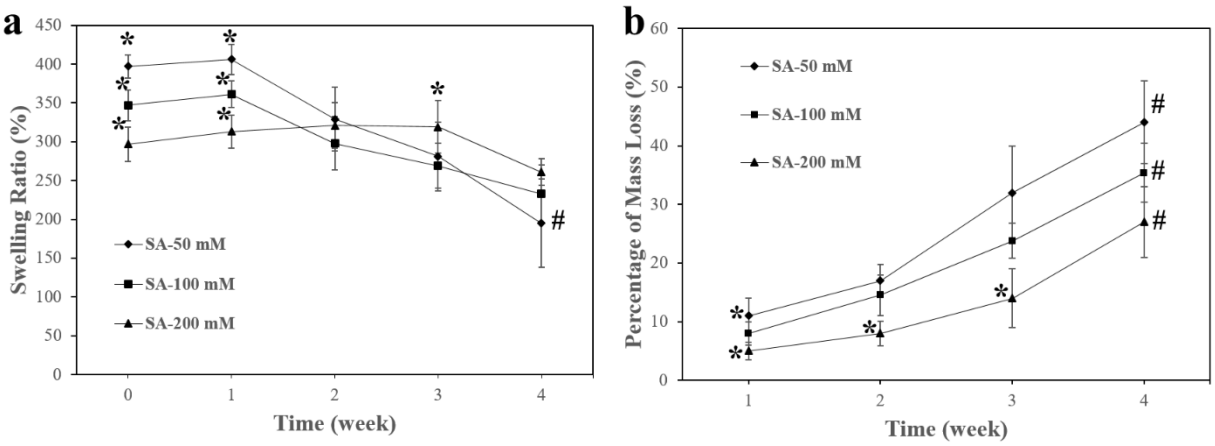

Figure 4.7 Swelling ratio (a) and percent weight loss (b) of porous hydrogel scaffolds at 37 °C. (* $p<0.05$, between groups. # $p<0.05$, over time, n=3)

4.4.4 Compressive Mechanical Properties

The compressive moduli of the three groups of hydrogel scaffolds generally decreased with time due to their time-dependent swelling and *in vitro* mass loss. At each time point, the compressive modulus increased with cross-linking density (Figure 4.8).

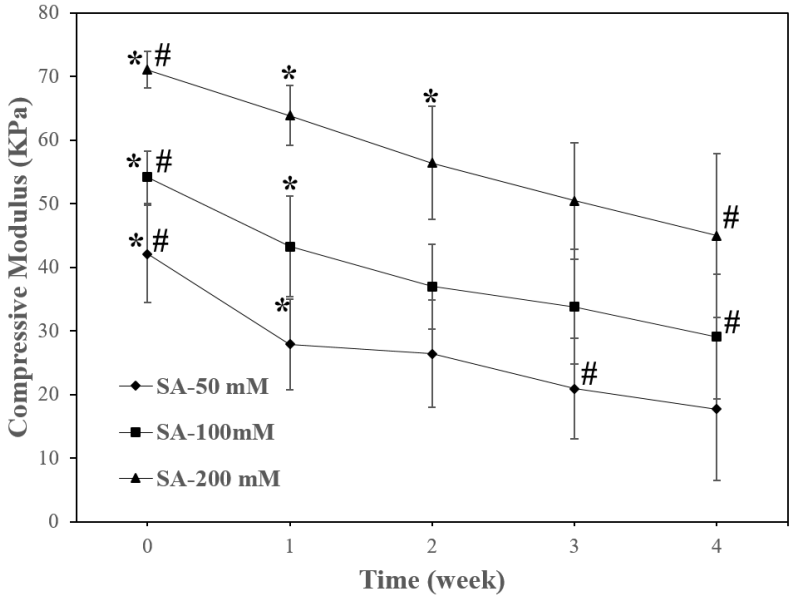

Figure 4.8 Compressive modulus of hydrogel scaffolds incubated in deionized water at 37 °C for various lengths of time (1, 2, 3, 4 weeks). (* $p<0.05$, between groups. # $p<0.05$, over time, n=3)

4.4.5 Protein Release Experiments

Due to the mild biofabrication conditions (room temperature), growth factors can be directly loaded into the precursor solutions and plotted to create scaffolds. BSA was used as a model protein to investigate the protein delivery ability of the plotted hydrogel scaffolds. The encapsulation efficiency for BSA was highest in the SA-200mM group, which was significantly higher than the SA-50mM group (Figure 4.9a). Around 80% of the BSA was released within the first 48 h in the SA-50mM and SA-100mM groups and 65% in the SA-200mM group (Figure 4.9b). Specifically, BSA demonstrated a slower protein release behavior with increasing the cross-linking density (Ca^{2+} concentration).

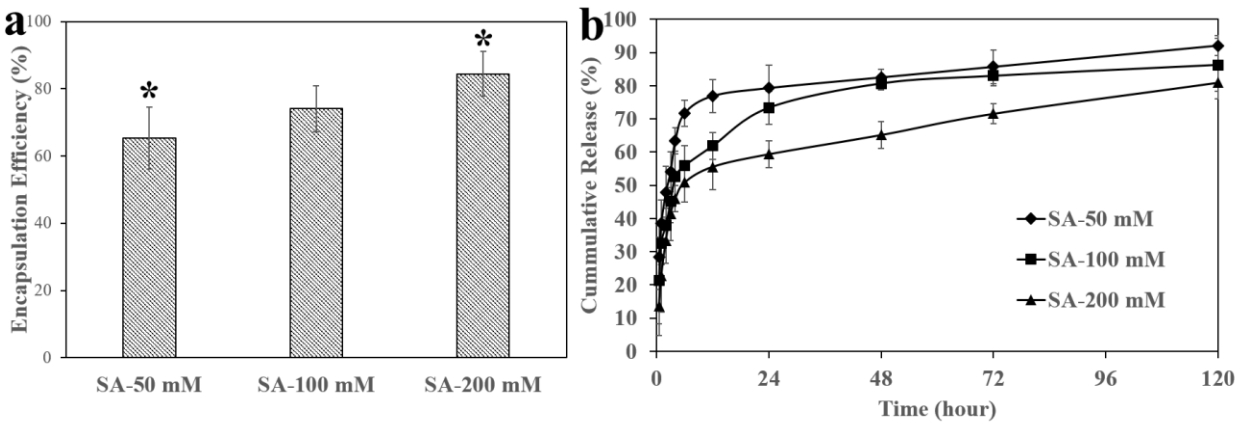

Figure 4.9 BSA encapsulation efficiency (a) and release behavior (b) from scaffolds in PBS solution (* $p<0.05$, pH 7.4, 37 °C, n=3).

4.4.6 Live/Dead Assay

Cell viability is an important parameter for cell-laden hydrogel constructs because it influences all cellular activities, including proliferation and differentiation. Cell viability was assessed with both a live/dead assay kit (Figure 4.10a-i) and as the change in cell number (Figure 4.10j) with time. Fluorescent images show a dominant population of live cells. Fluorescence images of the 3D bioplotted cell-laden hydrogel constructs show a homogeneous cell distribution that indicates successful mixing of cells in the SA hydrogel. Fluorescent images of cross-sectional views demonstrate that cell viability is not positionally dependent. Cell viability at day 1 was 76% but significantly increased to 84% by day 14. Cell number, as an indication of cell proliferation, increased slightly from the initial cell seeding density of 5×10^6 cells/mL to 5.5×10^6

cells/mL at day 1, then experienced a significant upward trend to 17×10^6 cells/mL by day 14 (Figure 4.10j). For the chondrocytes-laden hydrogel constructs, cell viability increased from day 1 to 14 (Figure 4.10k). MTT absorption also increased over time, indicating cell growth within the hydrogel constructs (Figure 4.10m).

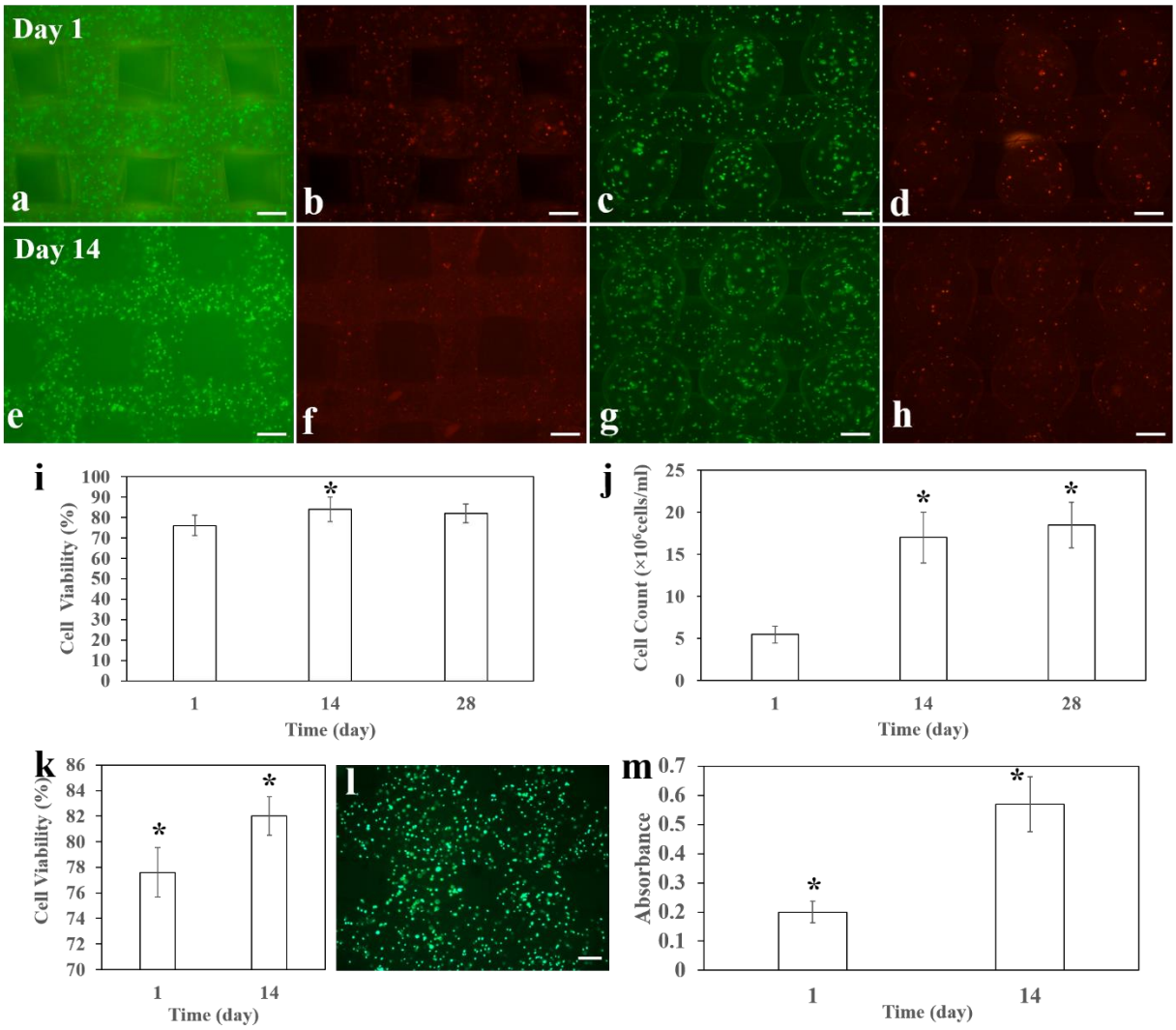

Figure 4.10 Fluorescent surface (a, b, e, f) and cross-sectional (c, d, g, h) images of the ATDC5 cell-laden hydrogel constructs showing live (green) and dead (red) cells after 1 day (a-d) and 14 days (e-h) of culture. Cell viability (i) and cell number (j) for various cell culture periods (1, 14, 28 days). (*$p<0.05$, compared to the cell viability and cell number at day 1 culture, n=3). Cell viability (k), representative live cells image of day 14 (l) and MTT assay (m) of embedded primary chick chondrocytes. (*$p<0.05$, n=3). Scale bar (a-h) = 200μm, scale bar (l) = 100μm.

4.4.7 Deposition of GAG and Collagen Type II

Cell-laden hydrogel constructs generally maintained their structural integrity and original shape throughout the culture period (Figure 4.11). The height of cell-laden hydrogel constructs decreased with time (Figure 4.11c), probably due to the gel contraction caused by the proliferating cells and deposition of ECM. Newly formed ECM was examined using Alcian blue staining to visualize GAG (Figure 4.12a, b, c) and immunocytochemistry for Collagen type II (Figure 4.12d, e).(48) Alcian blue stained sections demonstrate that cells secreted GAG after 7 d of culture. At day 14, cell number increased and more were secreting GAG. At day 28, many cells showed GAG deposition and the intensity of Alcian blue staining was higher than that at day 7 or day 14. Immunocytochemistry showed obvious expression of Collagen type II at day 14 and 28. For the chondrocytes-laden hydrogel constructs, Alcian blue and Collagen type II immunofluorescence staining reflected secretion of GAG and Collagen type II by primary chick chondrocytes, which are two main components of cartilage tissue matrix (Figure 4.12f, g). These results demonstrated that porous cell-laden hydrogel constructs fabricated in this study supported chondrogenic differentiation and ECM deposition.

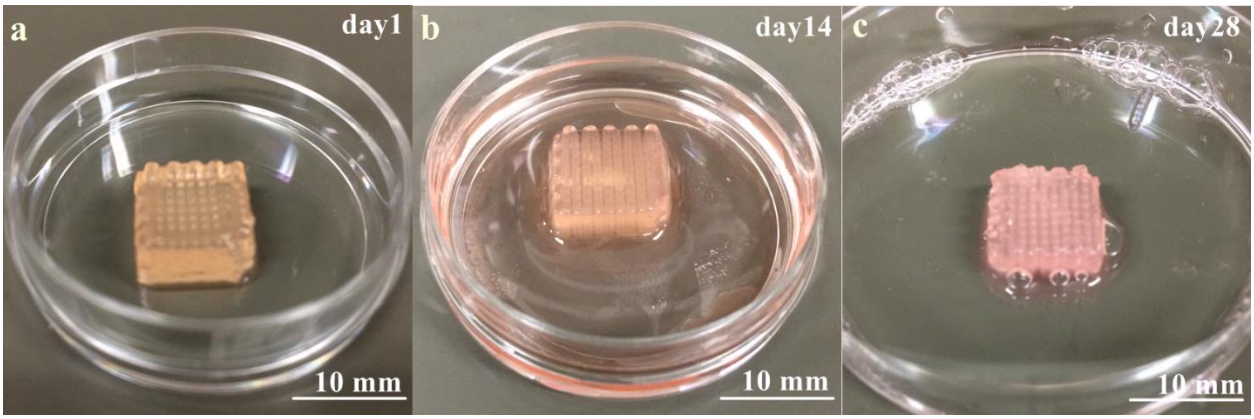

Figure 4.11 Digital photos of cell-laden hydrogel constructs after 1 (a), 14 (b), and 28 (c) days of culture.

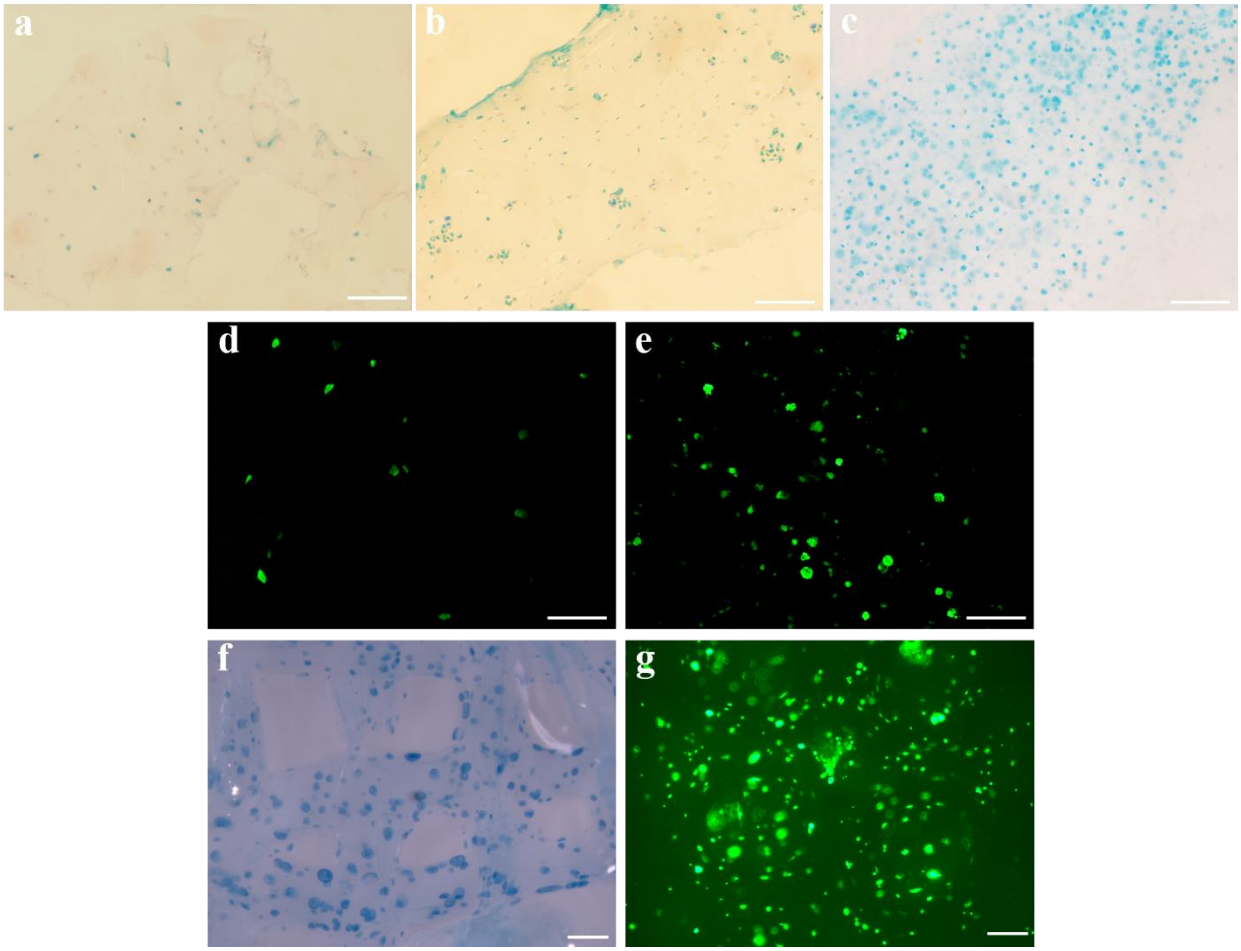

Figure 4.12 Accumulation of GAG (a, b, c) and Collagen type II (d, e) in ATDC5 cell-laden hydrogel constructs. Expression of GAG was analyzed by Alcian blue staining at day 7 (a), 14 (b) and 28 (c). Expression of Collagen type II was analyzed by immunofluorescent staining at day 14 (d) and 28 (e). Accumulation of GAG (f) and Collagen type II (g) in primary chick chondrocytes-laden hydrogel constructs. Scale bars=100μm.

4.5 Discussion

Advances in cartilage tissue engineering (CTE) depend upon reliable chondrogenic cell sources, appropriate scaffolds, and favorable culture conditions (e.g. suitable growth factors, nutrients and mass transfer) (49). The choice of appropriate scaffolding materials plays a fundamental role in successful CTE applications. Hydrogels are particularly attractive as scaffolding materials for CTE because their high fluid content closely mimics native ECM and they can homogenously suspend cells in a 3D microenvironment; this means that encapsulated

cells typically retain a rounded morphology that may facilitate the chondrocytic phenotype (50, 51). However, fabricating a predesigned external shape and obtaining a porous structure are still difficult to achieve due to the high-water content of hydrogels. Control over the scaffold's external shape helps to fill irregular cartilage defects, while the internal pores facilitate effective mass transfer. In this study, porous cell-laden hydrogel constructs were produced by a bioplotting technique supplemented with a submerged cross-linking technique.

Modelling and experimental studies show that cell viability is dependent on the needle type employed, with enhanced viability noted for conical needles compared with cylindrical needles (20, 52). and thus, a conical needle was used in this study. Linear PEI with a low molecular weight has been used in the field of tissue engineering and regenerative medicine to promote cells adhesion and proliferation (41) or as a material for tissue-engineered scaffold fabrication (42). PEI was used to pretreat the culture plates to promote adhesion of strands to the plotting surface since PEI pretreating helped to lower its contact angle and increase the contact area. This coating process is an important supplement to the 3D bioplotting technique since it helps to anchor the whole bioplotted scaffolds on the plotting surface and avoid possible deformation and undesired movement during the layer-by-layer deposition (Figure 4.3). PEI was also an indispensable addition in the cross-linking medium. Predesigned structure could not be achieved without PEI (Figure 4.3). This is probably due to the electrostatic attraction between the dispensed polyanionic SA strands and the polycationic PEI in the cross-linking medium that helps to maintain the cylindrical shape of dispensed strands.

Notably, small pores observed between deposited layers from the 3D reconstruction and optical images indicate that this fabrication technique withstood potential compression issues that may occur while depositing strands, thus preserving the space between layers (37). Time-dependent swelling, *in vitro* mass loss behavior and compressive modulus of the porous hydrogel scaffolds were demonstrated to be tunable by varying the Ca^{2+} concentration of the cross-linking medium. The loss of mechanical properties with time can be explained by alginate dissolution or decross-linking by calcium diffusion out of the matrix. The Young's modulus reported here is lower than that of articular cartilage (~0.4MPa) (53). This seems to be a common issue attributed to the use of the hydrogels (37). To overcome this problem, Malda et al. utilized synthetic polymer or printed polymeric microfibers to strengthen the printed hydrogel constructs (54, 55). Other researchers focused on employing advanced hydrogel materials to strengthen the

mechanical properties of the printed construct or induce embedded cells to secrete more ECM to enhance the mechanical properties (56, 57). Based on current results, the mechanical properties of printed hydrogel constructs can be improved through future research by designing various internal structures or supplementing with other materials.

The swelling ratios of the SA-50mM and SA-100mM hydrogels generally decreased over 4 weeks of incubation probably due to the loss of material from the polymer bulk (e.g., scission of the polymer backbone). For the SA-200mM group, decreasing the cross-linking density resulted in an increase in the swelling ratio. The decrease of swelling ratio observed after three weeks was probably because the influence of hydrogel mass loss on the swelling ratio prevails over the influence of reduced crosslinking density. The fabrication of porous hydrogel scaffolds was performed under mild conditions (room temperature) and thus proteins can be directly loaded into this fabrication system during scaffold production without denaturation. Two mechanisms are involved in the protein release from the SA hydrogel scaffolds: (1) proteins are released through the polymer network and (2) the rate of protein release increases with degradation of the polymer network (58). The latter is not thought to be a suitable method as it may lead to a burst release of the protein (59). Here, 80% of the BSA was released over 48h by the SA-50 and SA-100mM groups; the protein was released a little more slowly by the SA-200mM group. The mass loss of hydrogel scaffolds was around 10% after 1 week, which means that the BSA was released from the hydrogel scaffolds mainly through the polymer network. The fast protein release was probably because the low alginate concentration and the high-water content expedite the diffusion and transfer of the protein. Therefore, the protein release kinetics might be tuned by varying the polymer concentration or the initial cross-linking density. Given the mild fabrication conditions, other advanced materials or techniques could be incorporated in our biofabrication system to optimize the protein release profile.

The relatively low cell viability at day 1 could be due to the shear forces and inlet pressure applied to the cells when mixing with the SA solution or during dispensing. Despite the loss of cells during the embedding and bioplotting processes, the cell viability significantly recovered after 14 days of culture due to significant cell proliferation, as indicated by the higher cell viability compared to day 1(Figure 4.10i). Moreover, histology and immunocytochemistry results clearly demonstrate the deposition of cartilage ECM including GAG and collagens, which can create an integrated and dense network that forms the basis for the biomechanical properties

of articular cartilage (60). These results clearly demonstrate that this bioplotting-based fabrication technique is well suited for the bioprinting of living cells and supports chondrogenic cell differentiation.

Notably, a 2% polymer concentration was used in this study. Low viscosity increases the difficulty of fabricating the liquid gel precursors into hydrogel scaffolds, and mastering of a low viscosity fabrication technique would be of great help to future study. Previous studies increased the polymer concentration to improve the printability of the hydrogels. However, cells thrive best in a relatively aqueous environment, in which their migration and matrix deposition is not limited by the dense polymer network. The biofabrication technique introduced here enabled successful production of porous cell-laden hydrogel constructs from hydrogel precursors with a relatively low polymer concentration, which may be more desirable for the encapsulated cells. This biofabrication technique can also be considered as a versatile biofabrication platform that is compatible with various soluble biomaterials and growth factors (GF) and has various tunable properties (e.g., swelling, mechanical properties, degradation, GF release profile) that are relevant for potential applications in cartilage tissue engineering and regenerative medicine.

4.6 Conclusion

This study reports a facile bioplotting-based fabrication technique for the production of mechanically stable porous hydrogel scaffolds or cell-laden hydrogel constructs. Various properties including swelling ratio, *in vitro* degradation behavior, protein release profile, and mechanical properties can be tuned by controlling the Ca^{2+} concentration in the cross-linking medium. This biofabrication technique and the porous hydrogel scaffolds obtained can support high cell viability and deposition of cartilaginous ECM. The technique might also be compatible with various soluble biomaterials and GFs due to its hydrophilic nature. As such, this biofabrication technique is a versatile platform with potential applications to cartilage tissue engineering.

References

1. Awad HA, Wickham MQ, Leddy HA, Gimble JM, Guilak F. Chondrogenic differentiation of adipose-derived adult stem cells in agarose, alginate, and gelatin scaffolds. Biomaterials. 2004;25(16):3211-22.

2. Benoit DS, Schwartz MP, Durney AR, Anseth KS. Small functional groups for controlled differentiation of hydrogel-encapsulated human mesenchymal stem cells. Nature materials. 2008;7(10):816-23.

3. Chenite A, Chaput C, Wang D, Combes C, Buschmann M, Hoemann C, et al. Novel injectable neutral solutions of chitosan form biodegradable gels in situ. Biomaterials. 2000;21(21):2155-61.

4. Ma PX. Scaffolds for tissue fabrication. Materials today. 2004;7(5):30-40.

5. Hollister SJ. Porous scaffold design for tissue engineering. Nature materials. 2005;4(7):518-24.

6. Martin I, Wendt D, Heberer M. The role of bioreactors in tissue engineering. Trends Biotechnol. 2004;22(2):80-6.

7. Holy CE, Shoichet MS, Davies JE. Engineering three-dimensional bone tissue in vitro using biodegradable scaffolds: investigating initial cell-seeding density and culture period. J Biomed Mater Res. 2000;51(3):376-82.

8. Wendt D, Marsano A, Jakob M, Heberer M, Martin I. Oscillating perfusion of cell suspensions through three-dimensional scaffolds enhances cell seeding efficiency and uniformity. Biotechnol Bioeng. 2003;84(2):205-14.

9. Fedorovich NE, Alblas J, de Wijn JR, Hennink WE, Verbout AJ, Dhert WJ. Hydrogels as extracellular matrices for skeletal tissue engineering: state-of-the-art and novel application in organ printing. Tissue Eng. 2007;13(8):1905-25.

10. Peppas NA, Hilt JZ, Khademhosseini A, Langer R. Hydrogels in biology and medicine: from molecular principles to bionanotechnology. ADVANCED MATERIALS-DEERFIELD BEACH THEN WEINHEIM-. 2006;18(11):1345.

11. Zeng L, Chen X, Zhang Q, Yu F, Li Y, Yao Y. Redifferentiation of dedifferentiated chondrocytes in a novel three-dimensional microcavitary hydrogel. Journal of Biomedical Materials Research Part A. 2015;103(5):1693-702.

12. Wu D, Wang T, Lu B, Xu X, Cheng S, Jiang X, et al. Fabrication of supramolecular hydrogels for drug delivery and stem cell encapsulation. Langmuir. 2008;24(18):10306-12.

13. Wu D, Sun Y, Xu X, Cheng S, Zhang X, Zhuo R. Biodegradable and pH-sensitive hydrogels for cell encapsulation and controlled drug release. Biomacromolecules. 2008;9(4):1155-62.
14. Park H, Guo X, Temenoff JS, Tabata Y, Caplan AI, Kasper FK, et al. Effect of swelling ratio of injectable hydrogel composites on chondrogenic differentiation of encapsulated rabbit marrow mesenchymal stem cells in vitro. Biomacromolecules. 2009;10(3):541-6.
15. Khetan S, Guvendiren M, Legant WR, Cohen DM, Chen CS, Burdick JA. Degradation-mediated cellular traction directs stem cell fate in covalently crosslinked three-dimensional hydrogels. Nature materials. 2013;12(5):458-65.
16. Silva R, Fabry B, Boccaccini AR. Fibrous protein-based hydrogels for cell encapsulation. Biomaterials. 2014;35(25):6727-38.
17. Banks JM, Harley BA, Bailey RC. A tunable, photoreactive hydrogel system to probe synergies between mechanical and biomolecular cues on adipose-derived mesenchymal stem cell differentiation. ACS Biomaterials Science & Engineering. 2015.
18. Norotte C, Marga FS, Niklason LE, Forgacs G. Scaffold-free vascular tissue engineering using bioprinting. Biomaterials. 2009;30(30):5910-7.
19. Li Z, Gunn J, Chen M, Cooper A, Zhang M. On-site alginate gelation for enhanced cell proliferation and uniform distribution in porous scaffolds. Journal of Biomedical Materials Research Part A. 2008;86(2):552-9.
20. Billiet T, Gevaert E, De Schryver T, Cornelissen M, Dubruel P. The 3D printing of gelatin methacrylamide cell-laden tissue-engineered constructs with high cell viability. Biomaterials. 2014;35(1):49-62.
21. Ovsianikov A, Deiwick A, Van Vlierberghe S, Dubruel P, Möller L, Dräger G, et al. Laser fabrication of three-dimensional CAD scaffolds from photosensitive gelatin for applications in tissue engineering. Biomacromolecules. 2011;12(4):851-8.
22. Ma PX, Choi J. Biodegradable polymer scaffolds with well-defined interconnected spherical pore network. Tissue Eng. 2001;7(1):23-33.
23. Oh SH, Park IK, Kim JM, Lee JH. In vitro and in vivo characteristics of PCL scaffolds with pore size gradient fabricated by a centrifugation method. Biomaterials. 2007;28(9):1664-71.
24. Haraguchi Y, Shimizu T, Sasagawa T, Sekine H, Sakaguchi K, Kikuchi T, et al. Fabrication of functional three-dimensional tissues by stacking cell sheets in vitro. Nature protocols. 2012;7(5):850-8.

25. Gaetani R, Doevendans PA, Metz CH, Alblas J, Messina E, Giacomello A, et al. Cardiac tissue engineering using tissue printing technology and human cardiac progenitor cells. Biomaterials. 2012;33(6):1782-90.
26. Griffon DJ, Sedighi MR, Schaeffer DV, Eurell JA, Johnson AL. Chitosan scaffolds: interconnective pore size and cartilage engineering. Acta biomaterialia. 2006;2(3):313-20.
27. Lien S, Ko L, Huang T. Effect of pore size on ECM secretion and cell growth in gelatin scaffold for articular cartilage tissue engineering. Acta Biomaterialia. 2009;5(2):670-9.
28. Billiet T, Vandenhaute M, Schelfhout J, Van Vlierberghe S, Dubruel P. A review of trends and limitations in hydrogel-rapid prototyping for tissue engineering. Biomaterials. 2012;33(26):6020-41.
29. Fedorovich NE, De Wijn JR, Verbout AJ, Alblas J, Dhert WJ. Three-dimensional fiber deposition of cell-laden, viable, patterned constructs for bone tissue printing. Tissue Engineering Part A. 2008;14(1):127-33.
30. Khalil S, Nam J, Sun W. Multi-nozzle deposition for construction of 3D biopolymer tissue scaffolds. Rapid Prototyping Journal. 2005;11(1):9-17.
31. Wang X, Yan Y, Pan Y, Xiong Z, Liu H, Cheng J, et al. Generation of three-dimensional hepatocyte/gelatin structures with rapid prototyping system. Tissue Eng. 2006;12(1):83-90.
32. Tirella A, Orsini A, Vozzi G, Ahluwalia A. A phase diagram for microfabrication of geometrically controlled hydrogel scaffolds. Biofabrication. 2009;1(4):045002.
33. Khalil S, Sun W. Bioprinting endothelial cells with alginate for 3D tissue constructs. J Biomech Eng. 2009;131(11):111002.
34. DeForest CA, Anseth KS. Advances in bioactive hydrogels to probe and direct cell fate. Annual review of chemical and biomolecular engineering. 2012;3:421-44.
35. Malda J, Visser J, Melchels FP, Jüngst T, Hennink WE, Dhert WJ, et al. 25th anniversary article: engineering hydrogels for biofabrication. Adv Mater. 2013;25(36):5011-28.
36. Chang R, Nam J, Sun W. Direct cell writing of 3D microorgan for in vitro pharmacokinetic model. Tissue Engineering Part C: Methods. 2008;14(2):157-66.
37. Ahn S, Lee H, Bonassar LJ, Kim G. Cells (MC3T3-E1)-laden alginate scaffolds fabricated by a modified solid-freeform fabrication process supplemented with an aerosol spraying. Biomacromolecules. 2012;13(9):2997-3003.

38. Luo Y, Lode A, Wu C, Chang J, Gelinsky M. Alginate/Nanohydroxyapatite Scaffolds with Designed Core/Shell Structures Fabricated by 3D Plotting and in Situ Mineralization for Bone Tissue Engineering. ACS applied materials & interfaces. 2015;7(12):6541-9.
39. Rajaram A, Schreyer DJ, Chen DX. Use of the polycation polyethyleneimine to improve the physical properties of alginate–hyaluronic acid hydrogel during fabrication of tissue repair scaffolds. Journal of Biomaterials Science, Polymer Edition. 2015;26(7):433-45.
40. Bian L, Zhai DY, Tous E, Rai R, Mauck RL, Burdick JA. Enhanced MSC chondrogenesis following delivery of TGF-β3 from alginate microspheres within hyaluronic acid hydrogels in vitro and in vivo. Biomaterials. 2011;32(27):6425-34.
41. Lakard S, Herlem G, Propper A, Kastner A, Michel G, Valles-Villarreal N, et al. Adhesion and proliferation of cells on new polymers modified biomaterials. Bioelectrochemistry. 2004;62(1):19-27.
42. Khanam N, Mikoryak C, Draper RK, Balkus KJ. Electrospun linear polyethyleneimine scaffolds for cell growth. Acta biomaterialia. 2007;3(6):1050-9.
43. Armstrong CG, Bahrani AS, Gardner DL. In vitro measurement of articular cartilage deformations in the intact human hip joint under load. J Bone Joint Surg Am. 1979 Jul;61(5):744-55.
44. Nochos A, Douroumis D, Bouropoulos N. In vitro release of bovine serum albumin from alginate/HPMC hydrogel beads. Carbohydr Polym. 2008;74(3):451-7.
45. Yao Y, Wang Y. ATDC5: an excellent in vitro model cell line for skeletal development. J Cell Biochem. 2013;114(6):1223-9.
46. Izadifar Z, Chang T, Kulyk W, Chen X, Eames BF. Analyzing biological performance of 3D-printed, cell-impregnated hybrid constructs for cartilage tissue engineering. Tissue Engineering Part C: Methods. 2015.
47. Jang J, Seol Y, Kim HJ, Kundu J, Kim SW, Cho D. Effects of alginate hydrogel cross-linking density on mechanical and biological behaviors for tissue engineering. Journal of the mechanical behavior of biomedical materials. 2014;37:69-77.
48. Eames BF, De La Fuente L, Helms JA. Molecular ontogeny of the skeleton. Birth Defects Research Part C: Embryo Today: Reviews. 2003;69(2):93-101.
49. Hutmacher DW. Scaffolds in tissue engineering bone and cartilage. Biomaterials. 2000;21(24):2529-43.

50. Chung C, Burdick JA. Engineering cartilage tissue. Adv Drug Deliv Rev. 2008;60(2):243-62.
51. Vilela C, Correia C, Oliveira JM, Sousa RA, Espregueira-Mendes J, Reis RL. Cartilage repair using hydrogels: a critical review of in vivo experimental designs. ACS Biomaterials Science & Engineering. 2015.
52. Li M, Tian X, Schreyer DJ, Chen X. Effect of needle geometry on flow rate and cell damage in the dispensing-based biofabrication process. Biotechnol Prog. 2011;27(6):1777-84.
53. Liao I, Moutos FT, Estes BT, Zhao X, Guilak F. Composite three-dimensional woven scaffolds with interpenetrating network hydrogels to create functional synthetic articular cartilage. Advanced functional materials. 2013;23(47):5833-9.
54. Schuurman W, Klein T, Dhert W, Weeren P, Hutmacher D, Malda J. Cartilage regeneration using zonal chondrocyte subpopulations: a promising approach or an overcomplicated strategy? Journal of tissue engineering and regenerative medicine. 2015;9(6):669-78.
55. Visser J, Melchels FP, Jeon JE, van Bussel EM, Kimpton LS, Byrne HM, et al. Reinforcement of hydrogels using three-dimensionally printed microfibres. Nature communications. 2015;6.
56. Kesti M, Müller M, Becher J, Schnabelrauch M, D'Este M, Eglin D, et al. A versatile bioink for three-dimensional printing of cellular scaffolds based on thermally and photo-triggered tandem gelation. Acta biomaterialia. 2015;11:162-72.
57. Kesti M, Eberhardt C, Pagliccia G, Kenkel D, Grande D, Boss A, et al. Bioprinting Complex Cartilaginous Structures with Clinically Compliant Biomaterials. Advanced Functional Materials. 2015;25(48):7406-17.
58. George M, Abraham TE. Polyionic hydrocolloids for the intestinal delivery of protein drugs: alginate and chitosan—a review. J Controlled Release. 2006;114(1):1-14.
59. Huang X, Brazel CS. On the importance and mechanisms of burst release in matrix-controlled drug delivery systems. J Controlled Release. 2001;73(2):121-36.
60. Athanasiou KA, Darling EM, Hu JC. Articular cartilage tissue engineering. Synthesis Lectures on Tissue Engineering. 2009;1(1):1-182.

Chapter 5: Characterization of calcified cartilage matrix formation in homogeneous hydroxyapatite/alginate hydrogel and its printability

This chapter has been finished and ready for submission as You, F., Chen, X., Cooper, D., Eames, B. Characterization of calcified cartilage matrix formation in homogeneous hydroxyapatite/alginate hydrogel and its printability.

5.1 Abstract

Calcified cartilage formation plays an important role in a successful cartilage repair. However, a layer of calcified cartilage has not formed by current cartilage tissue engineering (CTE) strategies. To mimic native calcified cartilage, we hypothesized that the homogenously dispersed hydroxyapatite (HAP) within alginate (ALG) hydrogel promotes the deposition of characteristic matrix of calcified cartilage including Collagen type X and mineralized matrix. To test this hypothesis, a dispersant-sodium citrate (SC) was added to achieve homogenous mixing of HAP within ALG. Cell growth, extracellular matrix (ECM) production, and mineralization potential were evaluated in the presence or absence of HAP particles. Chondrocytes in gels with higher HAP content had higher mineralization potential, Collagen type X and minerals deposition. The printability of the composite hydrogel precursors was verified by printing porous scaffolds using a 3D Bioplotter. The results herein demonstrated that the presence of HAP in ALG hydrogel facilitates the deposition of calcified cartilage extracellular matrix (ECM) and thus is a promising design strategy for osteochondral interface regeneration.

Key words: calcified cartilage; hydroxyapatite; alginate; Collagen type X; minerals

5.2 Introduction

Osteoarthritis (OA) is a degenerative joint disorder characterized by articular cartilage lesions, severe joint pain, and loss of joint function (1). Surgeries are typically needed to treat OA due to the limited self-repair tendency of cartilage (2). Current surgical intervention such as autologous chondrocyte implantation (3), microfracture (4), osteotomy (5), joint replacement (6) are usually associated with donor site morbidity, undesirable fibrocartilage formation, or poor

long-term outcomes (7, 8). Cartilage tissue engineering (CTE) has shown promising to repair cartilage defects (9-11). Nevertheless, most current CTE strategies have not achieved successful regeneration of the osteochondral interface between the engineered cartilage and the subchondral bone. Although engineered osteochondral constructs have been explored to regenerate osteochondral defects (defects extending from articular cartilage to underlying subchondral bone), a stable osteochondral interface has yet to be formed within the construct. Notably, a layer of osteochondral interface is crucial for sustaining the structural integrity of engineered cartilage by curtailing ectopic mineralization and bone upgrowth, and preventing vascular invasion from bone in the full-thickness defects (12, 13). The native osteochondral interface consists of a layer of calcified cartilage, in which hypertrophic chondrocytes are embedded in a mineralized cartilage matrix. As an osteochondral interface, calcified cartilage also transmits force from pliable cartilage to stiff bone and serves as a structural barrier between cartilage and subchondral bone to ensure the pressurization of articular cartilage. As the last layer of cartilage next the bone, calcified cartilage also maintains the integrity of the osteochondral connection when compressive, tensile, and shear forces are transmitted from the viscoelastic joint cartilage to the stiff mineralized subchondral bone. The ideal scaffolding materials for osteochondral interface regeneration should promote the deposition of calcified cartilage matrix.

Formation of Collagen type X and mineralized matrix within scaffolds is the key to regenerating calcified cartilage. Previous results demonstrated the formation of Collagen type X with chondrocytes cultured directly on a calcium phosphate substrate (14). Also, published data indicated that cellular uptake of Ca^{2+} and inorganic phosphate (Pi) appeared to lead to the formation of complexes of amorphous calcium phosphate by chondrocytes (15). Inspired by these results, the present study employed hydroxyapatite (HAP) as a cue to induce the secretion of calcified cartilage matrix from chondrocytes. Alginate (ALG) hydrogels are cross-linked polymer networks holding large amounts of water and are good candidates for soft tissue engineering (16) due to their properties including efficient mass transfer, stimuli-responsiveness (17) and hydrophilic nature. HAP is widely present in natural mineralized tissue (18). Incorporating inorganic particles in polymeric hydrogels has been done before and is expected to introduce bioactive characteristics to the cross-linked network (19). Based on these findings, this study was aimed at designing and optimizing a composite ALG/HAP scaffold for calcified cartilage regeneration. Herein we hypothesize that the homogenously dispersed HAP within

ALG hydrogel promotes the deposition of characteristic matrix of calcified cartilage including Collagen type X and mineralized matrix.

Most common approach used to synthesize ALG/HAP composite is direct mixing hydrogel with hydroxyapatite particles (20, 21). However, such a physical mixing process is uncontrolled and usually leads to inhomogeneity of particle dispersion within polymer matrix. The heterogeneous distribution of these particles has a negative influence on experiment repeatability and not all embedded cells have access to mineral particles. Therefore, homogenization and intermixing of inorganic components within the polymeric networks remains a major engineering challenge for developing an ALG/HAP composite hydrogel.

An important objective of this study is, by exploiting a dispersant, the homogenous dispersion of mineral particles in hydrogel matrix can be achieved. Dispersants have been widely used for the stabilization of particle dispersion during ceramic processing (22, 23). Another advantage of even distribution of ceramic particles in hydrogel is facilitating 3D printing process. During the fabrication process, hydrogel precursors are usually stored in a syringe and ready to flow through a needle tip. Inhomogeneous dispersion of nanoparticles may lead to sedimentation of inorganic components and thus clog the needle tip.

In the current study, homogenous ALG/HAP composite hydrogels were prepared using a dispersant-sodium citrate (SC). Embedded chondrocyte viability, characteristic calcified cartilage matrix including Collagen type X and mineralized matrix were studied. In the end, porous ALG/HAP composite hydrogel scaffold will be fabricated by a 3D Biopoltter to verify the printability and dispersion outcomes of the ALG/HAP hydrogel system.

5.3 Materials and Methods

5.3.1 Cells Isolation and Culture

Primary chondrocytes were isolated from cartilaginous sternums of 14-day-old chick embryos (24). Chondrocytes from embryonic chick cartilage were used as the cells source due to the accessibility and abundant numbers and they also have been very well understood and characterized in terms of development and differentiation in tissue scaffolds under different culture conditions (25-29). A dozen of chick embryos were used to obtain sufficient numbers of primary cells without passaging them to minimize negative effects of monolayer passaging on chondrogenic differentiation. The sternums of chick embryos were carefully excised, chopped

and placed in digestion medium consists of 0.2% collagenase and 0.25% trypsin in Hank's buffered salt solution (HBSS) at 37℃ and 5% CO_2 for 2 hours. The digestion was terminated by adding Dulbecco's modified Eagle's medium (DMEM, Gibco) supplemented with 10% FBS. The obtained cell suspension was filtered through a 70 μm sterile Nitex and centrifuged at 200g for 10 minutes. The collected cell pellets were suspended and cultured in culture medium containing DMEM, 10% FBS, 2mM glutamine, 0.1 mg/mL kanamycin, 1% AA (100 U/mL penicillin, 0.1 mg/mL streptomycin, 0.25 μg/mL amphotericin B), and 0.01 mg/mL ascorbate. The cells were harvested at confluence by trypsinization and collected by centrifugation at 300 g for 10 min, followed by counting the cell number using a hemocytometer.

5.3.2 Synthesis and Characterization of Hydroxyapatite (HAP) Suspensions with the Addition of Dispersants

Sodium citrate tribasic dihydrate (SC, $Na_3C_6H_5O_7 \cdot 2H_2O$, Sigma-Aldrich) was added to DMEM. HAP particles were mixed into the SC-incorporated DMEM with the molar ratios of SC to HAP were 0.1:1, 0.125:1, 0.25:1, 0.5:1, 1:1, 2:1, 4:1, 8:1, 10:1 to determine the optimum ratio. The pH of the suspensions was measured using a standard pH meter (Pinnacle M530). The Zeta-potential of the suspensions was determined in triplicate using a Zetasizer (Brookhaven). Sedimentation characteristics of the prepared suspensions were monitored by adding 10 ml of suspension in 15 ml tubes and recording the settling height. For transmission electron microscopy (TEM), HAP suspensions with/without dispersants dropped onto a carbon-coated copper TEM grid and examined (Philips CM10). ALG/HAP composite hydrogel precursors were prepared by dissolving ALG in HAP suspensions in the absence or presence of SC. To examine the dispersion of the incorporated HAP particles in ALG matrix, ALG and HAP hydrogel precursors were lyophilized, coated with gold and examined by scanning electron microscopy (SEM, SU6600, HITACHI) equipped with energy dispersive spectroscopy (EDS). The elemental 2D-mapping of calcium and phosphorus was examined by EDS technique.

5.3.3 Preparation and Culture of Cell-laden ALG/HAP Composite Hydrogel Disks

SC was dissolved in DMEM and the obtained medium was filtered through a 0.22μm filter for sterilization. HAP suspensions were prepared in the SC-incorporated DMEM. ALG solution solutions were prepared by stir-bar mixing of alginic acid sodium salt in HAP suspensions under

sterile condition. The ALG/HAP solution was then mixed with cells suspension with a volume ration of 7:3 (solution volume to cells suspension) to reach a final cell density of 1.57×10^6 cells/ml. Three groups of samples were obtained: i) ALG, ii) ALG+1%HAP, and iii) ALG+2%HAP. ALG concentration was kept at 2.5% in all groups. Corresponding acellular controls for each group were prepared. 24-well culture plates were washed with DMEM prior to use. 1-ml syringe was used to inject 120μL cell/gel mixture to each well and waited until the mixture evenly cover the bottom of well which usually took 15-20 minutes. 1mL DMEM was added into each well followed by crosslinking ALG/HAP solutions with autoclaved 1mL 100 mM calcium chloride solution for 10 minutes. The crosslinking solution was replaced by culture medium and then culture plates were cultured in incubator at 37℃.

5.3.4 Cell Viability and Proliferation

Cell viability tests were conducted using calcein AM and ethidium bromide (EthD-1) solution (live/dead viability kit, Invitrogen) as recommended by the supplier. At each time point, cell-laden hydrogel scaffolds were removed from culture, washed with DMEM and incubated in 2μM calcein-AM and 1 μM EthD-1 solution in DMEM for 30 min at 37 ℃. The samples were washed with DMEM and imaged using a fluorescence microscope (Leica, Switzerland). Sequential images at different locations were captured to visualize cell distribution and viability of the embedded cells within the hydrogel. To quantitatively determine the cell viability, the stained cells were released by incubating cell-laden constructs in 50mM EDTA (diluted in DMEM) for 30 min at room temperature. Then the medium was pipetted to obtain an homogenous cell suspension mixture. Samples (n=3) were taken from the mixture of each disk and imaged under a coverslip on a glass microscope slide at 5-6 random locations to count live and dead cells. Cell number (n=3) was calculated using a hemocytometer to indicate the cell proliferation over the culture period.

5.3.5 Cartilaginous Matrix Deposition

Alcian blue staining was used to detect accumulation of glycosaminoglycans (GAGs) in the cell-embedded disks. The cell-embedded disks (n=3) were removed from culture, washed with DMEM and fixed in acetone and methanol solution (1:1) on ice for 15 minutes and then stained with 0.001 % Alcian blue in 3% acetic acid solution overnight. The stained constructs were

washed with 25% ethanol in 3% acetic acid for 1h and then washed with 50% ethanol in 3% acetic acid until obtaining a good background, and imaged using light microscopy.

Immunofluorescent staining was performed to detect the deposition of Collagen type II or Collagen type X. The disks (n=3) were harvested and washed with DMEM and fixed in 4% paraformaldehyde (PFA) in PBS at 4ºC on a shaking platform. The fixed samples were permeabilized with 0.5% Triton X-100 in PBS (PBS-T) for 5 min three times with shaking, followed by pre-treatment to block nonspecific reactions with blocking buffer (4% goat serum and 2% sheep serum in PBS-T) 2 hours while shaking at room temperature. For collagen staining, the constructs were incubated in anti-Col2 or anti-Col10 antibody (DSHB) in blocking buffer (1:100) overnight at 4ºC while shaking followed by rinsed with blocking buffer (30). The secondary immunoreaction was carried out with Alexa 488-conjugated goat anti-mouse IgG (1:1000, Invitrogen) in blocking buffer overnight at 4ºC, followed by rinsing with PBS-T. Fluorescent images were taken with a fluorescence microscope (Leica).

ImageJ was used to quantitatively analyze calcified cartilage matrix deposition (31). Four random regions of interest covered by Alcian blue and immunofluorescent stains were taken for each disk and appropriate threshold was applied to segment the stained areas (same threshold for all samples). For each time point, such segmentation was carried out to estimate the area covered by staining compared to the total area in the regions of interest.

5.3.6 Mineralization

Mineralization potential was quantitated by measuring alkaline phosphatase (ALP) activity, which was determined using an enzymatic assay based on the hydrolysis of p-nitrophenyl phosphate (pNP-PO4) to p-nitro-phenol (pNP). Briefly, the samples were lysed in 0.1% Triton-X solution for 15 min at 4ºC, then were added 50µL pNP-PO4 solution (Sigma) and allowed to react for 30 min at 37ºC. The reaction was stopped with 20µL 0.1 N NaOH (Sigma), and sample absorbance was measured at 405 nm using a microplate reader. ALP staining was done as follows. Samples were fixed in 4%PFA in PBS for 10 min and washed for 5 min in ALP buffer (100 mM Tris, pH 9.5; 50 mM MgCl2; 100 mM NaCl; 0.1% Tween 20), and incubated in BM Purple (Roche, USA) until strong signal appeared.

Mineral distribution was evaluated with Alizarin Red staining. Briefly, cell-embedded disks were fixed in 4% PFA for 20 min at room temperature. After PBS washing, disks were stained

with 0.1% Alizarin Red solution (pH=4.3) for overnight at ambient temperature and imaged with a Nikon optical microscope.

5.3.7 Rheology of Composite Hydrogel Precursors

Rheological properties of three groups of hydrogel precursors (2.5%ALG, 2.5%ALG+1%HAP, 2.5%ALG+2%HAP) were measured using a rheometer (AR G2, TA Instruments). Viscosity and shear stress were measured at 25 °C with a rotatory test setup by varying the shear rate from 0 to 200 1/s. Storage (G') and loss modulus (G'') were assessed by oscillatory tests by applying 5% strain within the linear viscoelastic region over a frequency range between 1 and 100 rad/s.

5.3.8 3D Printing of Composite Hydrogels

12-well tissue culture plates were pre-treated with sterile 0.1% (w/v) polyethylenimine (PEI, Alfa Aesar, MW: 60000) in PBS and incubated overnight at 37 °C. The PEI-doped plotting surfaces were flushed with double distilled water prior to fabrication. To form the composite hydrogel scaffolds, hydrogel precursor solutions were loaded into the low temperature dispensing head of the 3D-Bioplotter^{TM} (EnvisionTec, GmbH, Gladbeck, Germany). 3D porous scaffolds were produced by a sequential fiber deposition process. Briefly, the Bioplotter operates as a three-axis dispensing machine that deposits hydrogel precursors pneumatically on a stationary platform following the CAD model which contains the information for the layer-by-layer deposition (32). The gel precursors were dispensed through a 200 µm conical needle, using 0.02MPa pressure at dispensing speed of 8.5 mm/sec into a crosslinking medium containing 100mM calcium chloride, 0.1 % w/v PEI on the 0.1 % w/v PEI/PBS pretreated culture plate (30). By a layer-by-layer deposition process, scaffolds of 10mm×10mm×3.6mm with 20 layers of strands and 1 mm strand spacing were created.

5.3.9 Micro-CT Characterization of Printed Porous Hydrogel Scaffolds

Micro-CT imaging of printed composite hydrogel scaffolds was conducted by a Bruker micro-CT SkyScan 1172 (Kontich, Belgium) scanner. Samples were scanned with acquisition protocol that consisted of pixel size of 19.97 µm, X-ray tube settings of 40 kV and 250µA, rotation step of 0.1°, 1 mm aluminum filter, 10-frame averaging. Isotropic 2D slices of the

scaffolds were acquired from the projection datasets in a reconstruction procedure using NRECON V 1.6.10.1 (Skyscan 2011). The obtained data were exported into Amira software (Amira, USA) for 3D reconstruction.

5.3.10 Statistical Analysis

For quantitative analysis, Student's *t* tests were used to assess differences between two groups and multiple comparisons were performed via one-way ANOVA using SPSS software. Data are expressed as mean values ± standard deviation (SD), with p values <0.05 considered statistically significant.

5.4 Results

5.4.1 SC Can be Used to Stabilize HAP Suspensions

Sedimentation experiments were carried out to evaluate the effect of different molar ratios of SC to HAP on the stabilization of the HAP suspensions (Figure 5.1). SC can reduce sedimentation of HAP suspensions for the first 24h while the sedimentation of reference group without dispersant can be observed after 3h (Figure 5.1B, C). Stable suspensions without demarcation line for 24h were obtained when the molar ratio of SC to HAP was 0.25:1 or higher. Corresponding Zeta-potential measurements were carried out to reveal electrical charge on the HAP particles and the stability of HAP dispersions (Figure 5.1E). Overall, addition of SC led to an obvious increase in the negative Zeta-potential from values of +1 mV without SC to about -26 mV with a molar ratio of 10:1 (SC to HAP). pH values were tested to investigate the influence of SC on the pH. With the addition of SC, pH value suspension can go up to 9.4 when the molar ratio (SC: HAP) reach 10 (Figure 5.1F). TEM micrographs showed the morphology and dispersion state of the HAP particles in the absence (Figure 5.2A) or presence with SC (Figure 5.2B, the molar ratio of SC to HAP is 0.25:1). HAP spherical crystals were recognized in both groups with the size of 150-200 nm in diameter. The aggregation of particles was more obvious in the absence of SC while the HAP particles in the other group were well dispersed.

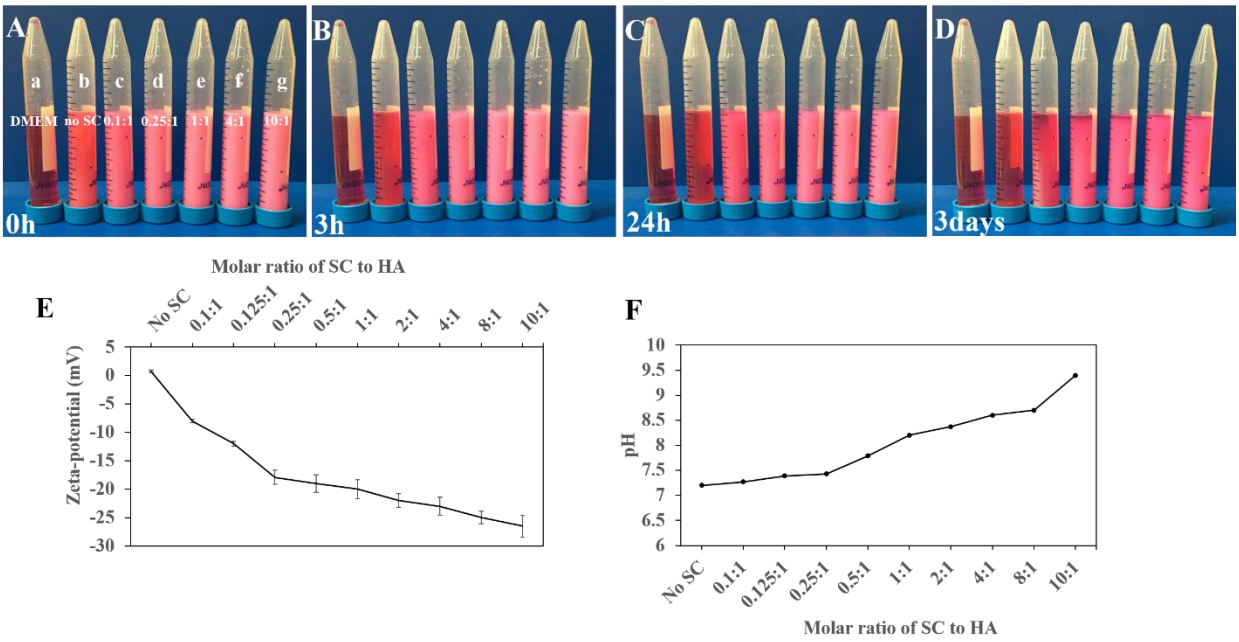

Figure 5.1 Influence of SC concentration on the stabilization of HAP suspensions. (A-D) Sedimentation behavior of HAP suspensions supplemented with SC. (E) Zeta-potential of HAP suspension in water as a function of SC addition. (F) pH of HAP suspension in DMEM as a function of SC addition.

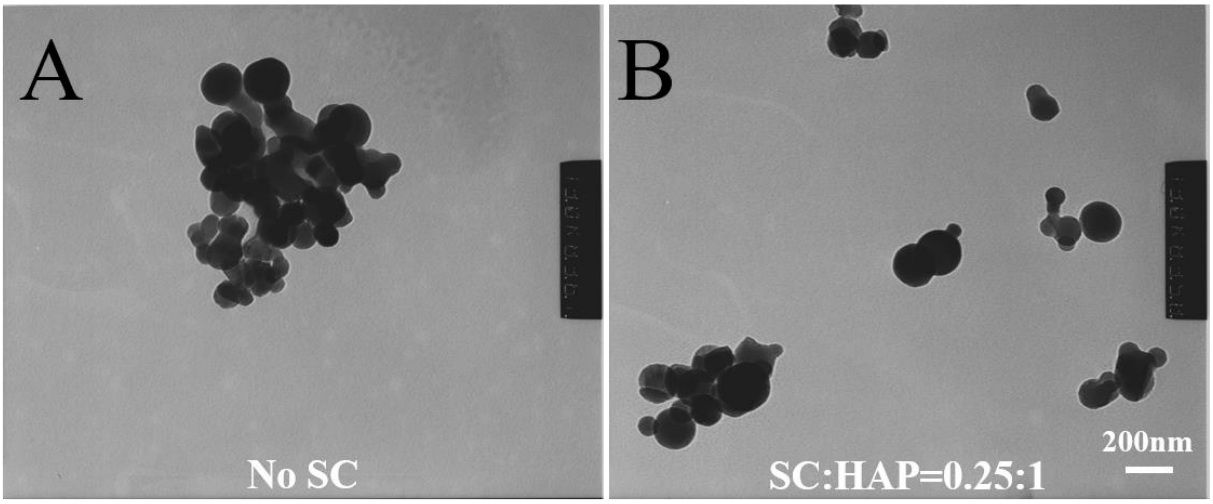

Figure 5.2 TEM micrographs of HAP particles in the absence (A) or presence (B) of SC.

5.4.2 Dispersion of HAP Particles in ALG Hydrogel is Analyzed by SEM

SEM micrographs and corresponding EDS analysis of composite hydrogel precursors were performed (Figure 5.3) to visualize the dispersion of HAP particles within the ALG hydrogel. The globular particles in the alginate matrix can be observed in groups with HAP (Figure 5.3D-E). However, the number and size of these globular particles in composites with dispersants (Figure 5.3C, E) were less and smaller than those without dispersants (Figure 5.3B, D), indicating that the addition of SC reduced the aggregation of HAP particles and promoted their dispersion in the alginate matrix. The heterogeneity of HAP particles in SC-free composites and the homogeneity of composites with SC were also confirmed by elemental mapping for calcium and phosphorus elements, both of which existed in HAP molecules. The distribution of calcium and phosphorus elements were very heterogeneous in SC-free groups (Figure 5.3G, I, L, N), suggesting the aggregation of HAP particles. In contrast, the elements distribution in composites with SC were nearly homogeneous and no obvious aggregation of calcium and phosphorus elements (Figure 5.3H, J, M, O), revealing that clustering of HAP particles in ALG matrix can be avoided by using SC.

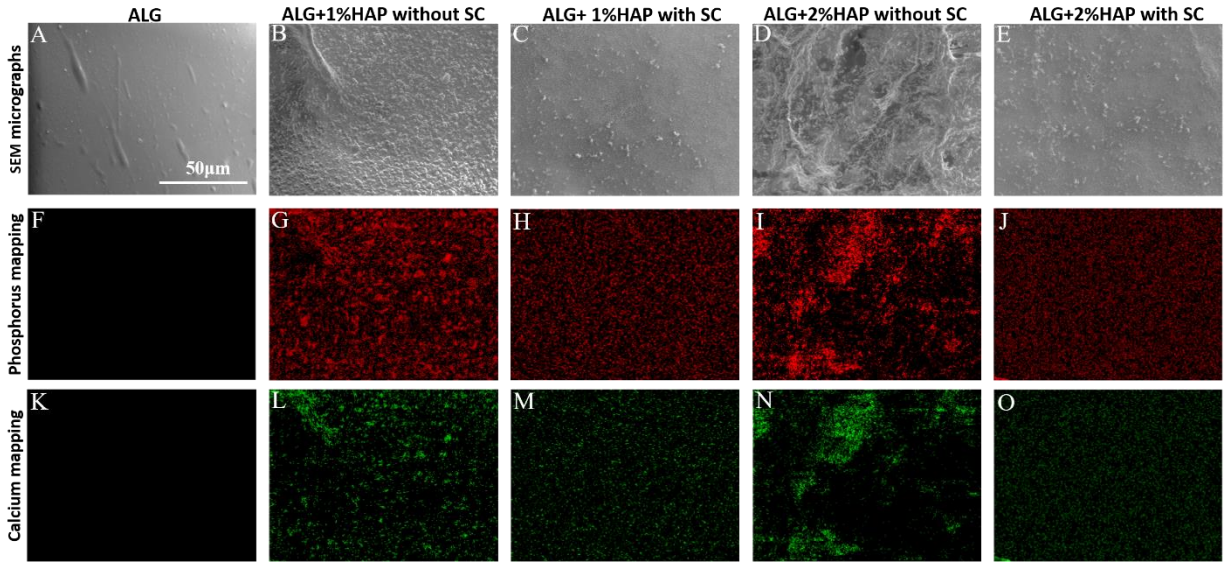

Figure 5.3 SEM micrographs and corresponding calcium and phosphorus mapping of three groups show the dispersion of HAP particles in ALG hydrogel.

5.4.3 Influence of the Addition of HAP Particles on Cytocompatibility

To ensure that the whole fabrication process and materials involved could provide a cytocompatible environment for chondrocytes, live and dead cells were visualized in composite

hydrogels. Fluorescent images showed most chondrocytes were alive and it can be recognized that a homogeneous distribution of encapsulated cells was achieved. All three groups showed a higher cell viability than 75% throughout culture period. The cell viability of ALG+1%HAP at Day14 was significantly higher than that of Day1 and meanwhile, same trend was observed for the group of ALG+2%HAP. Quantitative analyses suggested that cell numbers steadily increased during the culture period for each group, each showing a significant increase in cell number compared with earlier culture time points. At each timepoint, chondrocytes cultured in three composite hydrogels showed similar cell numbers during culture period.

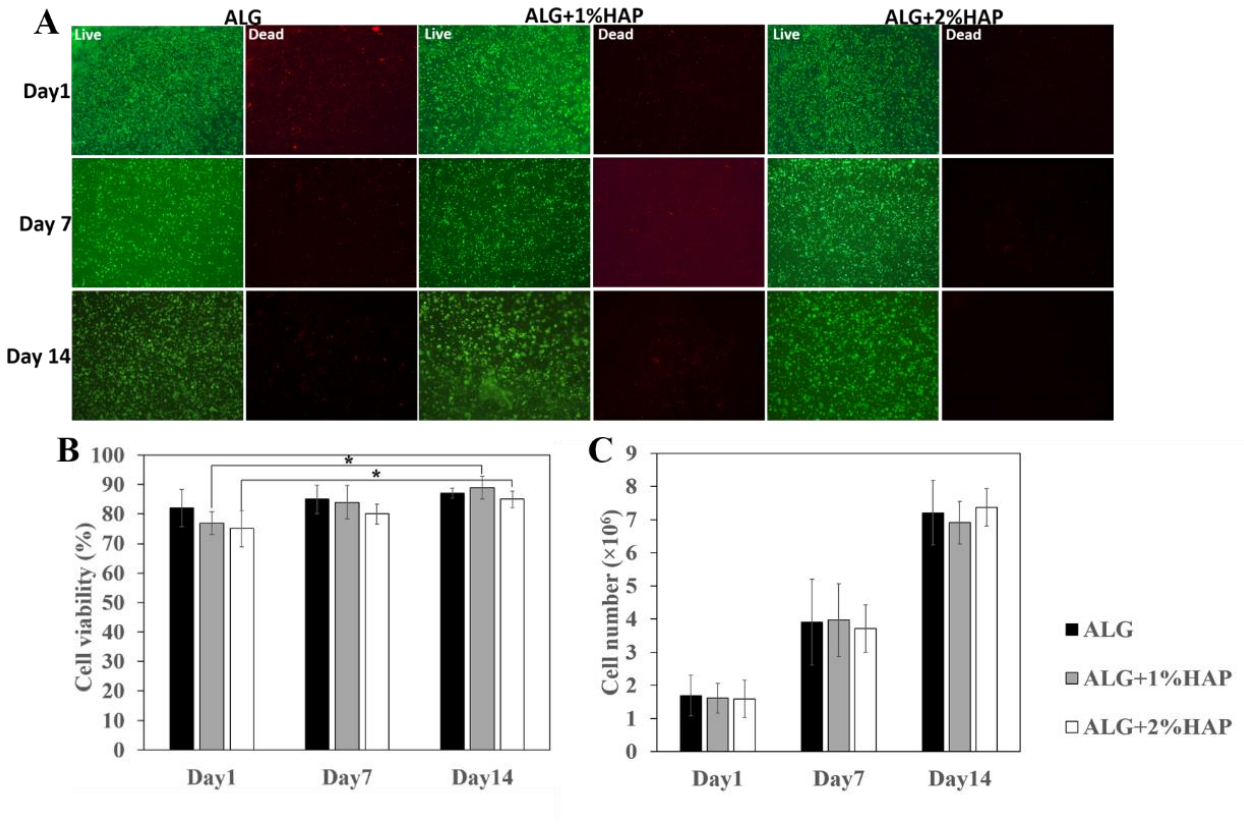

Figure 5.4 Fabrication process and materials supported cell survival and proliferation. (A) Fluorescent images showing live (green) and dead (red) cells. (B) Cell viability (*****$p<0.05$, n=3) and (C) cell number for various cell culture periods. At each timepoint, there is no significant difference in cell numbers among three groups. For each group, chondrocytes numbers increase significantly with culture (n=3).

5.4.4 Chondrocytes Secrete Cartilage Matrix within the Composite Hydrogel Disks

The addition of HAP phase into the ALG hydrogel did not have a significant effect on the chondrocytes viability and proliferation. Then, the influence of HAP presence on the cartilage matrix secretion was analysed. Alcian blue and Collagen type II immunofluorescence staining were used to detect the deposition of the two main components in cartilage ECM, glycosaminoglycans (GAGs) and Collagen type II, within the composite hydrogel disks during *in vitro* culture. Alcian blue staining demonstrating the GAGs synthesis was recognized around cells in all groups throughout *in vitro* culture. Less and smaller stained areas were seen at Day7 for three groups of composite hydrogels (Figure 5.5A, B, C). At Day14 and 28, areas of Alcian blue-stained matrix appeared to increase in numbers (Figure 5.5D, E, F) and size (Figure 5.5G, H, I) for all three groups. Relative area of Alcian blue-stained matrix was measured to quantitate these observations, and the results agreed with the trends observed in the images. Alcian blue-stained matrix increased over time for all three groups, being significantly higher at Day28 compared to Day 7 and 14 (Figure 5.5J). At Day 14, ALG+2%HAP showed least regions of Alcian blue-stained matrix than other two groups (Figure 5.5J). At Day28, ALG+2%HAP showed significant less Alcian blue stained area than that of ALG group.

Immunostaining showed the secretion of Collagen type II matrix around embedded cells in composite hydrogel disks after 28 days of culture for three groups (Figure 5.6). ALG group seemed to have less collage type II stained matrix than the other groups (Figure 5.6A, B, C). Embedded chondrocytes appeared to show comparable synthesis of Collagen type II for groups of ALG+1%HAP and ALG+2%HAP (Figure 5.6B, C). Quantitive analysis revealed the same trends observed in the staining images (Figure 5.6D). These results indicated that composite hydrogels offered a advantageous environment for chondrogenic differentiation and increased synthesis of cartilaginous ECM over long in vitro culture periods.

To test the hypothesis that the presence of HAP phase promotes synthesis of Collagen type X, the deposition of Collagen type X was detected by immunostaining at Day28. It can be observed from the images that Collage type X secretion increased with the amount of HAP phase addition (Figure 5.7A, B, C). Quantitate analysis demonstrated that chondrocytes in composite hydrogels with the presence of HAP phase secreted more Collagen type X than ALG group, and the amount of synthesized Collagen type X was positively related with content of added HAP phase. Therefore, the addition of HAP particles did induce the secretion of Collagen type X.

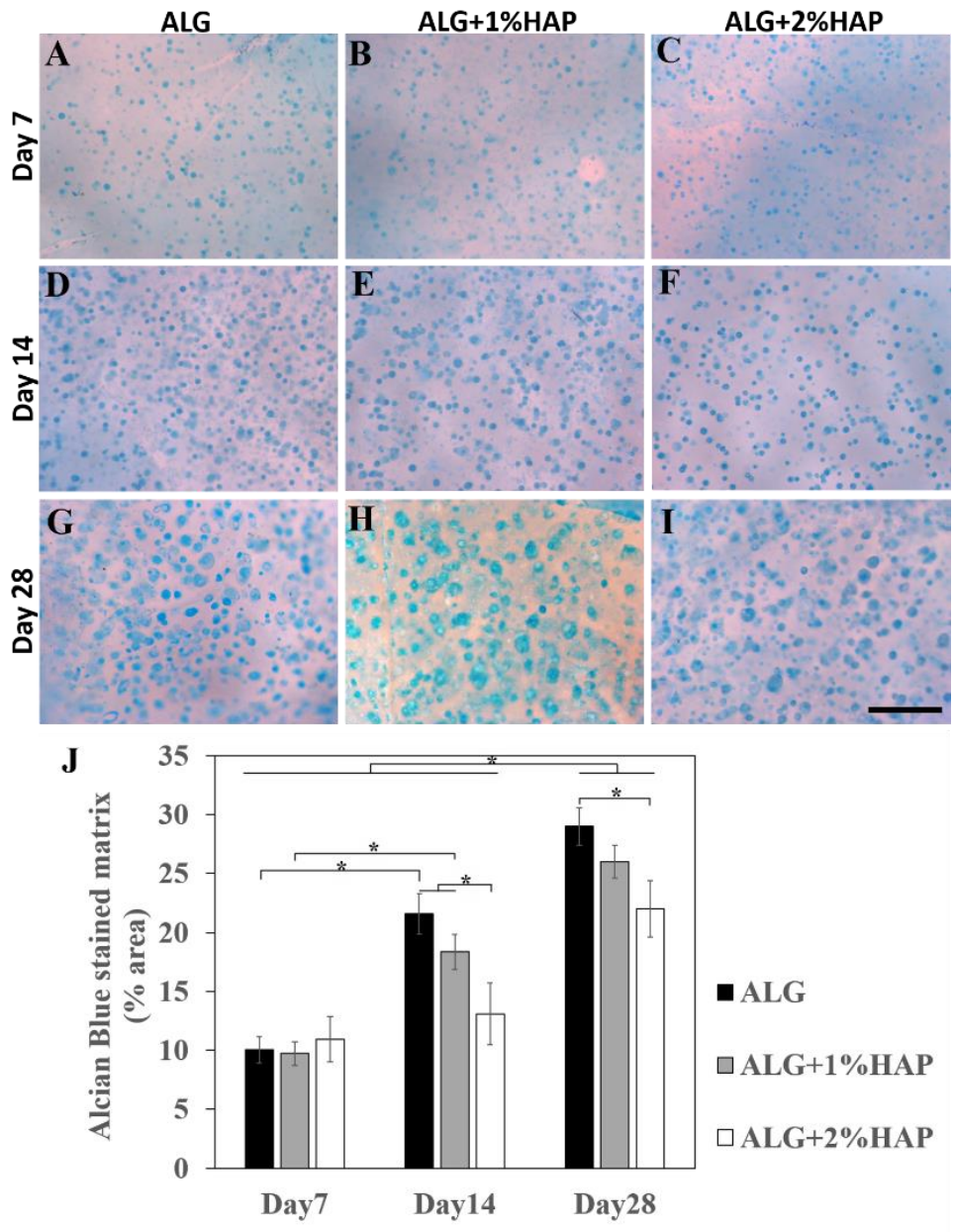

Figure 5.5 Composite hydrogels provide a favourable envirnment for increased synthesis of GAGs. (A) Increased secretion of Alcian blue-stained matrix in different gel disks over in vitro culture time (Scale bar=200μm). (B) Quantitative increase of Alcian blue-stained matrix over in vitro culture time for each group (*****$p<0.05$, n=4).

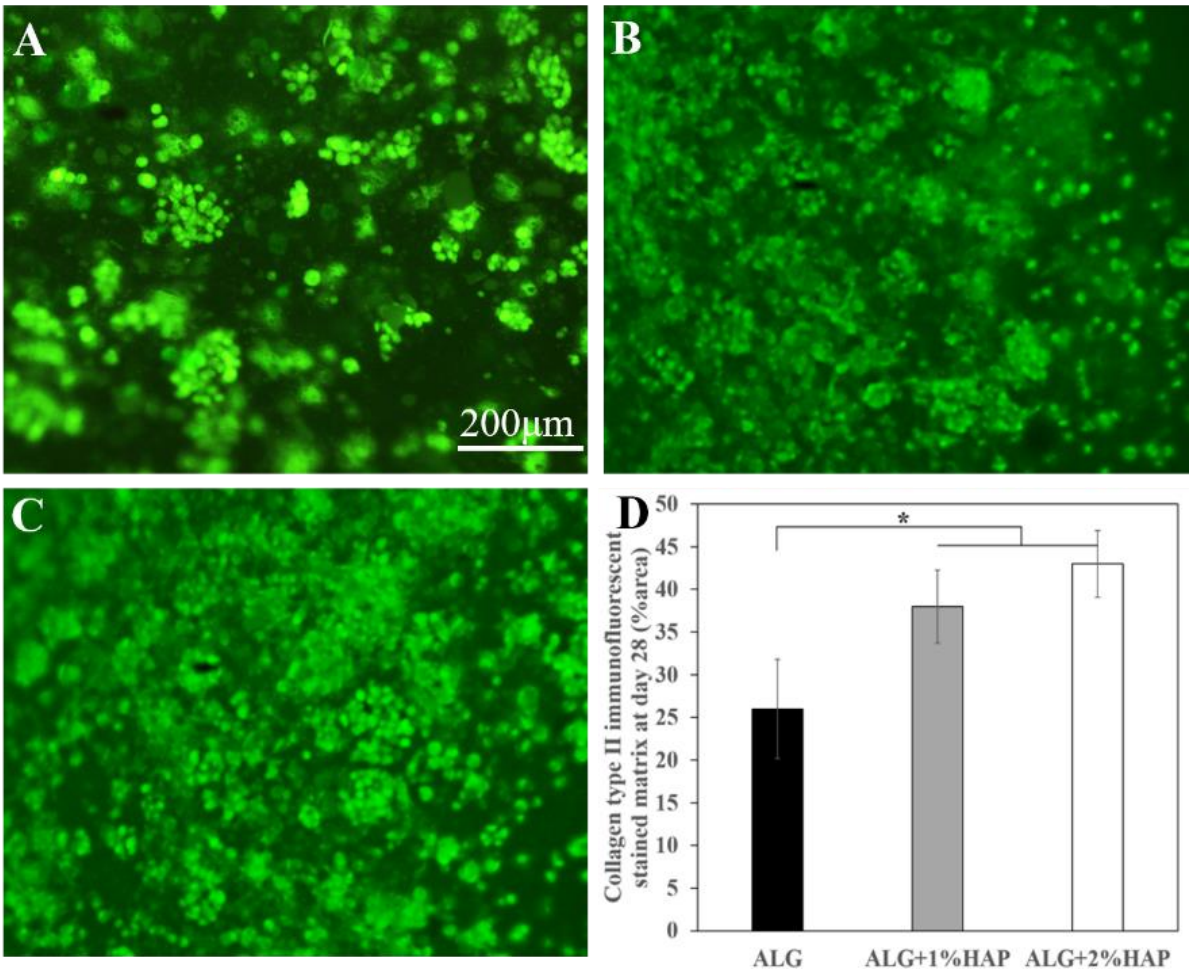

Figure 5.6 Collagen type II immunofluorescence staining demonstrates the deposition Collagen type II in (A)ALG, (B) ALG+1%HAP, (C) ALG+2%HAP composite gel disks after 28 days of culture (Scale bar=200μm). (C) shows the quantitation of Collagen type II immunostained area in gel disks after 28 days of culture (*****$p<0.05$, n=4).

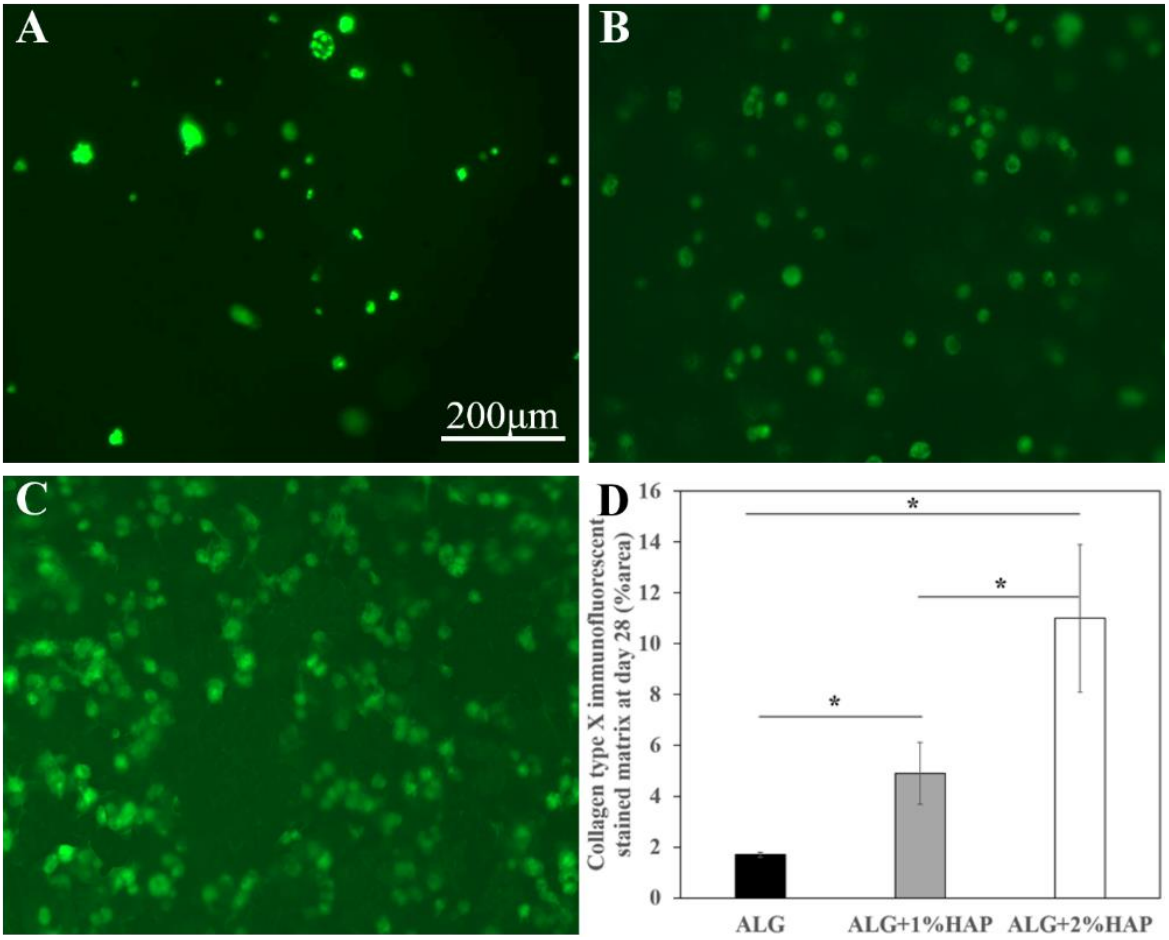

Figure 5.7 Collagen type X immunofluorescence staining demonstrates the deposition Collagen type X in (A)ALG, (B) ALG+1%HAP, (C) ALG+2%HAP composite gel disks after 28 days of culture. (C) shows the quantitation of Collagen type X immunostained area in gel disks after 28 days of culture (*****$p<0.05$, n=4).

5.4.5 Minerals Deposition Increases with HAP Content

Mineralization potential of chondrocytes in composite hydrogels was determined by ALP activity. After two weeks of culture, chondrocytes in the ALP+1%HAP and ALP+2%HAP scaffolds showed positive ALP staining while no obvious ALP staining was seen in ALG group (Figure 5.8A, B, C). At Day28, although ALP staining can be observed in all three groups, chondrocytes in ALP+1%HAP and ALP+2%HAP gels secreted more ALP (Figure 5.8D, E, F). ALP activity measurements indicated similar phenomenon, with ALP+1%HAP and ALP+2%HAP measured significantly higher ALP activity as compared to the ALP group and the highest ALP activity found in the 2% HA group (Figure 5.8G).

Alizarin red staining was applied to detect the mineral phase synthesized by embedded chondrocytes. During 14 days of culture, Alizarin red stained the cells and reflected the cells proliferation (Figure 5.9G-L). At Day28, obvious mineral deposition was observed for groups of ALG+1%HAP and ALG+2%HAP (Figure 5.9M, N, O). Control groups without cells were also stained to investigate the influence of pre-incorporated HAP particles on the Alizarin red staining outcomes (Figure 5.9A-F). Results have shown that these HAP particles were not stained by Alizarin red. Therefore, positive Alizarin red staining in ALG, ALG+1%HAP and ALG+2%HAP groups was mainly from cells and newly formed minerals. Compared with ALG, stronger staining in ALG+1%HAP and ALG+2%HAP at Day28 was a result of minerals deposited by chondrocytes. Quantitative characterization suggested the same results that ALG+1%HAP and ALG+2%HAP groups showed the highest amount of minerals secretion at Day28 (Figure 5.9P). This tested the hypothesis that the presence of HAP induced the chondrocytes secreted minerals.

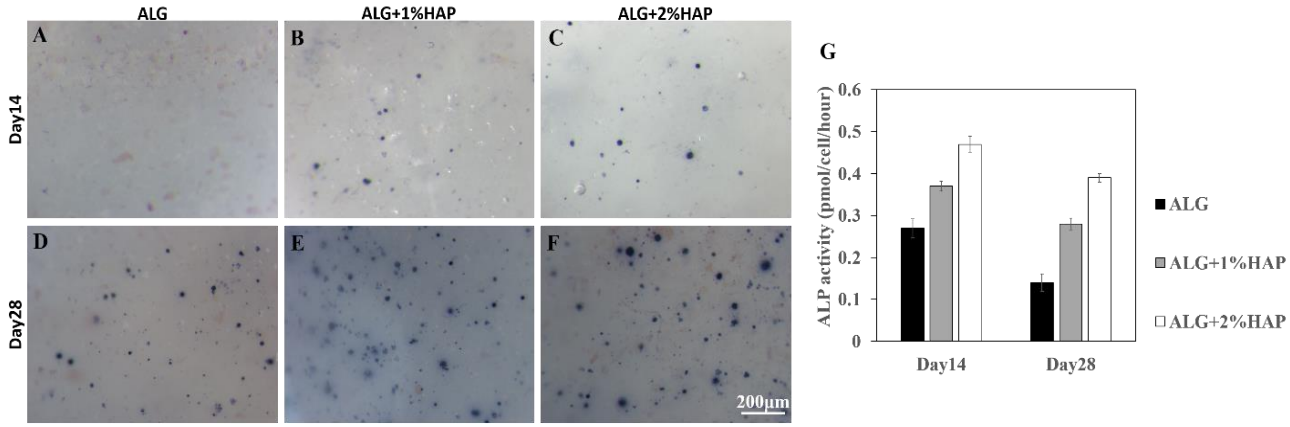

Figure 5.8 Mineralization potential was characterized by ALP staining and activity. ALP staining of three groups of composite hydrogels at Day 14 (A, B, C) and Day 28 (D, E, F). (G) ALP activity of chondrocytes in three groups of composite hydrogels at Day 14 and Day 28. For each group, there was significant difference of ALP activity between two time points. For each timepoint, there was significant difference among three groups.

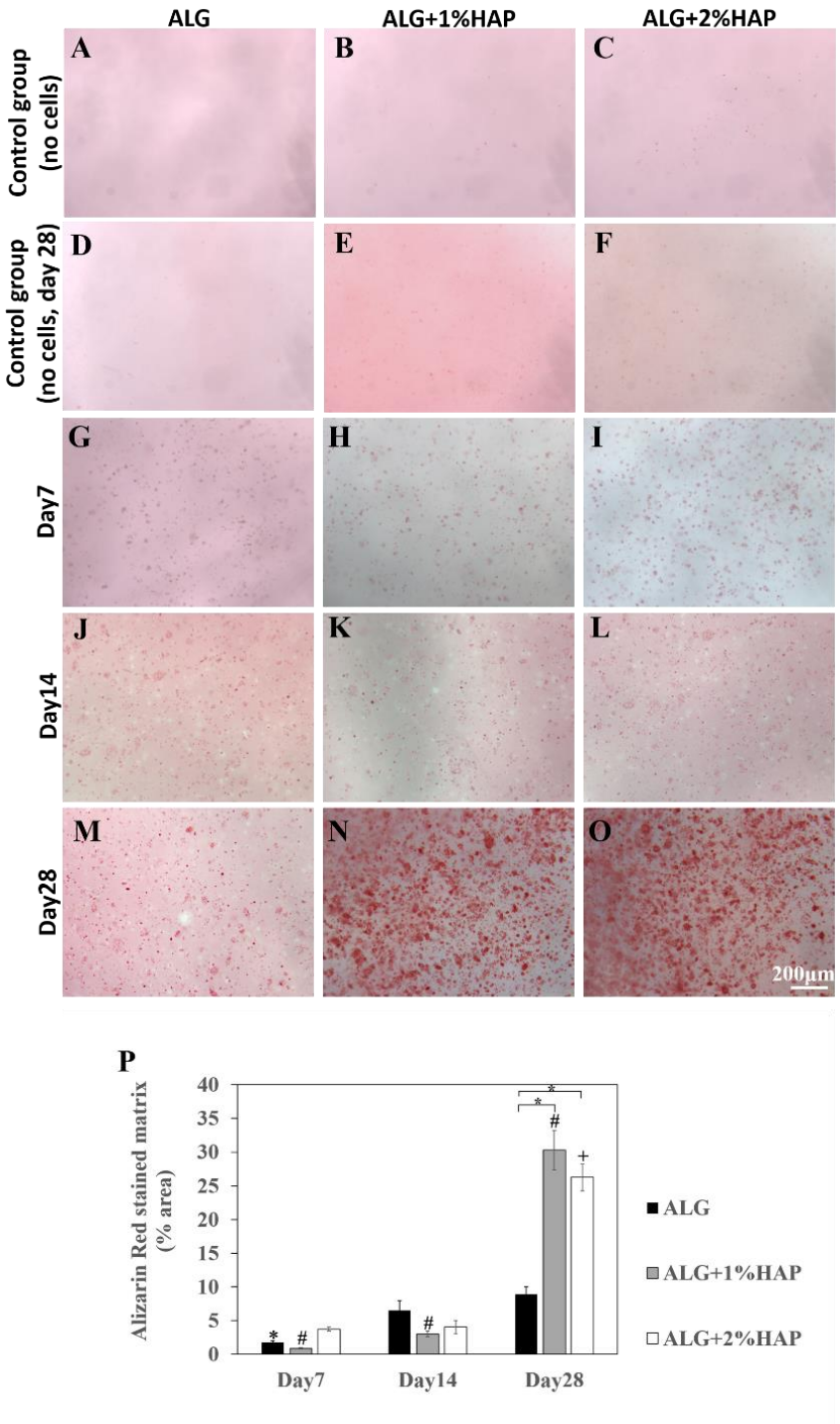

Figure 5.9 Alizarin red staining detected minerals deposition of ALG, ALG+1%HAP, and ALG+2%HAP groups. (A-O) Mineral deposition by encapsulated chondrocytes in three groups of hydrogels were stained by Alizarin red staining. (P) Quantitative increase of Alizarin red-stained matrix over *in vitro* culture time for each group ($^{*, +, \#}$ $p<0.05$, demonstrating significant difference over time for same group, *****$p<0.05$, demonstrating significant difference between different groups at day 28, n=4).

5.4.6 Printability of Composite Hydrogel Precursors is Verified by Successful Printing of Composite Hydrogels Scaffolds

3D printing possesses unique advantages to fabricate porous hydrogel scaffolds and it relies on the printability of the hydrogel precursors. Printability refers to the ability of materials to be printed to form and maintain a 3D construct with fidelity and integrity (33). Herein, we tested rheology to verify the printability of composite hydrogel precursors and successfully printed composite hydrogels scaffolds. Hydrogel precursor viscosity will greatly impact the fiber deposition and subsequent scaffold fabrication process. The shear rate dependent behavior of composite hydrogel precursor was provided for increasing HAP concentration, suggesting the non-Newtonian liquid behavior (Figure 5.10). All composite hydrogel precursors showed the shear thinning behavior, and viscosity increased with HAP concentration (Figure 5.10). Then, the ALG and ALG+1%HAP composite hydrogel precursors were loaded into bioprinter to print porous scaffolds by a layer-by-layer manner (Figure 5.11). To visualize the mineral particles dispersion and porous structure, printed scaffolds were analysed by micro-CT. It can be clearly seen from micro-CT images that the porous structure of the scaffold was completely interconnected for ALG and ALG+1%HAP groups. Thresholding is a method for image segmentation and can be used to create binary images (34). By changing the threshold value, materials with different density can be visualized. Porous structure is clearly observed when setting the threshold value at 90/255. For ALG+1%HAP group, even dispersion of mineral particles was clearly spotted when increasing the threshold value (Figure 5.11).

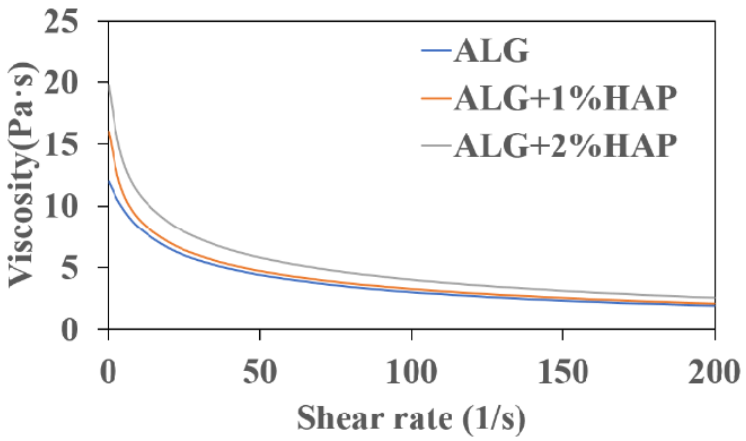

Figure 5.10 Viscosity of the three hydrogel composites with the addition of SC showed their shear thinning behavior.

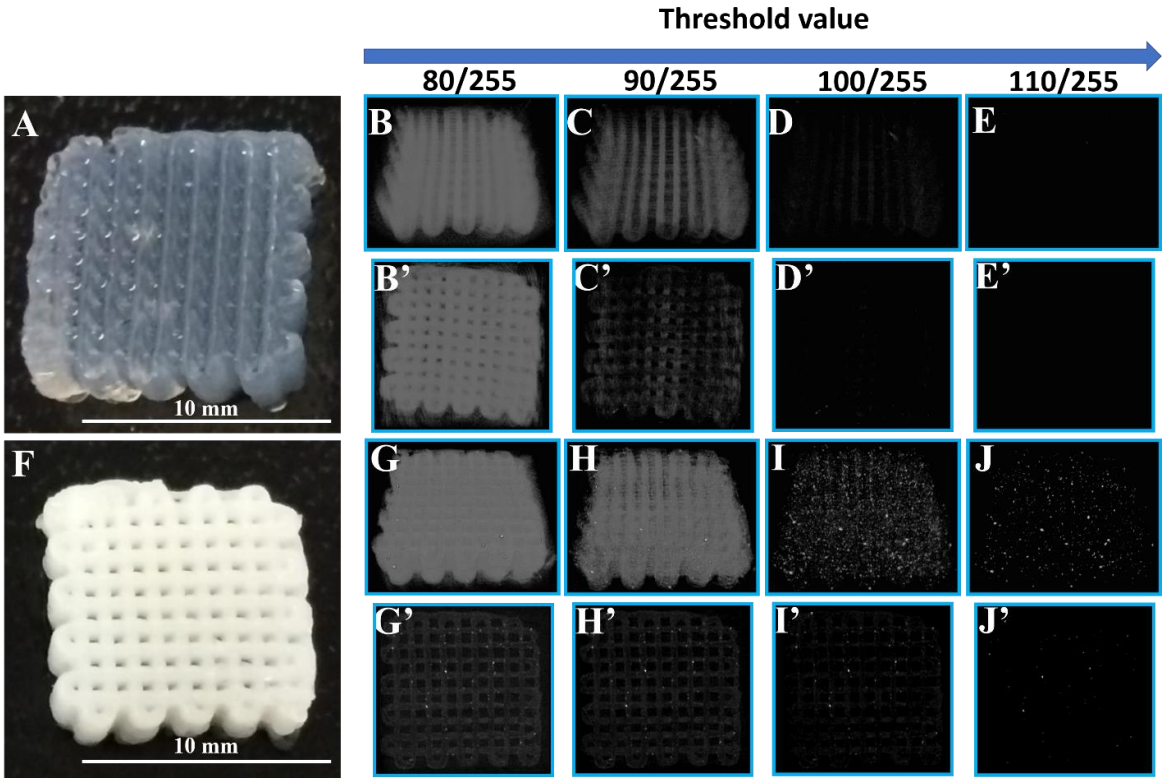

Figure 5.11 Digital pictures and micro-CT reconstruction of ALG and ALG+1%HAP hydrogel scaffolds. HAP particles are evenly dispersed in 3D-printed composite hydrogel. Digital pictures (A, F) and micro-CT reconstructions of ALG only (3D reconstructions: B-E; reconstructed slices: B'-E') and ALG+1%HAP (G-J, G'-J') scaffolds showed the porous structure of hydrogel scaffolds. Even dispersion of HAP particles was visualized by increasing the threshold value of reconstruction images for ALG+1%HAP group (G-J, G'-J').

5.5 Discussion

The goal of this study is to design and prepare ALG+HAP composite hydrogels for the formation of a calcified cartilage matrix. To achieve this goal, HAP particles need to be evenly dispersed within the alginate hydrogel matrices. It is also hypothesized that the homogenously dispersed HAP within ALG hydrogel promotes the deposition of characteristic matrix of calcified cartilage including Collagen type X and mineralized matrix. In the present study, HAP particles were well dispersed into alginate hydrogels with the addition of a surfactant-SC. The response of primary chick chondrocytes in ALG hydrogel with and without HAP was evaluated over time to test the hypothesis.

The HAP phase was stabilized and homogenously distributed in the aqueous solution by adding SC. The effect of SC on the stabilization of HAP suspensions was monitored by characterizing the sedimentation behavior. When increasing the molar ratio (SC to HAP) to 0.25 or higher, the HAP can be stabilized in the aqueous solution for at least 3 days (Figure 5.1). The stabilization effect of the dispersant is usually based upon the repulsive forces resulting from the adsorption of materials on the surface (stabilization by steric hindrance) and/or the overlapping of electrical double layers (electrostatic stabilization) (35, 36). Zeta-potential measurements of HAP suspensions showed that the electrical charge on the HAP nanoparticles was close to zero in the absence of SC. Therefore, there is no electrostatic repulsive forces could be able to counteract the attractive vander Waals forces among HAP crystals in suspension, which explains why HAP suspensions precipitated within 3h. Negative zeta-potential went up with the increase of SC in the HAP, demonstrating a strong initial increase during low SC concentrations ranges followed by a gradual increase at relative high SC concentration ranges (Figure 5.1E). By negatively charging HAP nanoparticles, electrostatic repulsive forces were established between these particles and in this way the HAP nanoparticles were very well dispersed in the medium. The critical molar ratio (SC to HAP) of 0.25 was necessary to stabilize the HAP suspensions, which corresponds a Zeta-potential of around -20 mV. The pH value varies from 7 to 7.5 when the molar ratio was lower than 0.25. A higher molar ratio than 0.25 would alkalize the suspension beyond the physiological level. Therefore, 0.25 was set as a critical molar ratio of SC to HAP for subsequent experiments.

It was also found that HAP phase was well dispersed in the alginate hydrogels. The dispersion state of HAP phase within the alginate hydrogel was examined by SEM and EDS.

Results showed that SC prevented the aggregation of the mineral phase within the alginate matrix at a SC/HAP molar ratio of 0.25, despite the increased HAP content. The stabilizing effect of HAP particles is not only attributed to the SC absorption on HAP particles, but also the alginate matrix, which is negatively charged at physiological pH owing to its isoelectric point of 5.4. The repulsions between alginate and negatively charged HAP crystals could increase the stability and dispersion of HAP in alginate matrix.

Cytocompatibility of composite hydrogels was evaluated by cell viability and proliferation. The addition of HAP particles into alginate hydrogels did not impair the cell viability. There was no significant difference in cell viability among three groups at Day1 and Day7. Cell viability of ALG was generally kept at similar level over culture period and live cells of both ALG+1%HAP and ALG+2%HAP groups demonstrated an increase from Day1 to Day14. This probably because cell viabilities recovered from initial cell viability, which might have been decreased by the increased stress exerted on cells from the mixing of mineral particles.

Embedded chondrocytes in all three groups displayed abundant synthesis of cartilage ECM. Alcian blue staining and Collagen type II immunostaining in three groups reflected the secretion of two major components of cartilage ECM, GAG and Collagen type II, further indicating the biocompatibility of composite hydrogels and preparation method. The addition of HAP into ALG hydrogels negatively influenced the GAG biosynthesis of chondrocytes at Day28. This was consistent with previously published research demonstrating decreased proteoglycan content may happen during cartilage mineralization (37).

All three groups expressed Collagen type X after 28 days of culture, which is a characteristic of calcified layers of articular cartilage (38, 39). It has been shown that after long time culture, embedded chondrocytes in alginate hydrogels would express Collagen type X (24), which was in accordance with the finding in the ALG group of the present study. Moreover, it was also found that the amount of newly formed Collagen type X was positively correlated with the content of added HAP. This was probably because HAP served as a reservoir of ions such as Ca^{2+} and Pi. It has been suggested that the exogenous Ca^{2+} and Pi markedly influenced Collagen type X synthesis (40-42).

It was observed that chondrocytes in ALG+1%HAP and ALG+2%HAP exhibited higher ALP activity than chondrocytes in ALG only group. The elevated mineralization potential observed here for groups with HAP addition were in accord with published research (43). ALP

activity showed a significant decrease from Day14 to Day28 which may be due to its normalization to cell numbers. ALP positive staining was observed in three groups at Day14, while stronger staining was seen in samples with the addition of HAP particles. Intense ALP staining can be observed at Day28 for three groups of composite hydrogels. The change in mineralization potential of chondrocytes were probably due to the presence of HAP particles. HAP can serve as a mediator that facilitated cell-to-cell interactions and induced the elevated ALP activity (44). It was believed that the mineralization process began at the location where ALP was detected in the matrix (45). When the expression of ALP was inhibited, calcification would not occur (46). Thereby the increase and expression of ALP was considered one of the markers showing that the calcification was occurring (47).

Abundant minerals deposits were stained at Day28 in ALG+1%HAP and ALG+2%HAP. This was understandable considering the fact that ALP began to express at Day14, which usually marked the start of mineralization process. To understand if the HAP particles serve as nucleation sites for mineralization during culture, control groups without cells were prepared and cultured for 28 days. Results did show the Alizarin red-stained areas, however, not as strong as cell-laden samples. This argues that the minerals deposition was mainly from chondrocytes rather than the nucleation effect of pre-incorporated HAP particles.

Porous composite hydrogel scaffolds were successfully printed by a 3D Bioplotter. Micro-CT images were obtained to visualize the porous structure and incorporated HAP particles. The boundaries of low-density materials like hydrogels seen in micro-CT scans are usually not as sharp as high-density materials like PCL (48) or hard tissue due to their lower linear attenuation coefficient. This is also the case for segmenting ALG scaffold structural information. When HAP was added into the alginate hydrogel, scaffold images could be extracted for morphometric analysis. Thus HAP could be used as a contrast agent for low-density materials. A shift of the threshold parameters can result in good quality micro-CT image deteriorated by noise and make these particles more visible. It can be observed from these images that HAP particles were evenly dispersed in the alginate matrix.

5.6 Conclusion

This study prepared composite hydrogels consist of ALG and HAP for application in calcified cartilage formation. HAP phase was homogenously dispersed within alginate matrices

with the addition of SC. The hypothesis that the presence of HAP in alginate hydrogel promotes the formation of calcified cartilage matrix including Collagen type X and minerals has been tested. The composite hydrogel precursors were successfully printed into porous hydrogel scaffolds, showing promising for its application in tissue engineering. These findings demonstrate that the ALG/HAP composite is promising for calcified cartilage formation and subsequent osteochondral interface regeneration.

References

1. Buckwalter JA, Saltzman C, Brown T. The impact of osteoarthritis: implications for research. Clin Orthop. 2004;427:S6-S15.

2. Hunziker EB. Biologic Repair of Articular Cartilage: Defect Models in Experimental Animals and Matrix Requirements. Clin Orthop. 1999;367:S135-46.

3. Knutsen G, Engebretsen L, Ludvigsen TC, Drogset JO, Grontvedt T, Solheim E, et al. Autologous chondrocyte implantation compared with microfracture in the knee. A randomized trial. J Bone Joint Surg Am. 2004 Mar;86-A(3):455-64.

4. Gudas R, Stankevičius E, Monastyreckienė E, Pranys D, Kalesinskas RJ. Osteochondral autologous transplantation versus microfracture for the treatment of articular cartilage defects in the knee joint in athletes. Knee Surgery, Sports Traumatology, Arthroscopy. 2006;14(9):834-42.

5. Brouwer RW, van Raaij TM, Bierma-Zeinstra S, Verhagen AP, Jakma TT, Verhaar JA. Osteotomy for treating knee osteoarthritis. The Cochrane Library. 2007.

6. Fortin PR, Penrod JR, Clarke AE, St-Pierre Y, Joseph L, Bélisle P, et al. Timing of total joint replacement affects clinical outcomes among patients with osteoarthritis of the hip or knee. Arthritis & Rheumatism. 2002;46(12):3327-30.

7. Bedi A, Feeley BT, Williams RJ. Management of articular cartilage defects of the knee. J Bone Joint Surg Am. 2010;92(4):994-1009.

8. Hunziker EB. Articular cartilage repair: basic science and clinical progress. A review of the current status and prospects. Osteoarthritis and cartilage. 2002;10(6):432-63.

9. Kuo CK, Li WJ, Mauck RL, Tuan RS. Cartilage tissue engineering: its potential and uses. Curr Opin Rheumatol. 2006 Jan;18(1):64-73.

10. Chung C, Burdick JA. Engineering cartilage tissue. Adv Drug Deliv Rev. 2008;60(2):243-62.

11. Izadifar Z, Chen X, Kulyk W. Strategic design and fabrication of engineered scaffolds for articular cartilage repair. Journal of functional biomaterials. 2012;3(4):799-838.

12. Hunziker E, Driesang I, Saager C. Structural barrier principle for growth factor-based articular cartilage repair. Clin Orthop. 2001;391:S182-9.

13. Lories RJ, Luyten FP. The bone–cartilage unit in osteoarthritis. Nature Reviews Rheumatology. 2011;7(1):43-9.

14. Allan K, Pilliar R, Wang J, Grynpas M, Kandel R. Formation of biphasic constructs containing cartilage with a calcified zone interface. Tissue Eng. 2007;13(1):167-77.

15. Wu LN, Ishikawa Y, Sauer GR, Genge BR, Mwale F, Mishima H, et al. Morphological and biochemical characterization of mineralizing primary cultures of avian growth plate chondrocytes: evidence for cellular processing of Ca2 and Pi prior to matrix mineralization. J Cell Biochem. 1995;57(2):218-37.
16. Vilela C, Correia C, Oliveira JM, Sousa RA, Espregueira-Mendes J, Reis RL. Cartilage repair using hydrogels: a critical review of in vivo experimental designs. ACS Biomaterials Science & Engineering. 2015;1(9):726-39.
17. Kopeček J. Hydrogel biomaterials: a smart future? Biomaterials. 2007;28(34):5185-92.
18. Hoppe A, Güldal NS, Boccaccini AR. A review of the biological response to ionic dissolution products from bioactive glasses and glass-ceramics. Biomaterials. 2011;32(11):2757-74.
19. Song J, Xu J, Filion T, Saiz E, Tomsia AP, Lian JB, et al. Elastomeric high-mineral content hydrogel-hydroxyapatite composites for orthopedic applications. Journal of Biomedical Materials Research Part A. 2009;89(4):1098-107.
20. Lin H, Yeh Y. Porous alginate/hydroxyapatite composite scaffolds for bone tissue engineering: preparation, characterization, and in vitro studies. Journal of Biomedical Materials Research Part B: Applied Biomaterials. 2004;71(1):52-65.
21. Turco G, Marsich E, Bellomo F, Semeraro S, Donati I, Brun F, et al. Alginate/hydroxyapatite biocomposite for bone ingrowth: a trabecular structure with high and isotropic connectivity. Biomacromolecules. 2009;10(6):1575-83.
22. Jewad R, Bentham C, Hancock B, Bonfield W, Best SM. Dispersant selection for aqueous medium pressure injection moulding of anhydrous dicalcium phosphate. Journal of the European Ceramic Society. 2008;28(3):547-53.
23. Bao Y, Senos A, Almeida M, Gauckler LJ. Rheological behavior of aqueous suspensions of hydroxyapatite (HAP). J Mater Sci Mater Med. 2002;13(7):639-43.
24. Izadifar Z, Chang T, Kulyk W, Chen X, Eames BF. Analyzing biological performance of 3D-printed, cell-impregnated hybrid constructs for cartilage tissue engineering. Tissue Engineering Part C: Methods. 2015;22(3):173-88.
25. Zhang Z, McCaffery JM, Spencer RG, Francomano CA. Growth and integration of neocartilage with native cartilage in vitro. Journal of orthopaedic research. 2005;23(2):433-9.

26. Zhang Z, McCaffery JM, Spencer RG, Francomano CA. Hyaline cartilage engineered by chondrocytes in pellet culture: histological, immunohistochemical and ultrastructural analysis in comparison with cartilage explants. J Anat. 2004;205(3):229-37.
27. Meier S, Solursh M. Ultrastructural analysis of the effect of ascorbic acid on secretion and assembly of extracellular matrix by cultured chick embryo chondrocytes. J Ultrastruct Res. 1978;65(1):48-59.
28. Walker E, Verner A, Flannery C, Archer C. Cellular responses of embryonic hyaline cartilage to experimental wounding in vitro. Journal of Orthopaedic Research. 2000;18(1):25-34.
29. Hirsch MS, Svoboda KH. Establishment of a whole-chick sternum model that recapitulates normal cartilage development. BioTechniques. 1998 Apr;24(4):632-6.
30. You F, Wu X, Zhu N, Lei M, Eames BF, Chen X. 3D Printing of porous cell-laden hydrogel constructs for potential applications in cartilage tissue engineering. ACS Biomaterials Science & Engineering. 2016;2(7):1200-10.
31. Schneider CA, Rasband WS, Eliceiri KW. NIH Image to ImageJ: 25 years of image analysis. Nature methods. 2012;9(7):671.
32. Billiet T, Gevaert E, De Schryver T, Cornelissen M, Dubruel P. The 3D printing of gelatin methacrylamide cell-laden tissue-engineered constructs with high cell viability. Biomaterials. 2014;35(1):49-62.
33. You F, Wu X, Chen X. 3D printing of porous alginate/gelatin hydrogel scaffolds and their mechanical property characterization. International Journal of Polymeric Materials and Polymeric Biomaterials. 2017;66(6):299-306.
34. Shapiro LG, Stockman GC. Computer Vision, 2001, 279-325.
35. Vishista K, Gnanam F. Role of deflocculants on the rheological properties of boehmite sol. Mater Lett. 2004;58(10):1576-81.
36. Hidber PC, Graule TJ, Gauckler LJ. Citric acid—a dispersant for aqueous alumina suspensions. J Am Ceram Soc. 1996;79(7):1857-67.
37. Buckwalter JA. Proteoglycan structure in calcifying cartilage. Clin Orthop. 1983;172:207-32.
38. Kirsch T, MARK K. Isolation of human type X collagen and immunolocalization in fetal human cartilage. European journal of biochemistry. 1991;196(3):575-80.

39. Reichenberger E, Aigner T, Von Der Mark K, Stöss H, Bertling W. In situ hybridization studies on the expression of type X collagen in fetal human cartilage. Dev Biol. 1991;148(2):562-72.
40. Thomas JT, Boot-Handford RP, Grant ME. Modulation of type X collagen gene expression by calcium beta-glycerophosphate and levamisole: implications for a possible role for type X collagen in endochondral bone formation. J Cell Sci. 1990 Apr;95 (Pt 4)(Pt 4):639-48.
41. Grant M. The structure and synthesis of cartilage collagen. The control of tissue damage. 1988:3-28.
42. Bonen DK, Schmid TM. Elevated extracellular calcium concentrations induce type X collagen synthesis in chondrocyte cultures. J Cell Biol. 1991;115(4):1171-8.
43. Khanarian NT, Jiang J, Wan LQ, Mow VC, Lu HH. A hydrogel-mineral composite scaffold for osteochondral interface tissue engineering. Tissue Engineering Part A. 2011;18(5-6):533-45.
44. Tsukamoto Y, Fukutani S, Mori M. Hydroxyapatite-induced alkaline phosphatase activity of human pulp fibroblasts. J Mater Sci Mater Med. 1992;3(3):180-3.
45. Omelon S, Georgiou J, Variola F, Dean MN. Colocation and role of polyphosphates and alkaline phosphatase in apatite biomineralization of elasmobranch tesserae. Acta biomaterialia. 2014;10(9):3899-910.
46. Fallon MD, Whyte MP, Teitelbaum SL. Stereospecific inhibition of alkaline phosphatase by L-tetramisole prevents in vitro cartilage calcification. Lab Invest. 1980 Dec;43(6):489-94.
47. Richards F, Boyer HWP. The Enzymes (3rd Edn.), Vol. 4. . 1971.
48. Olubamiji AD, Izadifar Z, Si JL, Cooper DM, Eames BF, Chen DX. Modulating mechanical behaviour of 3D-printed cartilage-mimetic PCL scaffolds: influence of molecular weight and pore geometry. Biofabrication. 2016;8(2):025020.

Chapter 6: Conclusions and Future Work

6.1 Conclusions

Hydrogel, as a water-swollen polymeric network, is attractive as a scaffolding material in cartilage tissue engineering. Hydrogels can closely mimic native cartilage ECM and thus provide a 3D culture microenvironment favorable for encapsulated chondrocytes. With hydrogels, it is also possible to achieve high cell seeding density, homogeneous cell distribution, and transduce mechanical stimuli to embedded chondrocytes. However, fabrication of hydrogel scaffolds with desired interconnective porosity and living cells is the key issue, which limits hydrogel's applications in CTE. To address this issue, the present study aimed to bioprint porous cell-laden hydrogel constructs for application in CTE. This aim was achieved through the following three specific objectives.

The first objective was to fabricate CTE scaffolds based on the bioprinting technique and to study the influence of scaffold design on the mechanical performance. For this, thermal/submerged ionic crosslinking process was employed to successfully bioprint porous alginate/gelatin hydrogel scaffolds. Six internal structures were designed and printed by varying stand orientation and strand spacing. The internal structures were found to play an important role in the mechanical properties of printed constructs. This finding provided researchers with a convenient way to modulate the mechanical performance of the printed hydrogel scaffolds.

The second objective was to develop a 3D bioplotting technique or process supplemented with the submerged cross-linking mechanism to fabricate alginate hydrogel constructs with living cells. In this regard, a Bioplotting technique supplemented with the submerged cross-linking mechanism was used to fabricate porous cell-laden alginate hydrogel constructs. *In vitro* biological performance of the printed constructs was evaluated and shown to favor the survival and proliferation of embedded chondrocytes, deposition of cartilage ECM including sulfated GAG and Collagen type II.

The third objective was to test the hypothesis that homogeneously dispersed hydroxyapatite in alginate hydrogel promotes the formation of calcified cartilage matrix. For this, by using SC, HAP phase was homogeneously dispersed in alginate hydrogel and the presence of HAP promoted the formation of calcified cartilage matrix including minerals and Collagen type X. Notably, composite hydrogel consists of HAP and alginate demonstrated good printability and was successfully printed.

To sum up, a bioprinting technique was developed to fabricate porous cell-laden hydrogel constructs. *In vitro* characterization of the printed constructs has shown to favor embedded chondrocytes survival and proliferation, and facilitated deposition of cartilage ECM including sulfated GAG and Collagen type II. This bioprinting approach utilized a submerged crosslinking process enabling the use of alginate solution with a concentration as low as 2%, which cannot be achieved by most other extrusion-based bioprinting techniques. Such a low polymer concentration would favor the cells migration and ECM production. Therefore, this bioprinting technique is a promising approach for CTE, providing a facile fabrication technique for other researchers to produce porous cell-laden hydrogel constructs facilitating cells survival and cartilage ECM production from low-viscosity hydrogel precursors.

To understand the versatility of the present bioprinting technique, another material-gelatin was mixed with alginate and printed. Since gelatin is a type of thermally crosslinkable polymer, a thermal crosslinking process was also combined with the submerged ionic crosslinking process. Results showed that the present bioprinting technique can be compatible with other crosslinkable polymers (e.g. gelatin) and crosslinking mechanisms (e.g. thermal crosslinking). Meanwhile, porous alginate/gelatin hydrogel scaffolds with various internal design were successfully printed and the mechanical properties of these constructs can be varied by changing internal structure. This finding allowed researchers to modify the properties of printed constructs by adding new biomaterials or changing the internal structure design.

Last, it was shown that the addition of HAP phase into the alginate matrix would promote the deposition of Collagen type X and minerals from embedded chondrocytes and thus can be an effective design used for calcified cartilage regeneration. This conclusion tested the hypothesis that the presence of HAP promotes the secretion of Collagen type X and minerals from chondrocytes. The finding showed an easy approach to induce the chondrocytes secrete calcified cartilage matrix and this result was consistent with previous finding that by mixing calcium phosphate with hydrogels, embedded chondrocytes could potentially produce mineralized cartilage matrix. To bring this forward, porous ALG/HAP scaffolds were also fabricated and demonstrated promising for use in CTE. In future study, two-layer cell-laden hydrogel constructs could be fabricated with upper layer mimicking cartilage and lower layer mimicking calcified cartilage. In future study, by printing this two-layer cartilage constructs, we will further test the

hypothesis that the calcified layer is required for mechanically-functional osteochondral constructs.

The conclusions drawn from this research and specific objectives that are fulfilled are summarized as follows:

- Bioprinting technique supplemented with a submerged crosslinking process was developed to successfully print porous chondrocyte-laden alginate hydrogel scaffolds with structural integrity and fidelity;
- Chondrocytes embedded in printed alginate hydrogel scaffolds were able to survive the bioprinting and submerged crosslinking process and the printed chondrocyte-laden alginate hydrogel constructs could support cartilage ECM deposition including GAGs and Collagen type II, and maintain a good structural integrity throughout the *in vitro* culture period;
- This present bioprinting technique demonstrated suitability to print other printable bio-inks (e.g. gelatin) by working with different crosslinking methods (e.g. thermal crosslinking). This finding makes it possible to tune the properties by mixing with other polymers.
- By varying the internal architecture parameters, the mechanical properties of the printed scaffolds can be tuned. Porosity, contact area between strands and spacing variation within printed scaffolds were three key factors that influence the mechanical performance of hydrogel scaffolds.
- With the addition of a surfactant-sodium citrate (SC), a ceramic phase HAP can be homogeneously distributed into alginate hydrogel matrix since the SC can negatively charge HAP particles and repulsive forces among particles helped to stabilize HAP suspension. A critical molar ratio of sodium citrate to HAP was determined as 0.25:1. Lower molar ratio than 0.25:1 cannot ensure a long-term homogenous dispersion of HAP particles.
- Chondrocytes mixed in the composite ALG/HAP hydrogel showed a high cell viability and synthesized calcified cartilage matrix including Collagen type X and minerals. Therefore, the composite hydrogel can potentially be used for calcified cartilage formation;

- The printability of the composite ALG/HAP hydrogel was verified by successfully printing the porous ALG/HAP hydrogel scaffold. Interconnected pore networks and pre-incorporated HAP particles can be visualized by adjusting the threshold value of reconstructed images.

6.2 Future Work

Based on the literature review and research results presented in this thesis, some recommendations for future research and suggested projects may be conducted in the future:

- Alginate, as a biocompatible material, possess unique advantages as bio-inks for bioprinting such as good printability and rapid crosslinking. However, lack of specific adhesion sites of alginate limits its application in tissue engineering. Other bioactive hydrogel-forming polymers (gelatin, collagen, and hyaluronic acid etc.) maybe mixed with alginate to improve its bioactivity. In this way, the bioactivity from other components and the good printability of alginate can be combined to fabricate tissue construct with better regeneration outcomes. Chapter 3, as an example, shows the possibility of incorporating other materials into the alginate and feasibility of combing various crosslinking mechanisms in current bioprinting technique.
- Growth factors are useful tools to enhance cartilage repair. Insulin-like growth factor transforming growth factor-β and bone morphogenetic protein have been shown to enhance cartilage formation alone or in combination. The mild conditions of current bioprinting process make it possible to include these growth factors in printed tissue constructs to stimulate cell proliferation and cartilage ECM deposition.
- Mechanical stimuli play an important part in the growth and development of articular cartilage. Hydrogel can transduce mechanical stimuli to embedded chondrocytes. Therefore, a study investigating effect of mechanical stimuli on ECM biosynthesis within the printed hydrogel constructs is strongly suggested.
- New approaches are needed to improve the mechanical properties of current printed tissue construct, which are inferior to native cartilage. These approaches may include: introducing other polymers into current system, varying the internal architecture, and co-depositing with thermoplastics et al.

- A reason of the poor cartilage self-repair capacity is its low chondrocyte density. Harvesting autologous chondrocytes is not an ideal way especially when considering the following monolayer cell expansion process may induce de-differentiation and the harvesting procedure will leave a donor site. In future study, stem cells may be introduced into the present bioprinting system. Stem cells viability, proliferation, and differentiation can be investigated in the current bioprinting system.
- The present study has shown promising cartilage matrix deposition within bioprinted constructs for *in vitro* studies. It is suggested that these printed constructs be implanted in animals such as immunodeficient mice, to investigate the structural integrity and long-term cartilage tissue regeneration of printed hydrogel constructs *in vivo*. With positive results, the functionality of printed hydrogel constructs should be studied to repair cartilage defects of articular joints in larger animals, like rabbit and pig, prior to moving the stage of applying them to humans.